ACOUSTIC TRANSDUCTION – MATERIALS AND DEVICES

Period 31 July 1996 to 31 December 1997

Annual Report

VOLUME III

OFFICE OF NAVAL RESEARCH
Contract No: N00014-96-1-1173

APPROVED FOR PUBLIC RELEASE – DISTRIBUTION UNLIMITED

Kenji Uchino

PENNSTATE

1855

THE MATERIALS RESEARCH LABORATORY
UNIVERSITY PARK, PA

REPORT DOCUMENTATION PAGE

Form Approved
OMB No. 0704-0188

1. AGENCY USE ONLY (Leave blank)	2. REPORT DATE	3. REPORT TYPE AND DATES COVERED
	05/01/98	ANNUAL REPORT 07/31/96-12/31/97

4. TITLE AND SUBTITLE
ACOUSTIC TRANSDUCTION -- MATERIALS AND DEVICES

5. FUNDING NUMBERS
ONR CONTRACT NO:
N00014-96-1-1173

6. AUTHOR(S)
KENJI UCHINO

7. PERFORMING ORGANIZATION NAME(S) AND ADDRESS(ES)
Materials Research Laboratory
The Pennsylvania State University
University Park, PA 16802

8. PERFORMING ORGANIZATION REPORT NUMBER

9. SPONSORING / MONITORING AGENCY NAME(S) AND ADDRESS(ES)
Office of Naval Research
ONR 321SS
Ballston Centre Tower One
800 N Quincy Street
Arlington, VA 22217-5660

Office of Naval Research
Regional Office Chicago
536 S Clark Str., Rm 208
Chicago IL 60605-1588

10. SPONSORING / MONITORING AGENCY REPORT NUMBER

11. SUPPLEMENTARY NOTES

12a. DISTRIBUTION / AVAILABILITY STATEMENT

12b. DISTRIBUTION CODE

13. ABSTRACT *(Maximum 200 words)*

SEE FOLLOW PAGE

14. SUBJECT TERMS

15. NUMBER OF PAGES

16. PRICE CODE

17. SECURITY CLASSIFICATION OF REPORT	18. SECURITY CLASSIFICATION OF THIS PAGE	19. SECURITY CLASSIFICATION OF ABSTRACT	20. LIMITATION OF ABSTRACT

GENERAL INSTRUCTIONS FOR COMPLETING SF 298

The Report Documentation Page (RDP) is used in announcing and cataloging reports. It is important that this information be consistent with the rest of the report, particularly the cover and title page. Instructions for filling in each block of the form follow. It is important to ***stay within the lines*** to meet ***optical scanning requirements***.

Block 1. Agency Use Only *(Leave blank)*.

Block 2. Report Date. Full publication date including day, month, and year, if available (e.g. 1 Jan 88). Must cite at least the year.

Block 3. Type of Report and Dates Covered. State whether report is interim, final, etc. If applicable, enter inclusive report dates (e.g. 10 Jun 87 - 30 Jun 88).

Block 4. Title and Subtitle. A title is taken from the part of the report that provides the most meaningful and complete information. When a report is prepared in more than one volume, repeat the primary title, add volume number, and include subtitle for the specific volume. On classified documents enter the title classification in parentheses.

Block 5. Funding Numbers. To include contract and grant numbers; may include program element number(s), project number(s), task number(s), and work unit number(s). Use the following labels:

C	- Contract	PR	- Project
G	- Grant	TA	- Task
PE	- Program Element	WU	- Work Unit Accession No.

Block 6. Author(s). Name(s) of person(s) responsible for writing the report, performing the research, or credited with the content of the report. If editor or compiler, this should follow the name(s).

Block 7. Performing Organization Name(s) and Address(es). Self-explanatory

Block 8. Performing Organization Report Number. Enter the unique alphanumeric report number(s) assigned by the organization performing the report.

Block 9. Sponsoring/Monitoring Agency Name(s) and Address(es). Self-explanatory.

Block 10. Sponsoring/Monitoring Agency Report Number. *(If known)*

Block 11. Supplementary Notes. Enter information not included elsewhere such as: Prepared in cooperation with...; Trans. of...; To be published in.... When a report is revised, include a statement whether the new report supersedes or supplements the older report.

Block 12a. Distribution/Availability Statement. Denotes public availability or limitations. Cite any availability to the public. Enter additional limitations or special markings in all capitals (e.g. NOFORN, REL, ITAR).

DOD	-	See DoDD 5230.24, "Distribution Statements on Technical Documents."
DOE	-	See authorities.
NASA	-	See Handbook NHB 2200.2.
NTIS	-	Leave blank.

Block 12b. Distribution Code.

DOD	-	Leave blank.
DOE	-	Enter DOE distribution categories from the Standard Distribution for Unclassified Scientific and Technical Reports.
NASA	-	Leave blank.
NTIS	-	Leave blank.

Block 13. Abstract. Include a brief *(Maximum 200 words)* factual summary of the most significant information contained in the report.

Block 14. Subject Terms. Keywords or phrases identifying major subjects in the report.

Block 15. Number of Pages. Enter the total number of pages.

Block 16. Price Code. Enter appropriate price code *(NTIS only)*

Blocks 17. - 19. Security Classifications. Self-explanatory. Enter U.S. Security Classification in accordance with U.S. Security Regulations (i.e., UNCLASSIFIED). If form contains classified information, stamp classification on the top and bottom of the page.

Block 20. Limitation of Abstract. This block must be completed to assign a limitation to the abstract. Enter either UL (unlimited) or SAR (same as report). An entry in this block is necessary if the abstract is to be limited. If blank, the abstract is assumed to be unlimited.

ABSTRACT

The report documents work carried out over the period 31 July 1996 to 31 December 1997 on a Multi-University Research Initiative (MURI) program under Office of Naval Research (ONR) sponsorship. The program couples transducer materials research in the Materials Research Laboratory (MRL), design and testing studies in the Applied Research Laboratory (ARL) and vibration and flow noise control in the Center for Acoustics and Vibration (CAV) at Penn State.

The overarching project objective is the development of acoustic transduction materials and devices of direct relevance to Navy needs and with application in commercial products. The initial focus of studies is upon high performance sensors and high authority high strain actuators. This objective also carries the need for new materials, new device designs, improved drive and control strategies and a continuing emphasis upon reliability under a wide range of operating conditions.

In *Material Studies*, undoubtedly major breakthroughs have occurred in the ultra-high strain relaxor ferroelectric systems. Earlier reports of unusual piezoelectric activity in single crystal perovskite relaxors have been amply confirmed in the lead zinc niobate : lead titanate, and lead magnesium niobate : lead titanate systems for compositions of rhombohedral symmetry close to the Morphotropic Phase Boundary (MPB) in these solid solutions. Analysis of the unique properties of 001 field poled rhombohedral ferroelectric crystals suggests new intrinsic mechanisms for high strain and carries the first hints of how to move from lead based compositions. A major discovery of comparable importance is a new mode of processing to convert PVDF:TrFE copolymer piezoelectric into a relaxor ferroelectric in which electrostrictive strains of 4% have been demonstrated at high fields. Both single crystal and polymer relaxors appear to offer energy densities almost order of magnitude larger than in earlier polycrystal ceramic actuators.

Transducer Studies have continued to exploit the excellent sensitivity and remarkable versatility of the cymbal type flextensional element. Initial studies of a small cymbal arrays show excellent promise in both send and receive modes, and larger arrays are now under construction for tests at ARL. New studies in constrained layer vibration damping and in flow noise reduction are yielding exciting new results.

In *Actuator Studies*, an important advance in piezoelectric generated noise control now permits wider use of acoustic emission as a reliability diagnostic technique. Joint studies with NRL, Washington have developed a completely new d_{15} driven torsional actuator and the CAV program element has designed an exciting high strain high force inchworm.

Finite element analysis continues to be an important tool for understanding the more complex composite structures and their beam forming capability in water. *Thin and Thick Thin Film Studies* are gearing up to provide the material base for micro-tonpilz arrays. New exploitation of ultra sensitive strain and permittivity measurements is providing the first reliable data of electrostriction in simple solids, and suggesting new modes for separating the polarizability contributors in dielectrics and electrostrictors.

APPENDICES

VOLUME I

GENERAL SUMMARY PAPERS

1. Ito, Y. and K. Uchino, Wiley Encyclopedia of Electrical and Electronics Engineering, J. G. Webster, Edit., (Partial Charge "Piezoelectricity"), John Wiley & Sons (1998). [in press].
2. Newnham, R.E., "Molecular Mechanisms in Smart Materials," MRS Bulletin (May 1997).
3. Swartz, S.L., T.R. Shrout, and T. Takenaka, "Electronic Ceramics R&D in the U.S., Japan, Part I: Patent History," The American Ceramic Society Bulletin **76** (8) (1997).

2.0 MATERIALS STUDIES

2.1 Polycrystal Perovskite Ceramics

4. Alberta, E.F., and A.S. Bhalla, "Piezoelectric Properties of $Pb(InNb)_{1/2}O_3$-$PbTiO_3$ Solid Solution Ceramics," J. Korean Phys. Soc. **32**, S1265-S1267 (February 1998).
5. Alberta, E.F. and A.S. Bhalla, "High Strain and Low Mechanical Quality Factor Piezoelectric $Pb[Sc_{1/2}Nb_{1/2})_{0.575}Ti_{0.425}]O_3$ Ceramics" (1997).
6. Zhang, Q.M. and J. Zhao, "Polarization Responses in Lead Magnesium Niobate Based Relaxor Ferroelectrics," Appl. Phys. Lett. **71** (12, 1649-1651 (1997).
7. Glazounov, A.E., J. Zhao, and Q.M. Zhang, "Effect of Nanopolar Regions on Electrostrictive Coefficients of a Relaxor Ferroelectric," Proceedings Williamsburg Meeting, Williamsburg, Virginia (1998).
8. Zhao, J. A.E. Glazounov, Q.M. Zhang, and B. Toby, "Neutron Diffraction Study of Electrostrictive Coefficients of Prototype Cubic Phase of Relaxor Ferroelectric $PbMg_{1/3}Nb_{2/3}O_3$," Appl. Phys. Lett. **72** (9), 1-3 (1998).
9. Park, S.-E., T.R. Shrout, P. Bridenbaugh, J. Rottenberg, and G.M. Loiacono, "Electric Field Induced Anisotropy in Electrostrictive $Pb(Mg_{1/3}Nb_{2/3})O_3$ - $PbTiO_3$ Crystals," Ferroelectrics (1997).
10. You, H. and Q.M. Zhang, "Diffuse X-Ray Scattering Study of Lead Magnesium Niobate Single Crystals," Phys. Rev. Lett. **79** (20), 3950-3953 (1997).
11. Zhao, J., V. Mueller, and Q.M. Zhang, "The Influence of the External Stress on the Electromechanical Response of Electrostrictive $0.9Pb(Mg_{1/3}Nb_{2/3})O_3$–$0.1PbTiO_3$ in the DC Electrical Field Biased State," J. Mat. Res. (1998).

VOLUME II

12. Yoon, S.-J., A. Joshi, and K. Uchino, "Effect of Additives on the Electromechanical Properties of $Pb(Zr,Ti)O_3$–$Pb(Y_{2/3}W_{1/3})O_3$ Ceramics," J. Am. Ceram. Soc **80** (4), 1035-39 (1997).
13. Hackenberger, W., M.-J. Pan, V. Vedula, P. Pertsch, W. Cao, C. Randall, and T. Shrout, "Effect of Grain Size on Actuator Properties of Piezoelectric Ceramics," Proceedings of the SPIE's 5th International Symposium on Smart Structures and Materials, San Diego, CA (March 1-5, 1998).

THIS PAGE LEFT INTENTIONALLY BLANK

Materials Studies–continued

14. Mueller, V. and Q.M. Zhang, "Shear Response of Lead Zirconate Titanate Piezoceramics," J. Appl. Phys. (1998).
15. Park, S.-E., M.-J. Pan, K. Markowski, S. Yoshikawa, and L.E. Cross, "Electric Field Induced Phase Transition of Antiferroelectric Lead Lanthanum Zirconate Titanate Stannate Ceramics," J. Appl. Phys. **82** (4), 1798-1803 (1997).
16. Yoshikawa, S., K. Markowski, S.-E. Park, M.-J. Pan, and L.E. Cross, "Antiferroelectric-to-Ferroelectric Phase Switching Lead Lanthanum Zirconate Stannate Titanate (PLZST) Ceramics)," Proceedings of SPIE's 4th Annual Symposium on Smart Structures and Materials, San Diego, CA (March 3-6, 1997).
17. Pan, M.-J., S.-E. Park, K.A. Markowski, W.S. Hackenberger, S. Yoshikawa, and L.E. Cross, "Electric Field Induced Phase Transition in Lead Lanthanum Stannate Zirconate Titanate (PLSnZT) Antiferroelectrics: Tailoring Properties through Compositional Modification" (1997).
18. Pan, M.-J., P. Pertsch, S. Yoshikawa, T.R. Shrout, and V. Vedula, "Electroactive Actuator Materials: Investigations on Stress and Temperature Characteristics," Proceedings of the SPIE's 5th International Symposium on Smart Structures and Materials, San Diego, CA (March 1-5, 1998).
19. Pan, M.-J. and S. Yoshikawa, "Effect of Grain Size on the Electromechanical Properties of Antiferroelectric-to-Ferroelectric Phase Switching PLSnZT Ceramics" (1997).

2.2 *Relaxor Ferroelectric Single Crystal Systems*

20. Service, R.F., "Shape-Changing Crystals Get Shiftier," Science **275**, 1878 (28 March 1997).
21. Shrout, T.R., S.-E. Park, C.A. Randall, J.P. Shepard, L.B. Hackenberger, "Recent Advances in Piezoelectric Materials" (1997).
22. Park, S.-E. and T.R. Shrout, "Ultrahigh Strain and Piezoelectric Behavior in Relaxor Based Ferroelectric Single Crystals," J. Appl. Phys. **82** (4), 1804-1811 (1997).
23. Park, S.-E. and T. R. Shrout, "Characteristics of Relaxor-Based Piezoelectric Single Crystals for Ultrasonic Transducers," IEEE Transactions, Ferroelectrics, and Frequency Control **44** (5), 1140-1147 (1997).
24. Park, S.-E. and T.R. Shrout, "Relaxor Based Ferroelectric Single Crystals for Electro-Mechanical Actuators," Mat. Res. Innov. **1**, 20-25 (1997).
25. Park, S.-E., M.L. Mulvihill, G. Risch, and T.R. Shrout, "The Effect of Growth Conditions on the Dielectric Properties of $Pb(Zn_{1/3}Nb_{2/3})O_3$ Single Crystals," Jpn. J. Appl. Phys. **36**, 1154-1158 (1997).
26. Mulvihill, M.L., L.E. Cross, W. Cao, and K. Uchino, "Domain-Related Phase Transionlike Behavior in Lead Zinc Niobate Relaxor Ferroelectric Single Crystals," J. Am. Ceram. Soc. **80** (6), 1462-68 (1997).
27. Park, S.-E., P.D. Lopath, K.K. Shung, and T.R. Shrout, "Relaxor-Based Single Crystal materials for Ultrasonic Transducer Applications" (1997).
28. Lopath, P.D., S.-E. Park, K.K. Shung, and T.R. Shrout, "$Pb(Zn_{1/3}Nb_{2/3})O_3/PbTiO_3$ Single Crystal Piezoelectrics for Ultrasonic Transducers" (1997).
29. Lopath, P.D., S-E. Park, K.K. Shung, and T.R. Shrout, "Single Crystal $Pb(Zn_{1/3}Nb_{2/3})O_3/PbTiO_3$ (PZN/PT) in Medical Ultrasonic Transducers" (1997).

Materials Studies–continued

2.3 New High Strain Polymer Materials

30. Su. J., Q.M. Zhang, C.H. Kim, R.Y. Ting, and R. Capps, "Effect of Transitional Phenomena on the Electric Field Induced Strain–Electrostrictive Response of a Segmented Polyurethane Elastomer" (1997).
31. Su, J., Q.M. Zhang, and R.Y. Ting, "Space-Charge-Enhanced Electromechanical Response in Thin-Film Polyurethane Elastomers," Appl. Phys. Lett **71** (3), 386-388 (1997).

VOLUME III

32, Su, J., Q.M. Zhang, P.-C. Wang, A.G. MacDiarmid, K.J. Wynne, "Preparation and Characterization of an Electrostrictive Polyurethane Elastomer with Conductive Polymer Electrodes," Polymers for Adv. Tech. (1998).
33. Zhang, Q.M., V. Bharti, and X. Zhao, "Giant Electrostriction and Relaxor Ferroelectric Behavior in Electron Irradiated Poly(vinylidene Fluoride-Trifluoroethylene) Copolymer," Science (1998).

3.0 TRANSDUCER STUDIES

3.1 Cymbal : Moonie : BB Composites

34. Newnham, R.E., "Composite Sensors and Actuators" (1997).
35. Steele, B.CH., R.E. Newnham, and A.G. Evans, "Ceramics, Composites, and Intergrowth," Current Opinion in Solid State & Materials Science **2**, 563-565 (1997).
36. Tressler, J.F. S. Alkoy, and R.E. Newnham, "Piezoelectric Sensors and Sensor Materials" (1997).
37. Tressler, J.F., S. Alko, A. Dogan, and R.E. Newnham, "Functional Composites for Sensors, Actuators, and Transducers" (1997).
38. Dogan, A., K. Uchino, R.E. Newnham, "Composite Piezoelectric Transducer with Truncated Conical Endcaps 'Cymbal'," IEEE Transactions on Ultrasonics, Ferroelectrics, and Frequency Control **44** (3), 597-605 (1997).
39. Dogan, A., J.F. Fernandez, K. Uchino, and R.E. Newnham, "The 'Cymbal' Electromechanical Actuator" (1997).
40. Tressler, J.F., W. Cao, K. Uchino, and R.E. Newnham, "Ceramic-Metal Composite Transducers for Underwater Acoustic Applications" (1997).
41. Tressler, J.F. and R.E. Newnham, "Doubly Resonant Cymbal-Type Transducers," IEEE Transactions on Ultrasonics, Ferroelectrics, and Frequency Control **44** (5), 1175-1177 (1997).
42. Tressler, J.F., W. Cao, K. Uchino, and R.E. Newnham, "Finite Element Analysis of The Cymbal-Type Transducer" (1997).
43. Tressler, J.F., W.J. Hughes, W. Cao, K. Uchino, and R.E. Newnham, "Capped Ceramic Underwater Sound Projector" (1997).

Transducer Studies–continued

VOLUME IV

44. Alkoy, S., P.D. Lopath, R.E. Newnham, A.-C. Hladky-Hennion, and J.K. Cochran, "Focused Spherical Transducers for Ultrasonic Imaging" (1997).
45. Alkoy, S., A. Dogan, A.-C. Hladky, P. Langlet, J.K. Cochran, and R.E. Newnham, "Miniature Piezoelectric Hollow Sphere Transducers (BBs)" (1997).
46. Zipparo, M.J., K.K. Shung, and T.R. Shrout, "Piezoceramics for High-Frequency (20 to 100 MHz) Single-Element Imaging Transducers," IEEE Transactions on Ultrasonics, Ferroelectrics, and Frequency Control **44** (5), 1038-1048 (1997).

3.2 Frequency Agile Transducers

47. Davis, C. and G.A. Lesieutre, "An Actively-Tuned Solid State Piezoelectric Vibration Absorber" (1997).
48. Davis, C.L., G.A. Lesieutre, and J. Dosch, "A Tunable Electrically Shunted Piezoceramic Vibration Absorber" (1997).
49. Lesieutre, G.A. and U. Lee, "A Finite Element for Beams Having Segmented Active Constrained Layers with Frequency-Dependent Viscoelastic Material Properties" (1997).
50. Hebert, C.A. and G.A. Lesieutre, "Rotocraft Blade Lag Damping Using Highly Distributed Tuned Vibration Absorbers," American Institute of Aeronautics and Astronautics (AIAA 98-2001).
51. Lesieutre, G.A. and C.L. Davis, "Can a Coupling Coefficient of a Piezoelectric Device be Higher than Those of its Active Material?," SPIE 4th Annual Symposium on Smart Structures and Materials, San Diego, CA (March 1997).

3.3 3-D Acoustic Intensity Probes

52. Lauchle, G.C., J.R. MacGillivray, and D.C. Swanson, "Active Control of Axial-flow Fan Noise," J. Acoust. Soc. Am 101 (1), 341-349 (1997).
53. McGuinn, R.S., G.C. Lauchle, and D.C. Swanson, "Low Flow-Noise Microphone for Active Noise Control Applications," AIAA Journal **35** (1), 29-34 (1997).
54. McGuinn, R.S., G.C. Lauchle, and D.C. Swanson, "Low Flow-Noise Pressure Measurements Using a "Hot-Mic," AIAA -97-1665-CP.
55. Capone, D.E., and G.C. Lauchle, "Designing a Virtual Sound-Level Meter in LabVIEW," Education/Acoustics, LabVIEW, National Instruments.

VOLUME V

4.0 ACTUATOR STUDIES

4.1 Materials : Designs : Reliability

56. Uchino, K., "Piezoelectric Actuators" (1997).
57. Uchino, K., "Overview: Materials Issues in Design and Performance of Piezoelectric Actuators," SPIE Mtg. (1997).
58. Uchino, K., "Shape Memory Ceramics," Chapter 8 (1997).

Actuator Studies–continued

59. Aburatani, H., S. Yoshikawa, K. Uchino, and J.W.C. deVries, "A Study of Acoustic Emission in Piezoelectric Multilayer Ceramic Actuator," Jpn. J. Appl. Phys. **37**, 204-209 (1998).
60. Aburatani, H. and K. Uchino, "Acoustic Emission (AE) Measurement in Piezoelectric Ceramics" (1997).
61. Aburatani, H. and K. Uchino, "The Application of Acoustic Emission (AE) Method for Ferroelectric Devices and Materials," 8th US-Japan Seminar (1997).
62. Uchino, K., "Reliability of Ceramic Actuators" (1997).

4.2 Photostrictive Actuators

63. Tonooka, K. P. Poosanaas, and K. Uchino, "Mechanism of the Bulk Photovoltaic Effect in Ferroelectrics," Proceedings of the 5th SPIE Mtg., San Diego, CA (1998).
64. Poosanass, P. A. Dogan, S. Thakoor, and K. Uchino, "Dependence of Photostriction on Sample Thickness and Surface Roughness for PLZT Ceramics," Proceedings of the 1997 IEEE Ultrasonics Symposium, Toronto, Ontario, Canada (October 1997).
65. Poosanaas, P. A. Dogan, A.V. Prasadarao, S. Komarneni, and K. Uchino, "Photostriction of Sol-Gel Processed PLZT Ceramics," J. Electroceramics **1** (1), 105-111 (1997).

VOLUME VI

66. Poosanaas, P., A. Dogan, A.V. Prasadarao, S. Komarneni, and K. Uchino, "Effect of Ceramic Processing Methods on Photostrictive Ceramics," J. Adv. Perf. Mat. (1997).
67. Thakoor, S., P. Poosanaas, J.M. Morookian, A. Yavrovian, L. Lowry, N. Marzwell, J. Nelson, R.R. Neurgaonkar, and K. Uchino, "Optical Microactuation in Piezoceramics" (1997).

4.3 New Torsional Amplifier/Actuators

68. Glazounov, A.E., Q.M. Zhang, and C. Kim, "Piezoelectric Actuator Generating Torsional Displacement from Piezoelectric d_{15} Shear Response," Appl Phys. Lett. (1997).
69. Glazounov, A.E., Q.M. Zhang, and C. Kim, "A New Torsional Actuator Based on Shear Piezoelectric Response," Proceedings of SPIE Smart Materials, San Diego, CA (March 1998).

4.4 High Force Amplifiers and Inchworms

70. Uchino, K., J. Zheng, A. Joshi, S. Yoshikawa, S. Hirose, S. Takahashi, and J.W.C. deVries, "High Power Characterization of Piezoelectric Materials" (1997).
71. Uchino, K., "High Electromechanical Coupling Piezoelectrics - How High Energy Conversion Rate is Possible," Mat. Res. Soc. Symp. Proc. **459**, 3-14 (1997).
72. Park, S.-E., V. Vedula, M.-J. Pan, W.S. Hackenberger, P. Pertsch, and T.R. Shrout, "Relaxor Based Ferroelectric Single Crystals for Electromechanical Actuators," Proceedings of the SPIE's 5th International Symposium on Smart Structures and Materials, San Diego, CA (March 1998).

Actuator Studies–continued

73. Koopmann, G.H. G.A. Lesieutre, B.R. Dershem, W. Chen, and S. Yoshikawa, "Embeddable Induced Strain Actuators Using Framed 3-3 Piezoceramic Stacks: Modeling and Characterization," Proceedings of the SPIE's 4th Annual International Symposium on Smart Structures and Materials, San Diego, CA (March 1997).
74. Driesch, P.L., G.H. Koopmann, J. Dosch, and H. Iwata, "Development of a Surface Intensity Probe for Active Control Applications," IMECE, Dallas, Texas (November 1997).
75. Galante, T., J. Frank, J. Bernard, W. Chen, G.A. Lesieutre, and G.H. Koopmann, "Design, Modeling, and Performance of a High Force Piezoelectric Inchworm Motor" (1997).
76. Galante, T.P., "Design and Fabrication of a High Authority Linear Piezoceramic Actuator: The PSU H3 Inchworm," Master of Science Thesis, The Pennsylvania State University (August 1997).
77. Lesyna, M.W., "Shape Optimization of a Mechanical Amplifier for Use in a Piezoceramic Actuator," Master of Science Thesis, The Pennsylvania State University (May 1998).

VOLUME VII

78, Uchino, K., "Piezoelectric Ultrasonic Motors: Overview," J. Smart Materials and Structures–Special Issue (1997).
79. Uchino, K., "Compact Piezoelectric Ultrasonic Motors," J. Medical Ultrasonics 24 (9), 1191-92 (1997).

5.0 MODELING and CHARACTERIZATION

5.1 Finite Element Methods

80. Qi, W. and W. Cao, "Finite Element Analysis and Experimental Studies on the Thickness Resonance of Piezocomposite Transducer," Ultrasonic Imaging **18**, 1-9 (1996).
81. Qi, W. and W. Cao, "Finite Element Study on Random Design of 2-2 Composite Transducer," SPIE **3037**, 176-180 (1997).
82. Geng, X. and Q.M. Zhang, "Evaluation of Piezocomposites of Ultrasonic Transducer Applications–Influence of the Unit Cell Dimensions and the Properties of Constituents on the Performance of 2-2 Piezocomposites," IEEE Transactions on Ultrasonics, Ferroelectrics, and Frequency Control **44** (4), 857-872 (1997).
83. Zhang, Q. and X. Geng, "Acoustic Properties of the Interface of a Uniform Medium-2-2 Piezocomposite and the Field Distributions in the Composite," Jpn. J. Appl. Phys. **36**, 6853-6861 (1997).
84. Geng, X. and Q.M. Zhang, "Analysis of the Resonance Modes and Losses in 1-3 Composites for Ultrasonic Transducer Applications," IEEE UFFC (1997).

APPENDIX 32

Polymers for Adv. Techn. (in press 1998).

Preperation and Characterization of an Electrostrictive Polyurethane Elastomer with Conductive Polymer Electrodes

J. Su and Q. M. Zhang,
Materials Research Laboratory,
The Pennsylvania State University, University Park, PA 16802, USA

P-C Wang and A. G. MacDiarmid
Department of Chemistry, University of Pennsylvannia
Philadelphia, PA 19104-6323

K. J. Wynne
Office of Naval Research, 331
Physical Science, Arlington, VA 22217

Preperation and Characterization of an Electrostrictive Polyurethane Elastomer with Conductive Polymer Electrodes

ABSTRACT

All-polymer electrostrictive soft films were firstly developed by depositing conductive polymer (polypyrrole) directly on both sides of solution cast electrostrictive polyurethane elastomer films. The final films are flexible with strong adhesion between the polyurethane film and the conductive polymer electrode. The conductivity of the polymer electrode is desirably good (the surface resistance is ~1000 Ω/□). The compatible interface between the electrode polymer and the electrostrictive polyurethane make acoustic and optical transparency of the all-polymer films significantly improved when compared with that of the metal electroded films. The all-polymer films exhibit also comparable dielectric properties with the gold electroded polyurethane films in the temperature range from -40°C to +80°C. The temperature range covers the soft segment related glass transition temperature of the polyurethane elastome, which is about -20°C. The films also show large electric field induced strain responses which are dependent on film thickness and measurement frequency. The electrostrictive characteristics in the all-polymer films show similarities to those of the films with gold electrodes under the identical measurement conditions.

Key words: Polypurrole conductive polymer, electrostrictive, polyurethane, dielectric properties, and all-polymer films.

INTRODUCTION

The recent studies on electromechanical properties of polymers showed that some thermoplastic polymer elastomers, especially segmented polyurethane elastomers, can exhibit very high electric field induced strain responses.[1] As promising materials for applications in transducer, sensor and actuator technologies,[2] these electromechanically active polyurethane elastomers have drawn more and more attentions of researchers and many experimental investigations have been conducted since the large electric field induced strain of this class polyurethane elastomers was reported.[3-8] However, increased interests in using electroactive polymeric materials for electro-acoustic and electromechanical applications also raise the issue of new electrode materials to meet requirments such as high optical and acoustic transparency, very small acoustic mismatching and reduced mechanical clamping effect. In the work reported here, an all-polymer electrostrictive system was firstly developed. In this system, a soft conductive polymer, polypyrrole, was directly deposited onto opposing surfaces of solution cast polyurethane films by an absorption polymerization method as electrodes replacing conventionally used metal electrodes, such as Al, Ag and Au etc.. The formed all-polymer polypyrrole/polyurethane/polypyrrole sandwich structure is flexable, and exhibit strong coherent interfaces, significantly improved acoustic and optical transparency[9,10] which are promising for improving the performance of electromechanical polymer materials in acoustic and optical applications. As our present interests, the dielectric and electric field induced strain properties of the films were characterized. The temperature dependence of the dielectric properties shows that the conductive polymer electrode is properly

functional, and the thickness and frequency dependence of the electric field induced strain responses in the all-polymer films show the characteristics similar to those of the films with gold electrodes under identical experimental conditions.

EXPERIMENTAL

Sample Preparation

Polyurethane films of various thicknesses were produced by a solution casting method followed by a 100°C annealing for 30 minutes. Thereafter, conductive polymer (polypyrrole) electrodes were deposited on opposing surfaces of the films by an in-situ deposition technique.[11,12] In the procedure, freshly distilled pyrrole were dissolved in distilled water. The pyrrole solution was then poured into another aqueous solution containing proper amounts of ferric chloride hexahydrate ($FeCl_3.6H_2O$) and doping agents to form a polymerizing solution. The prepared polyurethane films fixed on metal frames were immersed into the polymerizing solution and allowed to undergo the in-situ deposition of conductive polypyrrole onto both surfaces of the polyurethane films under ambient laboratory conditions. In order to obtain polypyrrole electrodes with desirable quality and thickness, the polyurethane films were removed from the polymerizing solution and rinsed with distilled water for ~10 seconds for several times during the deposition process. The resultant polypyrrole electrodes were smooth and coherent to the polyurethane films. The final thickness of the electrodes was about 300 Å. The surface electric resistivity measured using the AATCC test method 76-1987 was about 1000 Ω/□.

The procesing procedure and the schematic diagram of the polyurethane film with the conductive polymer electrode are shown in figures 1a, 1b and 1c.

Dielectric and Electric Field Induced Strain Measurements

The dielectric proeprties of the polyurethane films with the conductive polymer electrodes were characterized and compared to those of the polyurethane films with gold electrode with the same thickness as the conductive polymer ones in the temperature range from -40°C to 80°C. The heating rate employed was 2 °C/min which was controlled by a LakeShore 321 Autotuning Temperature Controller.

The electric field induced strain coefficient, R, (the electric field induced strain $S = RE^2$, where E is the applied electric field) of the polyurethane films having conduvtive polymer electrodes was measured as a function of the film thickness and frequency at room temperature using a piezoelectric bimorph-based cantilever dilatometer set up combined with a lock-in amplifier (Stanford Research System-SR830 DSP) and a high voltage supplier (KEPCO-BOP 1000M). The details of the technique is to be published in a separate paper.[13] The thickness and frequency dependence of the strain coefficient of the polymer electroded polyurethane films were compared with those of the films with gold electrodes.

RESULTS AND DISCUSSIONS

Temperarue dependence of the dielectric constant and loss of the polyurethane with conductive polymer electrodes are shown in figure 2, which are compared with the those of the films with gold electrodes. As can be seen, the two films show very similar

characteristics in the temperature range from -40°C to +35°C. The temperarue range investigated covers the soft segment related glass transition of the polyurethane elastomer, which is about -20°C. In the transition process, the dielectric loss of the polyurethane films with conductive polymer electrodes does not show significant difference when compared with that of the films with gold electrodes. These indicate that the conducitve polymer electrodes are properly functional and the direct deposition process did not change dielectric properties of the solution cast polyurethane films for the present research interests. However, when the temperature is higher than 35°C, the dielectric loss of the polyurethane films with conductive polymer electrodes starts increasing and becomes significantly higher than that of the films with gold electrode. The markedly increase in the dielectric loss might be a consequence of the dehydration phenomena in the conductive polypyrrle, which has been suggested by several researchers and should occur in the temperature range from 60 to 100 °C. [14-17]

Figure 3 shows the comparison of the electric field induced strain coefficient, R, of the polyurethane films, with conductive polymer electrodes and with gold electrodes. It can observed that 1) the stran coefficient, R, for both polymer electroded and gold electroded films, is increased when the sample thickness is decreased from 0.2 mm to 0.1 mm; 2) the strain coefficient, R, for both polymer electroded and gold electroded films show frequency dependence, increasing with the decrease in the measurement frequency; and 3) the polymer electroded films show higher R than the gold electroded ones at frequency higher than 10 Hz while the gold electroded films show more rapid increase in R than the polymer electroded ones with the decrease of frequency and the strain

coefficient, R, of the gold electroded films becomes higher than that of the polymer electroded ones when the frequency is lower than 10 Hz. As reported previously,[8] for the gold electroded films, the higher strain coefficient, R, in 0.1 mm films than that in 0.2 mm films and the rapid increase in the coefficient with decrease of frequency manifest the existence of interfacial charge and space charge distribution effects. For the polymer electroded films, as can be seen in the comparison, charge effects are still significant even though not as strong as those in the gold electroded films, or the increase of the strain coefficient with the decrease in frequency is not as rapid as that in the gold electroded films. The higher strain coefficient in the polymer electroded films in the higher frequency region might be considered as reflections of the less interfacial charge related enhancing effects and less mechanical restraint of electrodes [1] in the polymer electroded films than in the gold electroded films.

Figure 4a shows the thickness dependence of the strain coefficient, R, of the polymer electroded polyurethane films at different measurement frequencies: 2 Hz, 10 Hz, 100 Hz, and 1kHz. As can be observed, with the decrease of the sample thickness, the strain coefficient increases first and then starts to decrease at about 0.1 mm. Therefore, a maximum R is obtained and the lower the frequency is, the higher the strain coefficient is. When these results are compared with those obtained in studies on the gold electroded films, which are shown in figure 4b, the similarities in the electric field induced strain responses can be clearly noted. However, the gold eletroded films exhibit stronger frequency dependence than those which were polymer electroded. This can also be considered as an indication that the interfacial effects in the gold eletroded films is more

important than in the polymer electroded films, since the interfacial effects are strongly frequency dependent, especially at lower frequency. The mechanisms of the effects of interfacial/space charges on the electric field induced strain coefficient have been discussed in a previous publication as a new mechanism for generating enhanced electric field induced strain in electrostrictive materials.[8] According to the Poisson's relationship: $dE/dx = \rho(x)/\varepsilon$ (where E is the electric field, the $\rho(x)$ is the charge density at the position x along the thickness direction, and ε is the dielectric constant),[18] a non-uniform interfacial/space charge distribution can result in an enhanced local electric field profile along the thickness.[19-22] The depth of the enhanced field profile depnds on the transportability of charges. Therefore, the fraction of the enhanced field region will increase with a decrease of the sample thickness until a critical thickness is reached. The critical thickness is the thickness at which the neutralization and/or homogenization of the space charges might occur. The neutralization and/or homogenization will result in weakening of the non-uniformaty of the modified internal field. As a consequency, the enhanced electric field induced strain responses, which depends on the non-uniform filed profile, will start to decrease as observed in the figures 4a and 4b.

CONCLUSIONS

All-polymer electrostrictive soft films were developed by depositing conductive polymer (polypyrrole) directly onto solution cast electrostrictive polyurethane elestomer films. The films show ciherent polyurethane -polymer electrode interface and improved acoustic and optical transparency. The conductivity of the polymer electrodes is desirably

functional (the surface resistance is ~1000 Ω/□). The films exhibit comparable dielectric properties which are very similar to those of the polyurethane films with gold electrodes in the temperature range investigated. The large electric field induced strain responses and the characteristics of the thickness and frequency dependence in the all-polymer films are also found to be similar to those of the films with gold electrodes under same measurement conditions. The experimental results indicate the existence of interfacial charge effects in the all-polymer electrostrictive films. However, the effects are not as large as those in the gold electroded films.

ACKNOWLEDGMENT

This work was supported by the Office of Naval Research through grant No. N00014-96-1-0418.

REFERENCES

1. M. Zhenyi, J. I. Scheinbeim, J. W. Lee, and B. A. Newman, *J. Polym. Sci. Part B: Polym. Physi.*, **32**, 2721 (1994).
2. J. M. Herbert, "Ferroelectric Transducers and Sensors", Gordon and Breach Science Publishers, New York, 1982.
3. H. Wang, Q. M. Zhang, L. E. Cross, R. Ting, C. Coughlin, and K. Ritternmyer, *Proc. Int. Symp. Appl. Ferro.*, **9**, 182 (1994).
4. H. Wang, *Ph. D. Thesis*, The Pennsylvania State University, 1994.
5. J. Su, Q. M. Zhang, C.H. Kim, and R. Ting, in press, *J. Appl. Polym. Sci.*, (1997).
6. J. Su, C. H. Kim, Q. M. Zhang, V. Kugel, R. Ting, and R. Capps, in press, *Proc. Int. Symp. Appl. Ferro.* **10**, (1996).
7. Q. M. Zhang, J. Su, C. H. Kim, and R. Ting, *J. Appl. Phys.*, **81**, 2770 (1997).
8. J. Su, Q. M. Zhang, and R. Ting, accepted by *Appl. Phys. Lett.* for publication (1997).
9. T. Ueno, H. Arntz, S. Flesch and J. Bargon, *J. Macromol. Sci.*, **A25**(12), 1557 (1988).
10. Y. Tezuka, K. Aoki and K. Shinozaki, *Synthetic Metals*, **30**, 369 (1989).
11. R. V. Gregory, W. C. Kimbrell and H. H. Kuhn, *Synthtic Metals*. **28**, C823 (1989).
12. S. K. Manohar, A. G. MacDiarmid and A. J. Epstein, *Bull. Am. Phys. Soc.*, **34**, 3 (1989).
13. J. Su, P. Moses, and Q. M. Zhang, submitted to *Rev. Sci. Instruments* (1997).
14. B. C. Ennis and V. T. Truong, *Synthetic Metals*, **59**, 387 (1993).

15. M. Biswas and A. Roy, *J. Appl. Polym. Sci.*, **51**, 1575 (1994).

16. M. Biswas and A. Roy, *J. Appl. Polym. Sci.*, **60**, 143 (1996).

17. V. T. Truong, B. C. Ennis and M. Forsyth, *Polymer*, **36**, 1933 (1995).

18. G. M. Sessler, "Electrets", Topics in Appl. Phys., Vol. 33, Springer-Verlag, Berlin, (1980).

19. Y. Li, T. Gao, J. Liu, K. Liu, C. R. Desper, and Benjamin Chu, *Macromolecules*, **25**, 7365 (1992).

20. Y. Li, T. Takada, H. Miyata, and T. Niwa, J. Appl. Phys., **74**, 2725 (1993).

21. K. S. Suh, J. Y. Kim, C. R. Lee, and T. Takada, *IEEE Trans. Dielec. Electr. Insul.*, **3**, 201 (1996).

22. T. Takada, K. Soda, and K. Gotoh, *Jap. J. Appl. Phys.*, **29**, 1198 (1990).

FIGURE CAPTIONS

Figure 1 Schematic diagrams of the procedure of direct deposition of conductive polymer (polypyrrole) onto the surfaces of the solution cast electrostrictive polyurethane elastomer films. a) solution casting of polyurethane film, b) direct deposition of conductive polymer, and c) the polyurethane films with conductive polypyrrole on opposing surfaces.

Figure 2 Comparison of the dielectric constant and dielectric loss of conductive polymer electroded and gold electroded solution cast polyurethane films as a function of temperature, at 100 Hz.

Figure 3 Comparison of the electric field induced strain coefficient, R, of the conductive polymer electroded and gold electroded solution cast polyurethane films with the thickness of 0.1 mm and 0.2 mm, respectively, as a function of frequency. The solid lines were drawn to guide the eye.

Figure 4 Thickness dependence of the electric field induced strain coefficient, R, of a) the conductive polymer electroded polyurethane films and b) the gold electroded polyurethane films at various frequencies. The solid lines were drawn to guide the eye.

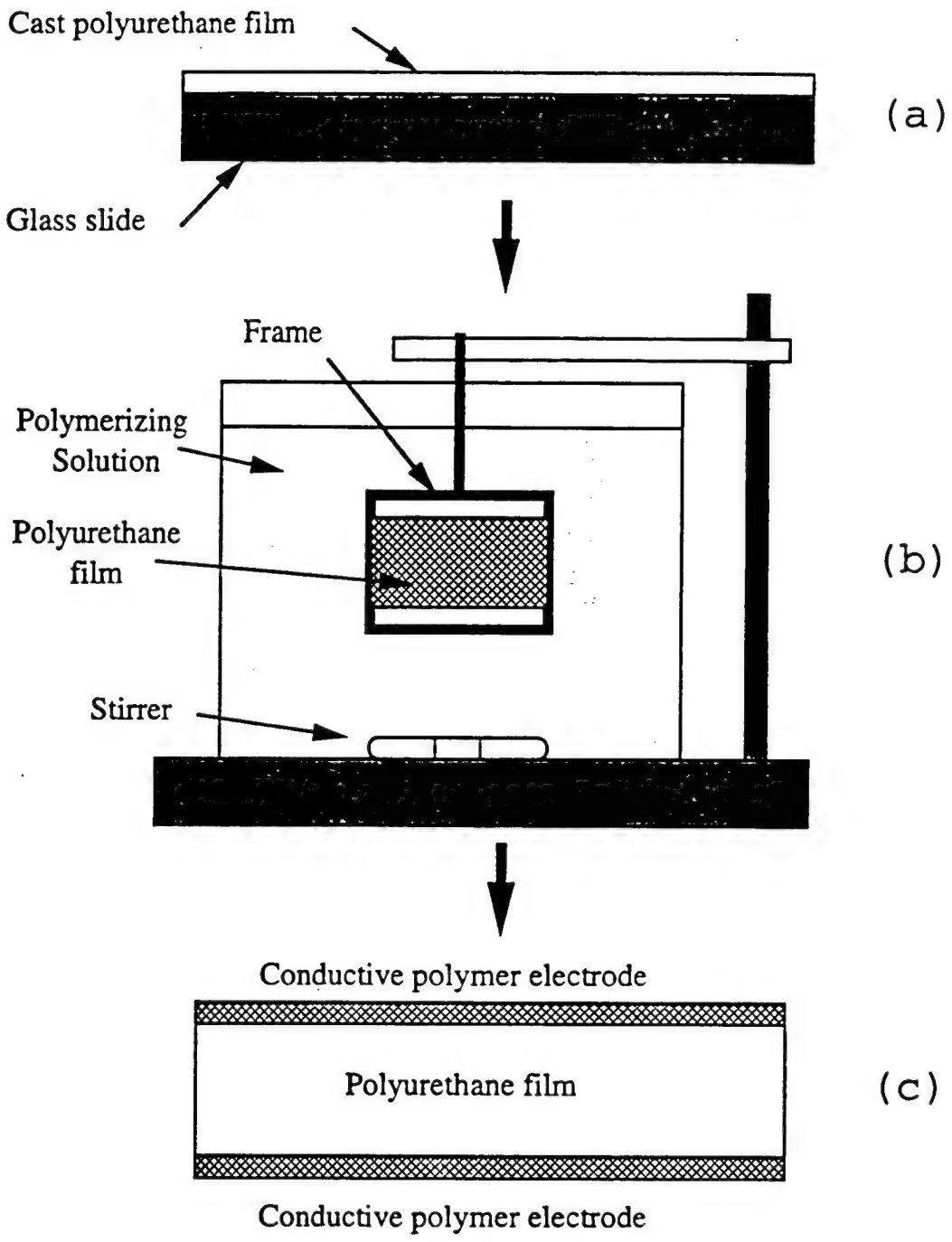
Cast polyurethane film
Glass slide
(a)
Frame
Polymerizing Solution
Polyurethane film
(b)
Stirrer
Conductive polymer electrode
Polyurethane film
(c)
Conductive polymer electrode

Fig. 1

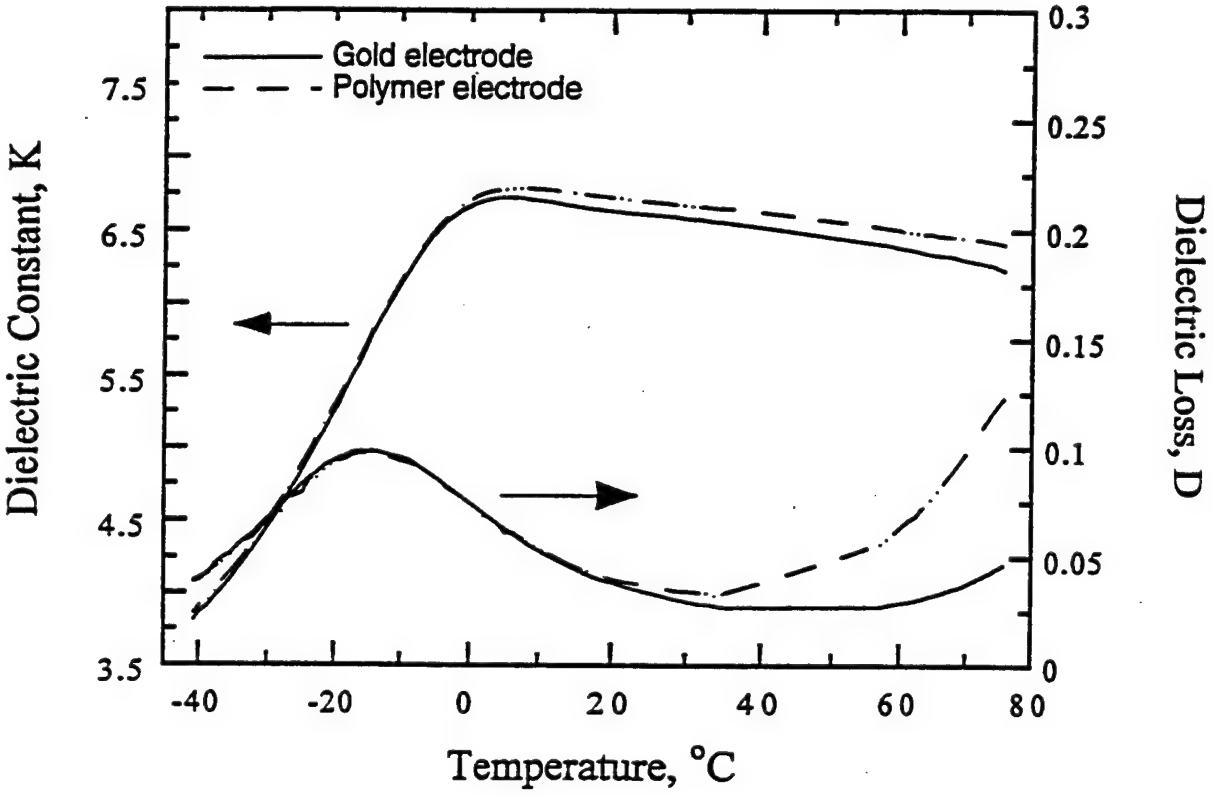
Gold electrode
Polymer electrode
Dielectric Constant, K
Dielectric Loss, D
Temperature, °C
7.5
6.5
5.5
4.5
3.5
0.3
0.25
0.2
0.15
0.1
0.05
0
-40
-20
0
20
40
60
80

Fig. 2

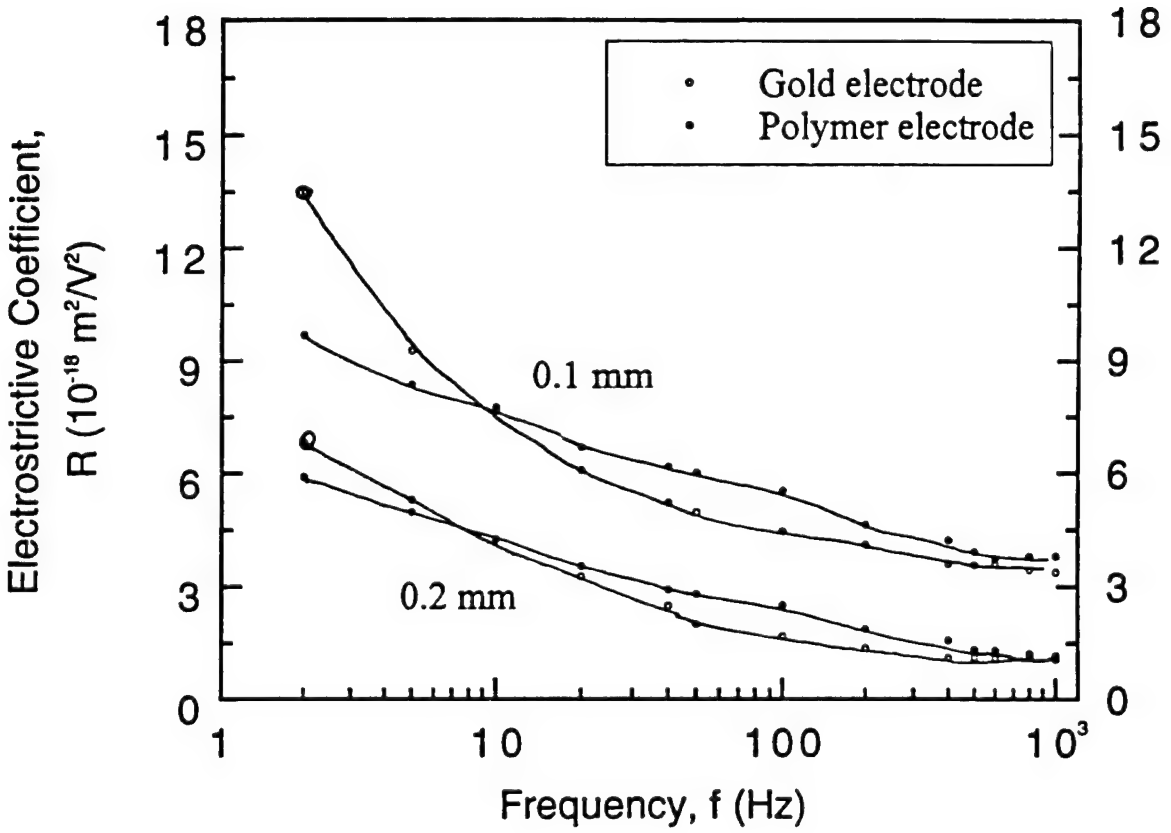
Gold electrode
Polymer electrode
0.1 mm
0.2 mm
Electrostrictive Coefficient,
R (10⁻¹⁸ m²/V²)
Frequency, f (Hz)
0
3
6
9
12
15
18
1
10
100
10³

Fig. 3

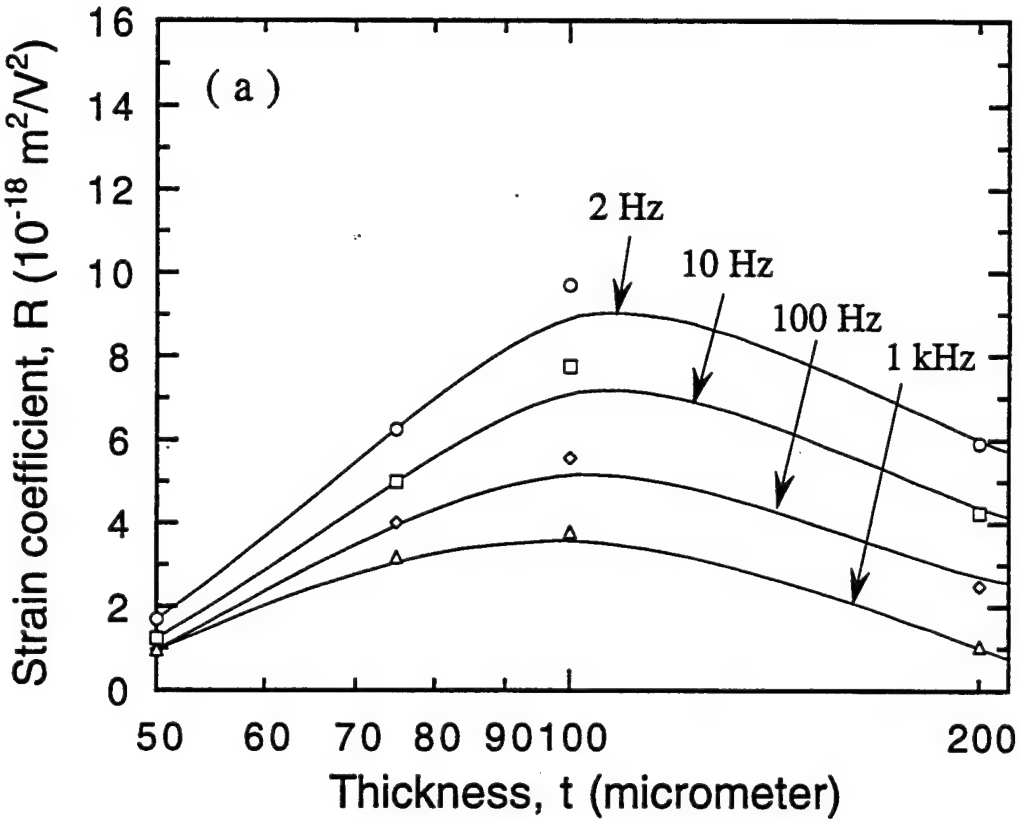
(a)
2 Hz
10 Hz
100 Hz
1 kHz
Strain coefficient, R (10^{-18} m^2/V^2)
Thickness, t (micrometer)
0
2
4
6
8
10
12
14
16
50
60
70
80
90
100
200

Fig. 4a

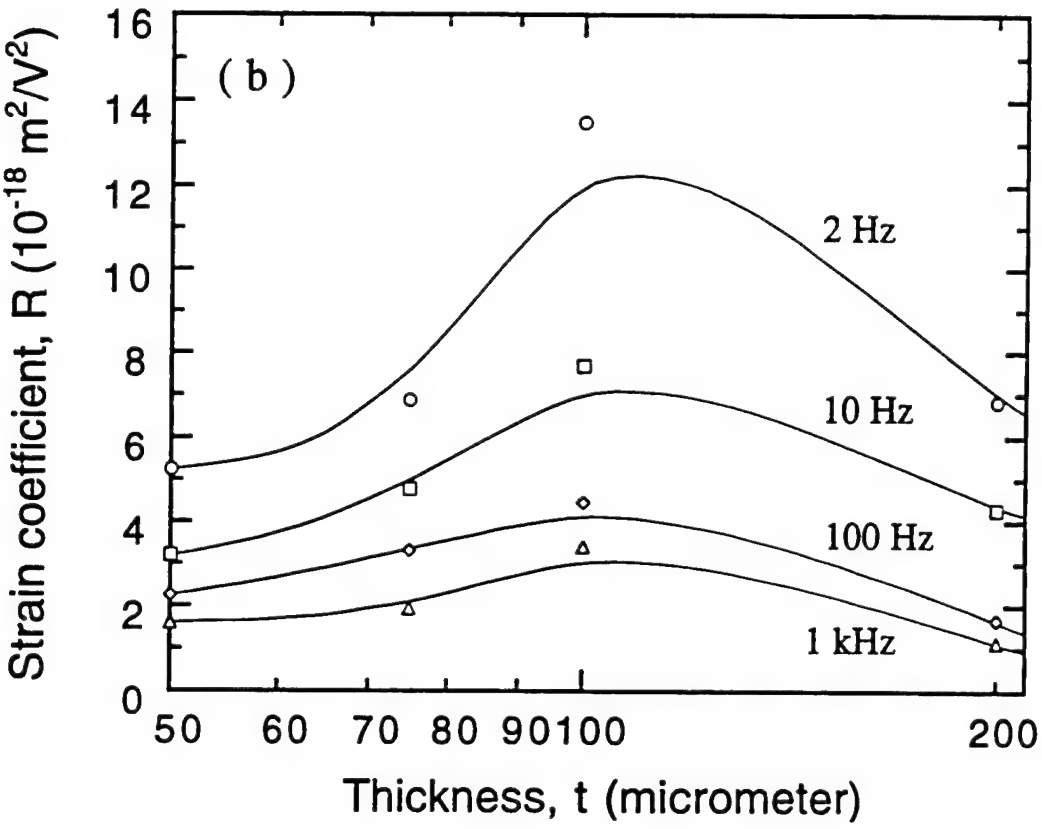
(b)
Strain coefficient, R (10^{-18} m^2/V^2)
16
14
12
10
8
6
4
2
0
2 Hz
10 Hz
100 Hz
1 kHz
50
60
70
80
90
100
200
Thickness, t (micrometer)

Fig. 4b

APPENDIX 33

Science (submitted 1997).

Giant Electrostriction and Relaxor Ferroelectric Behavior in Electron Irradiated Poly(vinylidene Fluoride-Trifluoroethylene) Copolymer

Q. M. Zhang, Vivek Bharti, and X. Zhao

Materials Research Laboratory and Department of Electrical Engineering

The Pennsylvania State University, University Park, PA 16802

Abstract:

An exceptionally high electrostrictive response has been observed in electron irradiated poly(vinylidene fluoride-trifluoroethylene) (P(VDF-TrFE)) copolymer. Moreover, experimental results show that the material exhibit typical relaxor ferroelectric behavior, which is the first relaxor ferroelectric polymer reported. These results suggest that the electron irradiation breaks up the coherent polarization domain in normal ferroelectric P(VDF-TrFE) copolymer into nano-polar regions which transforms the material into a relaxor ferroelectric with an ultrahigh electrostrictive response.

Materials which generate large mechanical actuation induced by external stimuli including electric field, temperature, and stress have attracted a great deal of attention in recent years. The development of smart materials and structures challenges the materials community to develop new materials with high strain levels, low hysteresis, fast response and high strain energy density. Although there are several active materials currently available, there are few that come meeting close to those requirements. For instance, piezoceramic and magnetostrictive materials, while possessing low hysteresis and fast response, suffer from low strain levels.[1,2] On the other hand, shape memory alloys generate high strain but are often associated with large hysteresis and very slow response.[3] In this paper, we report the discovery of an exceptionally high electric field induced strain with low hysteresis (electrostrictive) response from electron irradiated P(VDF-TrFE) copolymers. Furthermore, we present herein experimental evidence showing that in many respects, the material behaves like a ferroelectric relaxor, a class of materials under intensive investigation due to many peculiar features and their broad applications in actuators and transducers, capacitors, and electro-optical devices.[4,5]

Poly(vinylidene fluoride) (PVDF) and its copolymer P(VDF-TrFE) are semicrystaliine polymers and by proper sample treatments a ferroelectric phase (β-phase) can be induced in the crystalline region.[6,7] In compositions of P(VDF-TrFE) copolymers which exhibit a ferroelectric-paraelectric (F-P) transition, large lattice strains and sample dimensional changes have been observed in x-ray diffraction experiments and in thermal expansion experiments.[7-9] Such a large strain associated with the F-P transition is attractive for many electromechanical applications. One drawback associated with this large strain associated with the transition is the large hysteresis as observed in many experiments.[7,9] In this paper, we will show that by high energy electron irradiation, this large hysteresis can be eliminated and an exceptionally large electric field induced strain can be achieved.

The composition chosen for this study was P(VDF-TrFE) 50/50 which has a relatively low F-P transition temperature (70 °C). The copolymer was from Solvay & Cie of Bruxelles. The film used in this investigation was fabricated by hot pressing powder at 225 °C and then slowly

cooled down to room temperature. The film thickness was between 25 μm and 40 μm. The irradiation treatment was carried out in a nitrogen atmosphere with 3 MeV electrons and the dosage was in the range between 40 Mrad and 100 Mrad. Several temperatures were chosen for the irradiation. The results reported in this paper were obtained from films irradiated at 120 °C with 40 Mrad dosage. For the electric measurement, gold electrodes sputtered onto the film surfaces were used.

In this investigation, the electric field induced strain was characterized by a bimorph based strain sensor designed specifically for the polymer film strain measurement.[10] The polarization hysteresis loop was measured by a Sawyer-Tower circuit.[11] The frequency range for the polarization and strain measurement is from 1 to 10 Hz. The dielectric constant was evaluated by a HP multi-frequency LCR meter equipped with a temperature chamber. The elastic compliance was measured by a Dynamic Mechanical Analyzer in the frequency range from 1 to 200 Hz.[12]

Presented in figure 1A is the polarization hysteresis loop for P(VDF-TrFE) 50/50 film measured at room temperature before the electron irradiation. As expected, the material exhibits a well defined ferroelectric polarization loop with a coreceive field at 45 MV/m and a remanent polarization of 6.4 $\mu C/cm^2$. In contrast, the sample irradiated with 40 Mrad dosage at 120 °C exhibits a slim hysteresis loop and the polarization level of the sample is also reduced (figure 1B). A similar result was also obtained for samples irradiated at room temperature with 80 Mrad electron dosage. The result here is consistent with the early finding by Lovinger that electron irradiation of P(VDF-TrFE) can destroy the ferroelectricity in the material.[13]

Most interestingly, the films after the irradiation show a high strain response as shown in figure 2A. The strain under a field of 150 MV/m, which is the limit of the current experiment apparatus, can reach more than 4% and apparently the strain has not reached saturation at that field level. In addition, the strain response exhibits little hysteresis and follows an approximately electrostrictive relationship between the strain S and polarization P, $S= Q P^2$, where the proportional coefficient Q is the charge related longitudinal electrostrictive coefficient.[14] As

shown in figure 2B, the plot of S vs. P^2 is nearly a straight line, yielding the electrostrictive coefficient Q= -13.5 m^4/C^2.

Clearly, materials with such high electrostrictive strain are attractive for actuator, sensor, and transducer applications. However, in very soft polymers the Maxwell stress effect, originating from the Coulomb force of the charges, can deform the material to a high strain level.[15,16] Hence, another parameter, the strain energy density, is also used to evaluate an actuator material, which is proportional to $YS_m^2/2\rho$, where Y is the elastic modulus, S_m is the strain level, and ρ is the density of the material, respectively.[17] In Table 1, we compare the newly discovered irradiated P(VDF-TrFE) copolymer with several currently known materials, including the ferroelectric relaxor single crystal PZN-PT, discovered recently in this Laboratory and shown to possess an ultrahigh strain response.[18,19] Apparently, the electrostrictive P(VDF-TrFE) copolymer reported here exhibits a significantly improved performance.

Because prior to the irradiation P(VDF-TrFE) copolymer is a ferroelectric, one interesting question is whether the material after the irradiation is a simple dielectric or a ferroelectric. In order to answer this question, the polarization hysteresis loop was measured at lower temperatures. As shown in figure 3, we observed a gradual appearance of the polarization hysteresis loop with reduced temperatures. That is, the remanent polarization P_r (the polarization level at E=0 in the hysteresis loop) and coercive field E_c (the field level at P=0 in the hysteresis loop) slowly increase with reduced temperature, a feature reminiscent of relaxor ferroelectric behavior which has been investigated extensively in the past 4 decades in inorganic materials.[4]

The dielectric constant of the irradiated film is presented in figure 4 and it can be seen that the material has a broad dielectric constant peak T_m around room temperature which is below the F-P transition temperature (about 70 ^oC) observed in non-irradiated samples. This is consistent with early investigation.[20] However, unlike the dielectric peak associated with the F-P transition, the data in figure 4 shows that T_m shifts progressively towards higher temperature with frequency, another feature common to all the relaxor ferroelectrics. In addition, as shown in the insert of figure, the dispersion of T_m with frequency f can be modeled quite well with the Vogel-Folcher

law, $f=f_0 \exp[\frac{-U}{k(T_m - T_f)}]$, a relationship observed in many glass systems, where k is the Bolzman constant and T_f is the freezing temperature.[21,22] Hence, the result suggests that the material may belong to a dipolar glass system. The fitting of the data yields f_0=9.6 MHz, U =6.4x10^{-3} eV, and the freezing temperature T_f= 307 K (=34 °C), which is the temperature where the relaxation time of the system approaches infinity.

Figure 5 presents a comparison of variation of P_r with temperature between the samples before and after the irradiation. The sample before the irradiation exhibits a sharp drop of P_r with temperature at a temperature near 70 C, the F-P transition temperature. On the other hand, the change of P_r with temperature for the irradiated sample is more gradual, typical of ferroelectric relaxors. In addition, the derivative of P_r of the irradiated sample with temperature exhibits two broad peaks, one near -23 °C and the other near 32 °C. The one at -23 °C is related to the glass transition in the amorphous phase, indicating an increase of the amorphous phase in the irradiated sample compared with non-irradiated sample.[23] The one near 32 °C coincides closely with the freezing temperature determined from the dielectric constant (T_f=34 °C), consistent with the fact that below the freezing temperature, a macroscopic ferroelectric state can be induced by external fields in a ferroelectric relaxor.[24]

By drawing the analogy with the relaxor systems in inorganic materials, the results presented here suggest that the electron irradiation breaks up the coherent polarization domains in the normal ferroelectric crystalline region into nano-polar regions, resulting in the observed ferroelectric relaxor behavior.[9] To our knowledge, this is the first ferroelectric relaxor behavior observed in a polymeric system. Due to the large difference in the lattice constant between the ferroelectric and non-ferroelectric phases in P(VDF-TrFE) copolymers,[7,23] the gradual increase of polarization with field in the relaxor P(VDF-TrFE) copolymer produces a giant electrostrictive strain with a high strain energy density.

Table 1. Comparison of the Strain and Strain Energy Density

Materials	Y(GPa)	Typical S_m	$YS_m^2/2\rho$ (J/kg)
Piezoceramic[1]	64	0.1%	4.25
Magnetostrictor[2]	100	0.2%	21.6
PZN-PT Single Crystal[18]	7.7	1.7%	131
P(VDF-TrFE) electrostrictor	0.38	4%	160

References:

1. L. E. Cross, Ceramic Trans. **68**, 15 (1996).
2. K. B. Hathaway and Arthur E. Clark, MRS Bulletin, **18**, 34 (1993).
3. S. M. Wayman, MRS Bulletin, **18**, 49 (1993).
4. L. E. Cross, Ferro. **76**, 241 (1987).
5. G. H. Haertling, Ferro. **75**, 25 (1987).
6. A. J. Lovinger, Science **220**, 1115 (1983).
7. T. Furukawa, Phase Transition, **18**, 143 (1989).
8. K. Tashiro, K. Takano, M. Kobayashi, Y. Chatani, and H. Tadokoro, Ferro, **57**, 297 (1984); T. Yamada, T. Ueda, and T. Kitayama, J. Appl. Phys. **52**, 948 (1981).
9. A. J. Lovinger, D. D. Davis, R. E. Cais, and J. M. Kometani, Polymer **28**, 617 (1987).
10. J. Su, P. Moses, and Q. M. Zhang, Submitted to Rev. Sci. Instruments (1997).
11. J. K. Sinha, J. Sci. Instrum. **42**, 696 (1965).
12. DMA 2980, TA Instruments, Inc., New Castle, DE 19720.
13. A. J. Lovinger, Macromolecules, **18**, 910 (1985).
14. V. Sundar and R. E. Newnham, Ferro. **135**, 431 (1992).
15. Q. M. Zhang, J. Su, C. Kim, R. Ting,and R. Capps, J. Appl. Phys. **81**, 2770 (1997).
16. R. Pelrine, R. D. Kornbluh, and J. P. Joseph, Sensors and Actuators **A64**, 77 (1998).
17. V. Giurgiutiu and C. Rogers, J. Intel. Mater. Syst. and Struct. **7**, 656 (1996).
18. Seung-Eek Park and T. Shrout, J. Appl. Phys. **82**, 1804 (1997).
19. R. F. Service, Science **275**, 1878 (1997).
20. B. Daudin, M. Dubus, and J. F. Legrand, J. Appl. Phys. **62**, 994 (1987).
21. H. Vogel, Z. Phys. **22**, 645 (1921); G. S. Fulcher, J. Am. Ceram. Soc. **8**, 339 (1925).
22. E. Courtens, Phys. Rev. Lett. **52**, 69 (1984).
23. K. Tashiro, in Ferroelectric Polymers, H. S. Nalwa Ed. (Marcel Dekker, Inc. New York 1995), p. 43 .
24. R. Sommer, N. Y. Yushin, and J. J. van der Klink, Phys. Rev. **B48**, 13230 (1993).

25. We wish to thank L. E. Cross, R. Y. Ting, J. Lindberg, G. Kavarnos, and F. Tito for stimulating discussions. This work was supported by ONR through Grant No. N00014-97-1-0900 and NSF through Grant No. ECS-9710459.

Figure captions:

Figure 1. The polarization hysteresis loops of P(VDF-TrFE) 50/50 copolymer measured at room temperature. (a) Before irradiation; (b) After irradiation with 40 Mrad dosage at 120 °C.

Figure 2. (a) The strain-field dependence of P(VDF-TrFE) 50/50 copolymer after irradiation with 40 Mrad dosage at 120 °C. (b) The electrostrictive relation between the strain and polarization, where the strains at $P>0$ and $P<0$ regions are overlaped due to P^2 dependence of the strain. The deviation of the data from a straight line at S near zero is due to the zero point uncertainty of the measuring set-up.

Figure 3. The polarization hysteresis loops measured at lower temperatures which show the gradual increase of the remanent polarization and hysteresis.

Figure 4. The dielectric constant (solid lines) and dielectric loss (dashed lines) as a function of temperature for P(VDF-TrFE) 50/50 copolymer after irradiation with 40 Mrad dosage at 120 °C. The frequency is (from top to bottom curves for the solid lines and from bottom to top curves for the dashed lines): 100 Hz, 1 kHz, 10 kHz, 100 kHz, 300 kHz, 600 kHz, and 1 MHz. The insert shows the fitting of Vogel-Folcher law where the solid line is the fitting and circles are the data (the horizontal axis in the insert is temperature (K), and f is the frequency).

Figure 5. Remanent polarization P_r as a function of temperature before (solid line with open circles) and after (solid line with dots) the irradiation.

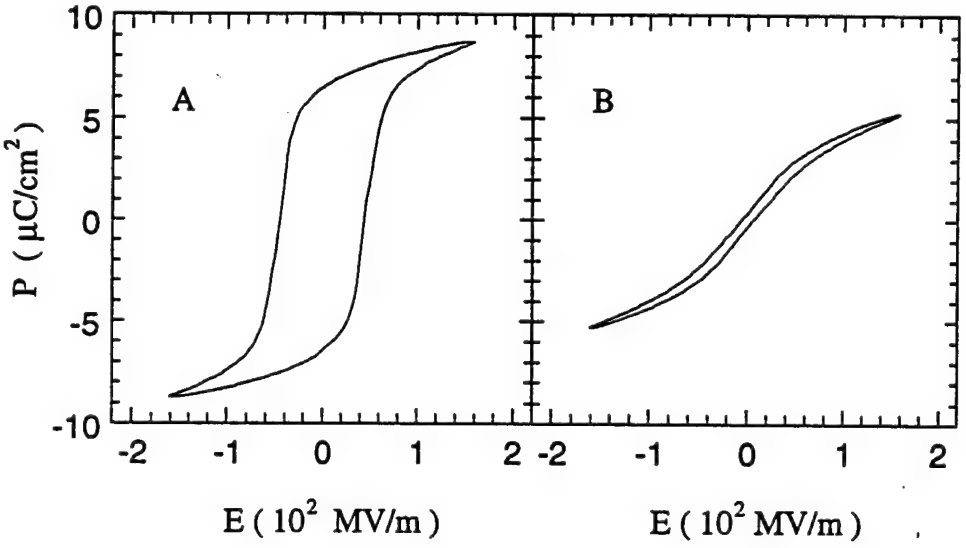

Fig. 1

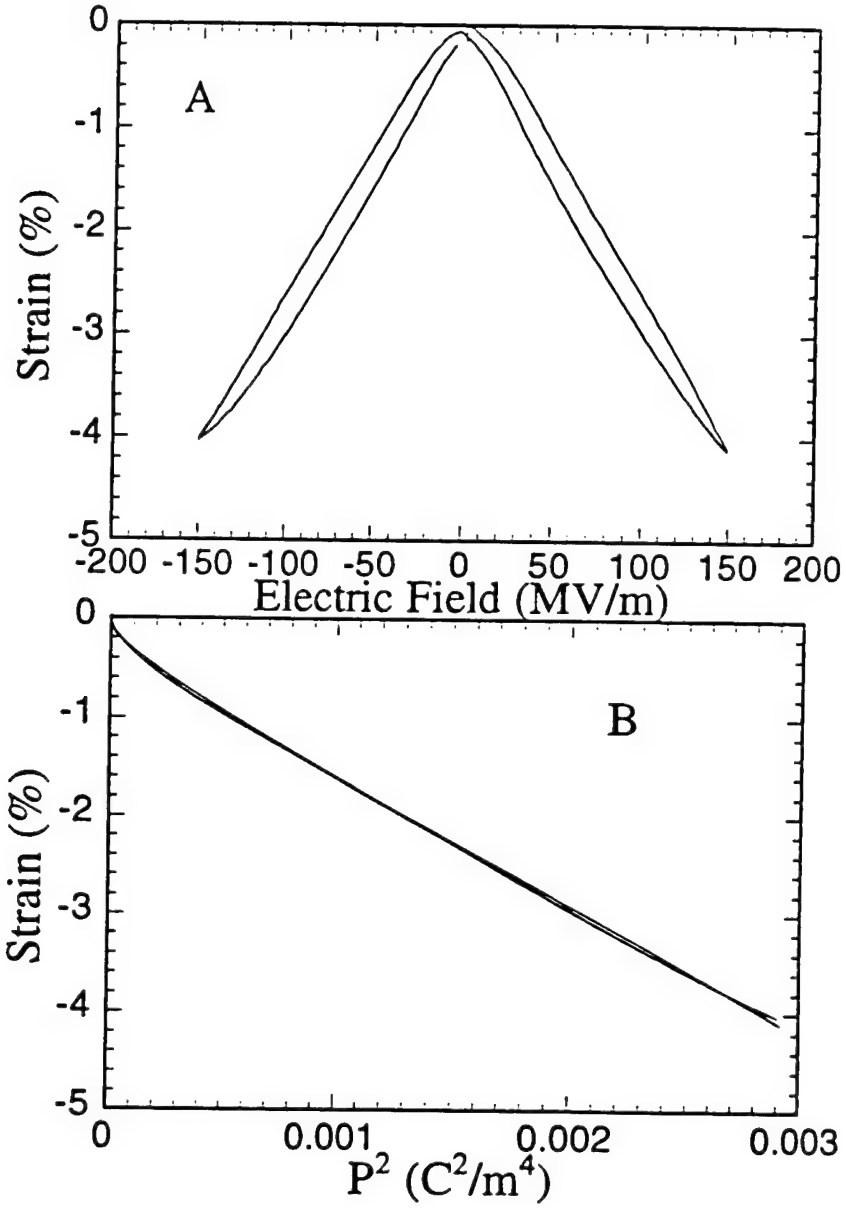
A
Strain (%)
0
-1
-2
-3
-4
-5
-200 -150 -100 -50 0 50 100 150 200
Electric Field (MV/m)
B
Strain (%)
0
-1
-2
-3
-4
-5
0
0.001
0.002
0.003
P² (C²/m⁴)

F. 2

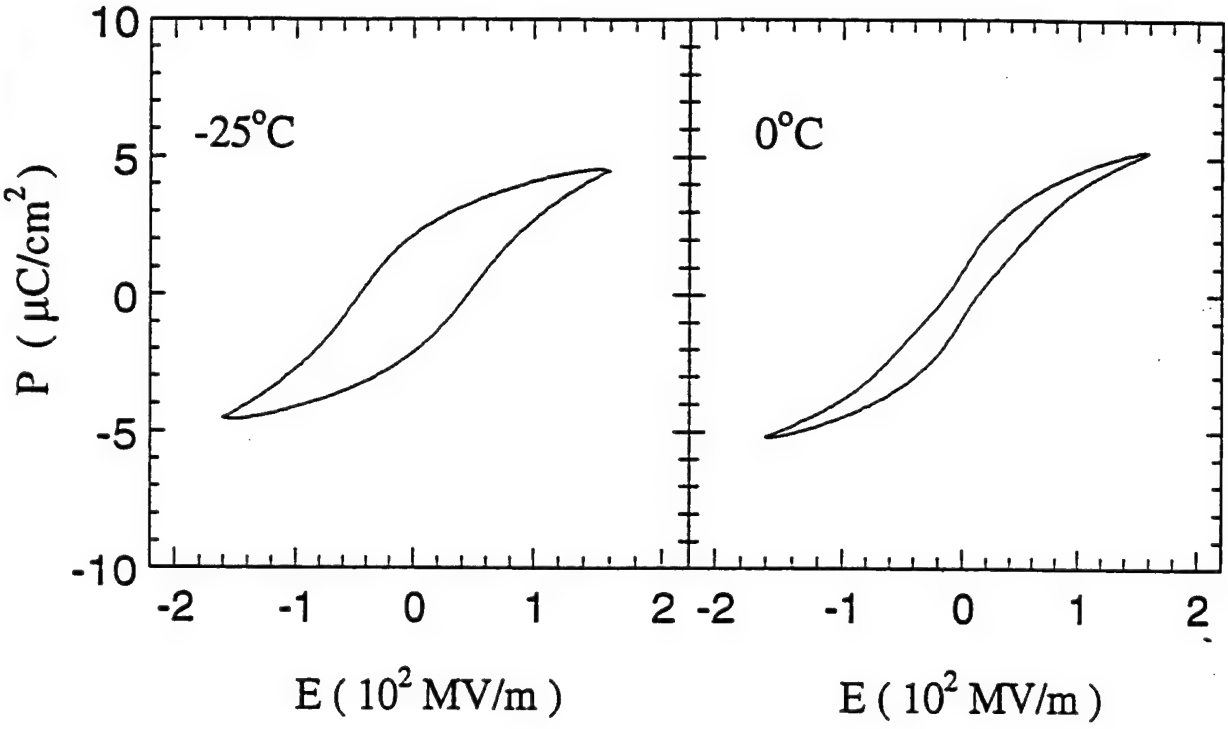

F. 3

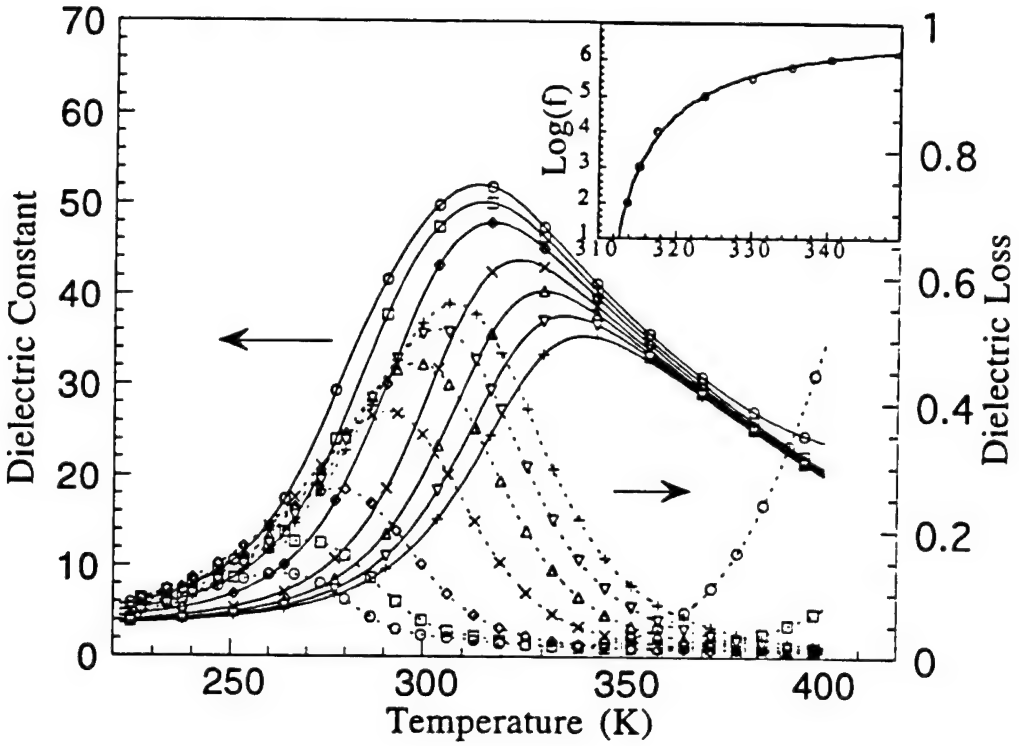
Dielectric Constant
Dielectric Loss
Temperature (K)
Log(f)
70
60
50
40
30
20
10
0
1
0.8
0.6
0.4
0.2
0
250
300
350
400
6
5
4
3
2
1
310
320
330
340

Fig. 4

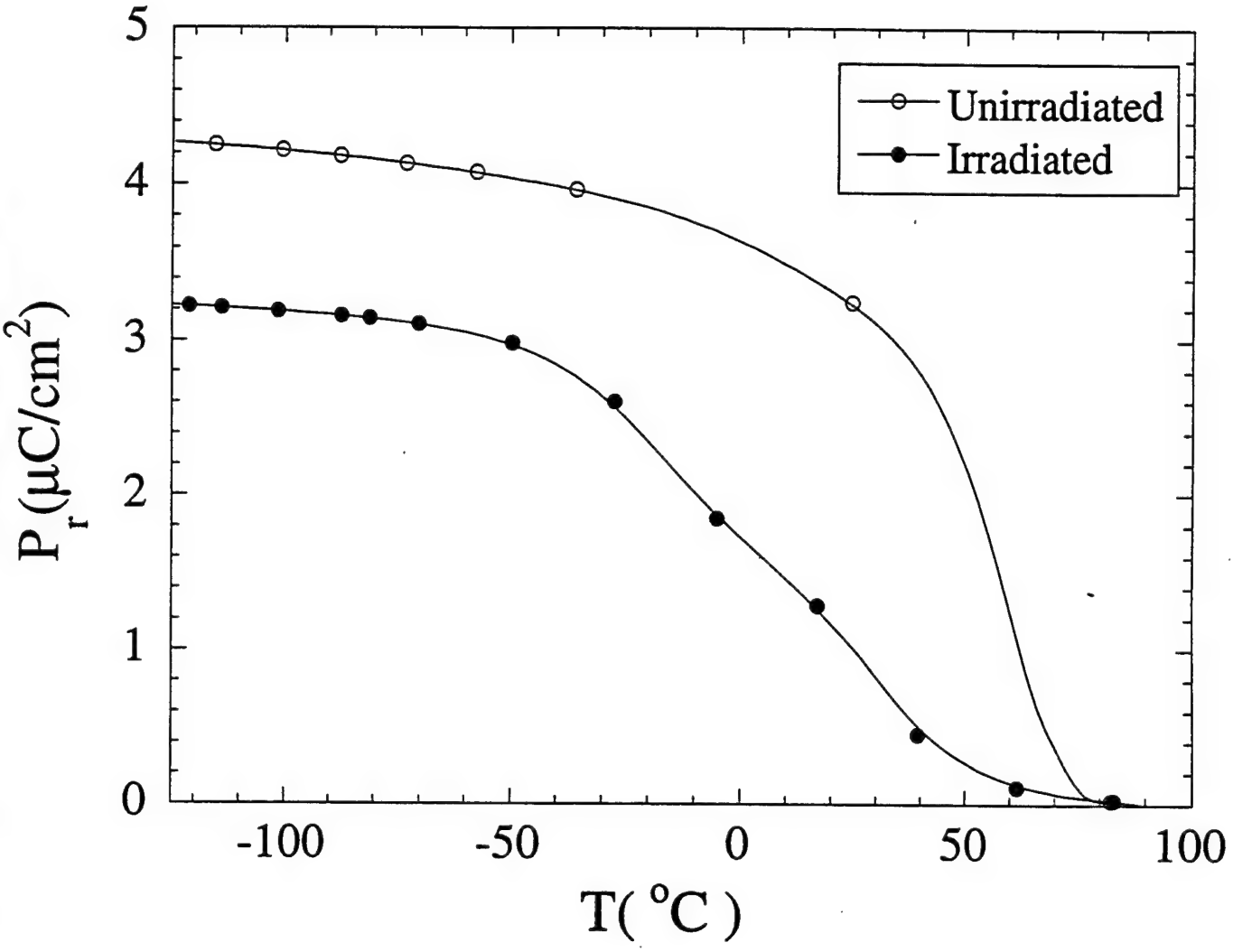

Fig. 5

TRANSDUCER STUDIES

Cymbal : Moonie : BB Composites

APPENDIX 34

COMPOSITE SENSORS AND ACTUATORS

ROBERT E. NEWNHAM*

Composite materials have found a number of structural applications but their use in the electronics industry has been relatively limited. As the advantages and disadvantages of electroceramic composites are better understood, we can expect this picture to change.

In this paper we review some of the composite sensor and actuator studies carried out in our laboratory during the past two decades. These functional composites make use of a number of underlying ideas including connectivity patterns leading to field and force concentration; the use of periodicity and scale in resonant structures: the symmetry of composite structures and its influence on physical properties; polychromatic percolation and coupled conduction paths: varistor action and other interfacial effects; sum, combination, and product properties; coupled phase transformation phenomena; and the important role that porosity and inner composites play in composite materials. These ideas provide a basic understanding of functional composites and have been discussed previously [1]. In the present paper, we describe several composite piezoelectrics and their applications. Several of these transducers mimic the geometries of the sound-sensing organs of fish: elongated feelers, vibrating air bladders, and spherical inner ears.

Early investigators concentrated on polymer-ceramic composites for use as hydrophones. Several interesting connectivity patterns [2] were developed including 3-3 structures made by the replamine process [3] and by fugitive phase technique [4]. Then came the more useful 1-3 composites consisting of parallel PZT fibers embedded in a polymer matrix. These structures were made by extrusion [5], by dicing [6], and more recently by injection molding [7] and lithographic lost-wax techniques [8]. The coupling between the ceramic fibers and the polymer matrix is important [11]. In optimizing hydrophone performance, the $d_h g_h$ product was chosen as a figure of merit. The 1-3 composite increases d_h and g_h by reducing the d_{31} piezoelectric coefficient and the dielectric constant while maintaining the large d_{33} coefficient.

The usefulness of the 1-3 composite in high frequency applications for non-destructive testing and medical diagnostics was recognized later [9]. Biomedical transducers require resonant frequencies in the 1-10 MHz range, high electromechanical coupling coefficients, low acoustic impedance, and broad bandwidth. The 1-3 transducers manufactured by Siemens [8] have thickness resonances of 5-10 MHz, coupling coefficients $k_t = 0.67$, $K = 600$, $\tan\delta < 0.025$, and a mechanical Q about 10.

* Intercollege Materials Research Laboratory, Pennsylvania State University, University Park, PA 16802-4801, USA.

Poling is sometimes difficult for the long, slender PZT fibers used in 1-3 composites. Electric breakdown often occurs before poling is complete, and the transducer is ruined. Lower poling and driving fields are obtained when the spaghetti-like PZT fibers are replaced with macaroni-like PZT tubules. When electroded inside and out, the thin-walled tubes are poled and driven radially at relatively modest voltages. Radial motions are coupled to length-wise displacements through the d_{31} coefficient. Effective piezoelectric constants of about 8000 pC/N and large $d_h g_h$ products are achieved with these composites [10]. Other variants on the basic 1-3 structure include the 1-2-3 composite with transverse load bearing fibers [11], and the 1-3-0 composite with a foamed polymer matrix [12], and the interesting woven fiber composites devised by Safari and co-workers [13].

Perhaps the simplest piezoelectric composite is the 0-3 transducer made by dispersing ceramic particles in a polymer matrix. The NTK Piezo-Rubber films and cables are used as flexible hydrophones, keyboards, blood pressure cuffs, and musical instruments. They are made by hot-rolling $PbTiO_3$ particles into a chloroprene rubber matrix [14].

Composites with 1-3 and 3-2 connectivity were prepared by drilling either circular or square holes in prepoled PZT blocks. Drilling was carried out in a direction perpendicular to the poled axis and by filling the drilled holes with epoxy [15]. On samples optimized for hydrophone performance, the g_h and $d_h g_h$ coefficients were about 4 and 40 times greater, respectively, for the 1-3 composites; and 25 and 150 times greater for the 2-3 composites compared to those of solid PZT.

BB transducers are made from hollow spheres of PZT a few millimeters in diameter, about the same size as the metallic pellets used in air rifles (BB guns). PZT BBs are mass produced by a patented forming process [16] in which air is blown through a PZT slurry of carefully controlled viscosity. The hollow spheres are 1-6 mm in diameter with wall thickness of 0.1 mm. Densities are about 1.3 g/cm^3 giving the BB a low acoustic impedance close to that of water and human tissue. When embedded in a polymer matrix to form a 0-3 composite the BB spheres are surprisingly strong, and able to withstand large hydrostatic pressure without collapse. Close-packed transducer arrays are easily assembled.

When electroded inside and out, and poled radially the BB becomes an omnidirectional transducer suitable for underwater or biomedical applications. For spheres 2.6 mm is diameter with 90 mm thick walls, the resonant frequencies are 700 kHz for the breathing mode (d_{31}) and 10 MHz for the wall thickness mode (d_{33}). BBs are small enough to be used in catheters for non-invasive surgery to act as beacons, sensors, and actuators.

In recent years, piezoelectric and electrostrictive ceramics have been used in many actuator applications [17]. To meet these needs a new type of composite actuator based on a flextensional transducer has been developed [18]. This ceramic-metal composite actuator, or "moonie" consists of either a piezoelectric ceramic disc or a multilayer stack, sandwiched be-

tween two specially designed metal end caps. This design provides a sizable displacement, as well as a large generative force. In other words, it bridges the gap between the two most common types of actuators, the multilayer and the bimorph. The shallow spaces under the end caps produce a substantial increase in strain by combining the d_{33} and the d_{31} contributions to the ceramic. It is attractive for hydrophone. transceiver and actuator applications, and is especially advantageous for use as a non-resonant, low frequency projector in deep water [19].

REFERENCES

[1] R.E. Newnham, J. Mat. Edu. **7** (1985) 601.
[2] R.E. Newnham, D.P. Skinner and L.E. Cross. Mat. Res. Bull. **13** (1978) 525.
[3] D.P. Skinner, R.E. Newnham and L.E. Cross. Mat. Res. Bull. **13** (1978) 599.
[4] T.R. Shrout, W.A. Schulze and J.V. Biggers. Mat. Res. Bull. **14** (1979) 1553.
[5] K.A. Klicker, J.V. Biggers and R.E. Newnham. J. Am. Ceram. Soc. **64** (1981) 5.
[6] H.P. Savakus, K.A. Klicker and R.E. Newnham. Mat. Res. Bull. **16** (1981) 677.
[7] C.P. Bowen, T.R. Shrout, R.E. Newnham and C.A. Randall, Journal of Int. Mat. Syst. & Struct. **6** (1995) 159-168.
[8] G. Preu, A. Wolff and D. Crames. U. Bast Euro-Ceramics II **3** (1991) 2005.
[9] T.R. Gururaja, W.A. Schulze, L.E. Cross. R.E. Newnham, B.A. Auld and Y.J. Wang, EKE Transactions on Ultrasonics **32** (1985) 481, 499.
[10] W. Pan, Q.M. Zhang. A. Bhalla and L.E. Cross. J. Am. Ceram. Soc. **72** (1989) 571.
[11] M.J. Haun. R.E. Newnham and W.E. Schulze. Adv. Ceram. Mat. **1** (1986) 361.
[12] M.J. Haun and R.E. Newnham, Ferroelectrics **68** (1986) 123.
[13] V.F. Janas and A. Safari, J. Am. Ceram. Soc. **78** (1995) 2945.
[14] H. Banno. Ferroelectrics **50** (1983) 329.
[15] A. Safari. S. DaVanzo and R.E. Newnham. Ferroelectrics **50** (1983) 257.
[16] R. Meyer. H. Weitzing, Q.C. Xu. Q.M. Zhang. R.E. Newnham and J.K. Cochran, J. Amer. Ceram. Soc. **77** (1994) 1669.
[17] K. Uchino. Mat. Res. Soc. Bull. **18** (1993) 42.
[18] Y. Sugawara, K. Onitsuka, S. Yoshikawa, Q. Xu, R.E. Newnham. and K. Uchino, J. Am. Ceram. Soc. **75** (1992) 996.
[19] Q.C. Xu, S. Yoshikawa, J. Belsick. and R.E. Newnham, IEEE Transactions on Ultrasonics, Ferroelectrics and Frequency Control, **38** (1991) 634.

APPENDIX 35

Ceramics, composites and intergrowths

Editorial overview

Brian CH Steele*, Robert E Newnham† and Anthony G Evans‡

Addresses
*Centre for Technical Ceramics, Imperial College, South Kensington, London SW7 2AY, UK; e-mail: b.steele@ic.ac.uk
†The Pennsylvania State University, 251-A Materials Research Laboratory, University Park, PA 16802-4801, USA; e-mail: bobnewnham@psu.edu
‡Division of Applied Sciences, Harvard University, Pierce Hall, 29 Oxford Street, Cambridge, MA 02138, USA

Current Opinion in Solid State & Materials Science 1997, 2:563–565

Electronic identifier: 1359-0286-002-00563

Abbreviations
MEMS microelectromechanical systems
MLC multilayer ceramic capacitor

Multilayer ceramic capacitors

Recent developments in the multibillion dollar capacitor market are summarized by Yukio Sakabe (pp 584–587), Chief Ceramic Engineer of the Murata Manufacturing Company, the world's leading producer of multilayer ceramic capacitors (MLCs). The dielectric ceramic materials used in these passive devices have evolved to meet ever-increasing demands for miniaturization, higher-frequency operation, stable response over a wide temperature range, improved reliability, and reduced manufacturing costs. Meeting these market demands requires the development of the new dielectric materials and improved manufacturing methods for reducing dielectric layer thickness in MLCs. An example is the current worldwide activity involving Ni electrodes as a replacement for the more expensive Ag and Ag-Pd electrodes.

Capacitors are an indispensable part of virtually every electronic circuit. The growth in the MLC market parallels that of IC (integrated circuit) chip production. TV sets, tape recorders, personal computers, and other consumer electronic systems typically contain 100 or more capacitors. In combination with resistors, inductors, and ICs, capacitors perform a variety of functions including coupling circuits, bypass filters, tuning and resonance circuits, power supplies and temperature compensators.

A survey of ongoing R&D in the United States and Japan was recently conducted to identify future developments in electronic ceramics [1]. Since 1990, 391 US patents were issued in the field of dielectric ceramics, with Japanese and US companies receiving nearly 90% of the total. The patent review indicated some interesting differences between the Japanese and American development strategies. US companies were more aggressive in developing new dielectric compositions for conventional X7R and Z5U $BaTiO_3$-based capacitors, while Japanese manufactures concentrated on new microwave formulations and Pb-based relaxor ferroelectric dielectrics.

Currently nearly all passive circuit elements are incorporated in electronic circuits as surface-mounted discrete components, but the picture is changing rapidly because of the small sizes of MLC chips. By the year 2005, industry experts predict that only 20% will be discrete, with 40% integrated into interconnecting substrates, and the remaining 40% deposited directly on-chip as part of the active silicon IC die. As pointed out by Sakabe in his article on 'Multilayer ceramic capacitors', component manufacturers need to respond rapidly to these changes.

Extruded honeycomb ceramics

Pronob Bardhan (pp 577–583), Director of Ceramic Research and Development at the Sullivan Park Research of Corning Inc, has summarized recent activity in 'Ceramic honeycomb filters and catalysts'. For the past 20 years, cellular catalytic reactors made from extruded cordierite have been used successfully for automobile emissions control. The honeycomb ceramic substrates coated with precious metal catalysts have proven to be the best method for reducing automotive air pollution, despite the tightened emission standards imposed from time to time. As pointed out in Bardhan's article, sizeable reduction in cell size and wall thickness of the extruded substrates, coupled with improved catalysts, were required to meet the new, more stringent standards.

Three Corning employees, Rodney Bagley, Irwin Lachman and Ronald Lewis, were honored last year by the International Academy of Ceramics for developing the catalytic convertor. An historical account of the research and development program at Corning in the early 1970s has just been published [2]. The key inventions were the extrusion process [P1] and a low thermal expansion ceramic suitable as a catalyst substrate in severe environments [P2].

Extruded cellular ceramics have now become the substrate of choice for many applications replacing crimped and wrapped substrates and bead-type reactors. The unique ultra-low expansion cordierite ceramic has withstood the harsh thermal shock environment of automobile exhaust and catalyst light-off with over 2×10^{12} km and 2.5×10^{9} years of accumulated service in automobiles and trucks. They are the most widely used automobile emissions control device in the US Europe and Japan.

As described in Bardhan's report, extruded ceramic substrates are also used for pollution control in wood stoves, diesel engines and in the control of nitrous

oxide from coal, gas, and oil-fired combustion burners. In materials processing, cellular molten metal filters have significantly improved the quality of cast iron parts.

Quartz crystal growth

Millions of the quartz units produced annually are used in telecommunications and radio communications where precise frequency control, both in transmission and reception, is essential for reliable communication [3]. Time-keeping, one of the earliest applications of piezoelectric quartz, has also grown considerably both in precision and market share. Precision quartz resonators have achieved levels of a few parts in 10^{14} for one second sample times. The millions of quartz crystal oscillators used in inexpensive wrist watches possess long-term stabilities of one part in a million per year. Other applications include timing elements in computers, surface wave correlators, instrumentation filters and sensors for use in detecting miniscule changes in temperature, pressure, or chemical composition.

Most of the quartz crystals used in industry today are grown synthetically by a hydrothermal process carried out in steel-wall autoclaves 5–10 m long and 1 m in diameter. Seed crystals are mounted in racks in the upper half of the autoclave, while pieces of pure silica in the lower half provide nutrient for the growing crystals. The autoclave is filled with water and heated to about 350°C, increasing the pressure to about 2,000 atmospheres. Under these conditions SiO_2 becomes quite soluble. Crystal growth proceeds by deposition on the seed crystals kept at a slightly cooler temperature. Crystals measuring $2 \times 3 \times 15$ cm grow in about a month.

Joseph F Balascio and Theodore Lind (pp 588–592), two outstanding process engineers from Motorola, have updated the field in their article. 'The growth of piezoelectric alpha quartz crystals'. Concerns about various types of impurities, as well as water content and dislocation density, have arisen because of the industry drive to tighter standards over longer time periods. Higher resonant frequency have led to the use of photolithography in miniaturizing the quartz resonants. Current R & D efforts are concentrated on the standardization of starting materials and the use of computer-aided modelling of the growth process.

The importance of interfaces in electroceramics has long been recognised in the operation of ceramic oxide semiconductor barrier devices such as varistors and positive temperature coefficient resistors. Accordingly the survey by Jamnik and Maier (pp 600–603) includes recent publications about the transport of electronic species across grain boundaries. However, an important feature of the survey is the prominence given to transport of ions across ceramic interfaces. The technological applications (e.g. Steele [4]) require rapid ion transport across ceramic interfaces. It is interesting, therefore, to read about novel techniques to study mass transport across, for example, single grain boundaries in doped $SrTiO_3$ bicrystals, as well as innovative theoretical approaches for the interpretation of the experimental observations of ionic transport across space-charge regions. Additional techniques and much more data are urgently required for further progress in this topic in order to provide a basic understanding for the technological applications of these materials. Fortunately progress is being made in modelling the cathodic reduction of oxygen associated with porous oxide electrodes used in solid oxide fuel cells, and it appears that the injection of oxygen ions into the surface of ceramic electrolytes is relatively facile. Mass transport across and along interfaces is one of the basic processes involved in the sintering of ceramic materials, and recent developments in this area are also surveyed.

The ubiquitous presence of water vapour in the environment used to process ceramic oxides means that it is always necessary to consider whether the observed properties of the oxide are being influenced by dissolved water. This is particularly true of acceptor doped perovskite and rare-earth oxides, where the transport properties can be dominated by the relatively large concentrations of interstitial protons. The review by Norby and Larring (pp 593–599) summarises our present knowledge about the concentration and transport of protons in oxide ceramics, including the role of grain boundaries, where segregated species can influence the distribution of protons. The mechanism of proton transport is being clarified by a variety of techniques, including computer simulation studies, and an important feature of the survey is a correlation between the concentration of dissolved water and the molar density of oxygen ions in selected oxide structures. Using this correlation it is possible to evaluate the likely influence of protons as a function of the partial vapour pressure of water and of temperature. Finally, it should be noted that technological applications of proton conducting ceramics, such as hydrogen sensors in molten aluminium, are emerging and there is also interest in mixed protonic–electronic ceramic conductors for chemical membrane reactors.

The use of sol-gel processing routes for the preparation of bio-active ceramic coatings and devices provides the focus for the survey by Hench (pp 604–610). Clinical use of bioceramics is rapidly expanding for a variety of exciting applications as recent investigations are providing more information about the type and mechanism of the response of biological tissue. Active biological molecules entrapped within the sol-gel pore network are accessible to external reagents and if appropriate, can also be modified by photochemical reactions as the gel matrix is usually transparent to UV light and visible wavelengths. It is important to note that porous sol-gel networks provide heterogeneous nucleation sites for the growth of biologically active hydroxy-carbonate-apatite (HCA) which is found in all known bioactive materials. Whilst the mechanism of nucleation and growth of HCA on silica gel substrates remain controversial the ability of sol-gel networks to form HCA is already being exploited in

surface coatings on titanium implants which yield a strong interfacial attachment to bone which is superior to plasma sprayed hydroxy apatite coatings. Additional applications of sol-gel materials in biology and medicine include sol-gel matrices with immobilised enzymes and antibodies, and their use as biological and chemical sensors. Clearly these materials are going to provide a fruitful source of both interdisciplinary theoretical investigations and medical/biological applications in the next millennium.

Developments in MEMS

MEMS (microelectromechanical systems) technology has developed from the Si world and has for much of its existence been practised by electrical engineers. However, as the potential for producing small mechanical systems became apparent, mechanical and materials engineers seized the opportunity to make unique small things, such as micro-pumps and accelerometers. This involvement, in turn, leads to a realisation that the exclusive use of Si imposed limitations. That is, a much wider range of opportunities would be possible if other materials could be fabricated at comparable spatial resolutions, using related combinations of etching and deposition. The prime candidate for this materials expansion was SiC, because it was familiar to electrical engineers, based on its potential as a high temperature semiconductor. From a thermomechanical perspective, SiC has the advantage (relative to Si) of exceptional high temperature durability (except under reducing conditions), as well as remarkable abrasion and wear resistance. It also has high thermal conductivity and a low thermal expansion coefficient. This combination of properties has led to concepts for its use in mini-engines [5], in addition to mini-pumps, valves and so on. The status of SiC MEMS fabrication technology is elaborated in the article by Zorman *et al.* (pp 566–570), with some discussion of applications. The particularly important issue of residual stress development upon oxidation and deposition is addressed thoroughly.

MEMS devices based on Si or SiC are inherently passive. In order to achieve actuation capability, an active material must also be used, preferably as a film deposited onto the SiC substructure. In principle, electrical, magnetic or thermal actuation can be used for this purpose. However, thin film ferroelectrics and magnetorestrictives compatible with MEMS fabrication have yet to be convincingly demonstrated. The emphasis has thus been on shape memory materials, particularly NiTi alloys. These materials have the greatest power density (in kilowatts per kilogram) among all active materials. This capability is used to advantage in bulk form for the warping of large structures, for gripping and so on. However, because of the thermal actuation mode, bulk shape memory systems can only operate at low frequencies, have low efficiency and are prone to fatigue. These limitations are substantially circumvented in thin film form, because thermal transients are short and the effective heat capacity is low. Operational frequencies in the 0.1 kHz range have been cited for films which, in combination with their high authority attribute, suggest considerable opportunity for active MEMS elements comprising NiTi alloys deposited on SiC. The second part of the Zorman *et al.* article addresses the technology of shape memory thin films deposited on SiC, with this potential in prospect.

Refractory ceramics

Research on refractory ceramics has largely been conducted in industry, with low levels of academic involvement. The pace and focus of research progress in the field reflects this situation. The article by Moore (pp 571–576) provides a current assessment of the areas and themes that are the forefront of the field. Foremost among the new interests is the use of numerical simulations to predict the physical and chemical responses of the refractory materials during operation. Progress appears to be hindered by the paucity of temperature dependent materials properties and of methods for their efficient measurement. Such properties are particularly difficult to acquire, because of the severe conditions (of temperature and environment) that refractories experience in operation. That is, the thermomechanical responses are viscoplastic and inherently much more complex to model, than say, the incompressible elastic/plastic constitutive behaviour that characterises the performance of most metallic structures. Yet, the insights to be gained from modelling are considerable and an appeal is made to establish precompetitive research agendas for refractories that would provide the tools and data that industry needs to proceed along this path.

Moore's article strongly emphasises the trend in industry to supplant cast refractory shapes with unitary liners. This trend changes the engineering requirements and research needs. Some basic chemistry issues related to bonding emerge as central to this approach, as well as to the characterisation and control of the rheology of the slurry systems. Comparable issues are confronted in cement and concrete technology. There are clear opportunities for research initiatives that would greatly enhance the ability of this industry to improve product quality and reliability.

References

1. Swartz SL, Shrout TR, Takenaka T: **Electronic Ceramics R & D in the US Japan.** *Am Ceram Soc Bull* 1997, **76**:59–65.
2. Bagley RD, Lachman IM, Lewis RM: **Extruded cordierite substrates for automotive emissions control.** In *Role of Ceramics in a Self-Sustaining Environment.* Edited by Pampuch R, Haberko K. Faenza, Italy: Techna Srl; 1997.
3. Bottom VE: *Introduction to Quartz Crystal Unit Design.* New York: Van Nostrand Reinhold Co; 1982.
4. Steele BCH: **Ceramic ion conducting membranes.** *Curr Opin Solid State Mater Sci* 1996, 1:683-691.
5. Epstein EH, Senturia SD: **Macro power from micro machinery.** *Science* 1997, **276** 1211.

Patents

P1. Bagley RD: **Extrusion method for forming thin-walled honeycomb structures.** *US Patent* 3 790 654; 1974.

P2. Lachman IM, Lewis RM: **Anisotropic cordierite monolith.** *US Patent* 3 885 977; 1975.

APPENDIX 36

PIEZOELECTRIC SENSORS AND SENSOR MATERIALS

James F. Tressler, Sedat Alkoy, and Robert E. Newnham

Materials Research Laboratory, The Pennsylvania State University,
University Park, PA 16802

ABSTRACT

This paper reviews the current trends and historical development of piezoelectric sensors and sensor materials technology. It begins with a discussion of the bases of piezo- and ferroelectric activity, followed by an overview of the most commonly used piezoelectric ceramic: lead zirconate titanate (PZT). A discussion of the properties and applications of piezoelectric crystals and additional piezoelectric ceramics is followed by a description of several sensor configurations prepared from bulk ceramics. An extensive review and comparison of piezoelectric ceramic - polymer composite sensors based on the connectivity of the constituent phases is also presented. We conclude our discussion of sensor configurations with recent examples of piezoelectric ceramic - metal composite sensors, and expected future developments in the area of piezoelectric sensors.

INTRODUCTION

Piezoelectricity is a phenomenon exhibited by non-centrosymmetric crystals whereby an electric polarization (i.e. charge) is induced in the material upon the application of a stress. Conversely, it is the development of an induced strain which is directly proportional to an applied electric field. The latter phenomenon is known as the converse effect and is utilized in actuation. The former is called the direct effect and is used in sensing dynamic pressure changes, changes in acceleration (from shock or vibration), and changes in force [1]. Whether a material that belongs to one of the piezoelectric point groups actually exhibits measurable piezoelectricity has to be measured experimentally [2].

Through proper design and selection of materials, the frequency range that piezoelectric materials can detect changes in force or motion can range from below 1 Hz to above several MHz. Displacements in the μm range can be precisely measured as can force changes from mN to kN. The rugged solid-state construction of industrial piezoelectric ceramic sensors enables them to operate under most harsh environmental conditions, including dirt, oil, and most chemical atmospheres. They perform well over a wide temperature range and resist damage from severe shock and/or vibration [3].

Piezoelectricity exists in some naturally occurring crystals such as quartz; however, the bulk of the piezoelectric materials used for commercial sensing applications come from synthetic polycrystalline ferroelectric ceramics, such as PZT. Ceramics offer the advantage of high strength and ease of fabrication in general, especially into complex shapes and large area pieces. This paper will review the significant piezoelectric ceramic sensor materials, composite sensor configurations, and some typical applications.

FERROELECTRICITY

Ferroelectrics are a class of piezoelectric materials that exhibit a spontaneous polarization that is reorientable under a realizable electric field (≈ 10^6 V/m). Ferroelectric oxides with the perovskite, tungsten bronze, pyrochlore, and bismuth titanate layer structures all have high dielectric constants and high electromechanical coupling coefficients. In addition, all contain corner-linked octahedral networks of Ti^{4+}, Nb^{5+}, or other d^0 ions. These transition-metal elements are the highly polarizable "active" ions promoting ferroelectricity and the high permittivity and piezoelectric constants required for sensing. With reference to the periodic table, there are two major groups of active ions, both of which are near electronic "crossover" points where different types of atomic orbitals are comparable in energy and where hybrid bond formation is prevalent. The first group, typified by Ti^{4+}, Nb^{5+}, and W^{6+}, consists of d^0 ions octahedrally coordinated to oxygen. For Ti^{4+}, the electronic crossover involves the $3d$, $4s$, and $4p$ orbitals, which

combine with the sigma and pi orbitals of its six O^{2-} neighbors to form the $(TiO_6)^{8-}$ complex. The bond energy of the complex can be lowered by distorting the octahedron to a lower symmetry. This leads to molecular dipole moments, ferroelectricity, large dielectric constants, and piezoelectricity. A second group of active elements contributing to polar distortions in ceramic dielectrics are the lone-pair ions having two electrons outside a closed shell in an asymmetric hybrid orbital. Among oxides, the most important of these lone-pair ions are Pb^{2+} and Bi^{3+}, which are involved in a number of ferroelectrics ($PbTiO_3$, $Bi_4Ti_3O_{12}$, $PbNb_2O_6$) with high Curie temperatures. In many of these compounds, Pb^{2+} and Bi^{3+} are in pyramidal coordination with oxygen and therefore contribute to the spontaneous polarization [4].

PIEZOELECTRIC PZT

Most piezoelectric ceramic sensor formulations are based on PZT (a registered trademark of Clevite Corporation), which has become a common acronym for the solid solutions of nominal composition 52-54 mole % lead zirconate ($PbZrO_3$) and 46-48 mole% lead titanate ($PbTiO_3$). PZT is one of a number of ferroelectric substances crystallizing with the perovskite structure. Lead atoms are positioned at the corners of the unit cell and oxygens at the face centers. Both lead and oxygen ions have radii of about 1.4 Å. Together they make up a face-centered cubic array, having a lattice parameter of about 4 Å. Octahedrally coordinated titanium or zirconium ions are located at the center of the unit cell.

Upon cooling from high temperature, the crystal structure of PZT undergoes a displacive phase transformation with atomic displacements of about 0.1 Å. For titanium-rich compositions, the point symmetry changes from cubic m3m to tetragonal 4mm at the Curie temperature. The tetragonal state with its spontaneous polarization along [001] persists to 0 K. These structural changes are shown in Figure 1.

To make use of these piezoelectric ceramics with their large polarizations, compositions near a second phase transition are chosen. At the Curie point, PZT converts

from a paraelectric state with the cubic perovskite structure to a ferroelectric phase located near a morphotropic phase boundary between the tetragonal and rhombohedral states. Very large piezoelectric coupling between electric and mechanical variables is obtained near this phase boundary.

Polycrystalline ferroelectric ceramics (Curie point group ∞∞m) such as PZT, initially contain randomly oriented polarized regions within each grain called domains. These domains form upon cooling through the Curie temperature in order to minimize the total elastic energy in the ceramic [2]. Because of this polarization randomness, polycrystalline ferroelectrics do not exhibit the piezoelectric effect. Piezoelectricity can be induced, however, by applying a static electric field larger than the saturation field but smaller than the breakdown field at elevated temperatures below the ferroelectric Curie point where the domains are easily aligned. This process is known as poling. Poling orients the domains by reversal, or by a change through angles that depend on the crystal structure so that the spontaneous polarization has a component in the direction of the poling field [5] and imparts conical symmetry (∞m). When the electric field is removed, some of the more highly strained domains revert to their initial position (depolarization), but a large majority remain aligned (remnant polarization), resulting in the material being permanently poled.

For a poled ceramic having symmetry ∞m, d_{31}, d_{33}, and d_{15} are the appropriate tensor coefficients. Both intrinsic and extrinsic contributions to these piezoelectric coefficients exist. The intrinsic effects coming from the distortions of the crystal structure under mechanical stress appear in Figure 2. Under mechanical stress parallel to the dipole moment, there is an enhancement of the spontaneous polarization P_s along x_3. When stress is applied perpendicular to the dipole moment, electric charges develop transversely. These are the d_{33} and d_{31} effects, respectively. When the dipole is tilted by shear stress, charges appear on the side faces, the d_{15} coefficient. There are extrinsic contributions to the

piezoelectric coefficient as well. These can be extremely large, often involving the domain wall motions.

Titanium-rich compositions in the PZT system favor a tetragonal modification with sizable elongation along [001] (for a total of six equivalent directions) and a large spontaneous polarization in the same direction. A rhombohedral ferroelectric state is favored for zirconium-rich compositions. In this case, the polarization and distortion are along [111], giving rise to eight possible equivalent domain states. The compositions that pole best lie near the morphotropic boundary between the rhombohedral and tetragonal ferroelectric phases. For these compositions, there are 14 possible equivalent poling directions over a very wide temperature range (-50°C to +200°C). This explains in part why the ceramic piezoelectric coefficients are largest near the morphotropic boundary. Phase changes between the rhombohedral and tetragonal phases also occur during the poling process [4].

The addition of dopants to PZT can have a profound impact on its properties. Donor dopants cause cation (metal) vacancies in the crystal structure which enhance domain reorientation and hence the extrinsic contribution to the piezoelectric coefficients. As a result, these electrically 'soft' PZTs (such as those designated as 5A and 5H) have large piezoelectric coefficients, large permittivity, high electrical losses, large electromechanical coupling factors, very high electrical resistance, low mechanical quality factors, and a low coercive field [6]. Acceptor dopants, on the other hand, cause oxygen vacancies. These oxygen vacancies pin the domain walls, with the defect dipoles aligning with the spontaneous polarization within a domain [2]. This leads to an electrically 'hard' PZT (e.g. those with designations 4 and 8). A hard PZT is characterized by low piezoelectric coefficients, low permittivity, low losses, low electrical resistivity, high Q_m, and a high coercive field [7]. Isovalent substitutions tend to reduce the Curie temperature and hence increase the room temperature permittivity [8]. Multivalent ions, which substitute for either

Ti^{4+} or Zr^{4+}, serve to reduce aging effects [9]. A listing of the more commonly used dopants is provided in Table 1.

SENSOR CHARACTERIZATION

The sensitivity of a piezoelectric is taken to be equal to the open circuit voltage that it generates due to an applied stress, or g•t, where 'g' is the relevant piezoelectric voltage tensor and t is the thickness of the piezoelectric element. The sensitivity needs to be sufficiently high so that the generated signal can be detected above the background noise. In practice, the generated signal is small and has to be enhanced by an appropriate charge or voltage amplifier. The sensitivity is maximized when the 'g' coefficient is maximized. The 'g' coefficient is related to the 'd' coefficient through the dielectric constant, K, as follows: $g=d/K\varepsilon_o$, where ε_o is the permittivity of free space. Typically, a large dielectric constant, or capacitance, is also desirable for sensors in order to overcome the losses associated with the cables. Unfortunately, an increase in dielectric constant results in a lower voltage coefficient, as seen in the aforementioned equation. Another important parameter of a piezoelectric material is the electromechanical coupling coefficient, k which can be defined as;

k^2 = (stored mechanical energy / input electrical energy)

or

k^2 = (stored electrical energy / input mechanical energy)

When operating in the hydrostatic mode, i.e. when the incident stress is equal on all sides, the tensor coefficients are represented as $d_h=d_{33}+2d_{31}$ and $g_h=g_{33}+2g_{31}$. A figure-of-merit, the $d_h \bullet g_h$ product, is often reported as a measure of the quality of the sensing capability of the piezoelectric element or to compare different hydrophone materials [10]. Quantitatively, it is used to ascertain the type of amplifier required in the electronic circuitry to overcome the self-noise of the system, and in the case of composites should be normalized by the volume of the device in order to make accurate comparisons [11].

PIEZOELECTRIC SENSOR MATERIALS

Crystals

Although some piezoelectric crystals, such as quartz and rochelle salt, occur in nature, they are more commonly grown synthetically. To be of practical use, however, they have to be oriented and cut along specific crystallographic directions so as to obtain the best piezoelectric response. A listing of the more significant piezoelectric crystals, along with their best piezoelectric coefficient, is given in Table 2.

Quartz is still used quite extensively in accelerometers [1]. Lithium sulfate (because of its large g_h coefficient) and tourmaline are two piezoelectric crystals still used in commercial hydrophones, the latter earmarked for shock and blast measurements [12]. Rochelle salt still sees some limited use on one type of sonic blast sensor [12]. Lithium niobate ($LiNbO_3$) and lithium tantalate ($LiTaO_3$) are both used as high temperature acoustic sensors because they both maintain high sensitivity up to 400°C [13]. Other high-temperature piezoelectric crystals with good thermal stability include the perovskite layer structure (PLS) ferroelectrics such as $Sr_2Nb_2O_7$ and $La_2Ti_2O_7$ which have Curie temperatures of 1342°C and 1500°C, respectively [13]. Polar glass ceramics, which are grown by conventional crystal growing techniques, are of interest for hydrophone applications [13]. Because of their very stable piezoelectric properties, natural crystals are best suited for sensor applications in which a variable has to be monitored over long periods of time [1].

Ceramics

The first polycrystalline ferroelectric ceramic was barium titanate ($BaTiO_3$), which has the perovskite structure, and was discovered independently by researchers in the United States, Japan, and the Soviet Union in 1943. Its superiority over single crystals was recognized immediately and it remained the primary electroceramic material until the discovery of lead zirconate titanate (PZT) in 1954 by Jaffe et al. [8,13]. Barium titanate has

the disadvantage of difficulties in sintering due to anomalous grain growth during firing [14].

The solid solution of lead zirconate and lead titanate (PZT), which also has the perovskite crystal structure, was described previously. A complete description of its piezoelectric properties is shown in Table 3. While individual manufacturers of PZT use proprietary formulas for each composition, in general, PZT-5 is Nb-doped, PZT-6 is Cr-doped, PZT-7 is La-doped, and PZT-4 is Fe-doped [14]. Often, PZT types are reported by their US Navy designations as Type I, II, or III. Type I is a hard PZT with a T_c greater than or equal to 310°C. Type II is a soft PZT with a Curie temperature of greater than or equal to 330°C. Type III is a very hard PZT with a T_c of greater than or equal to 290°C. Type IV is barium titanate with nominal additives of 5% calcium titanate and 0.5% cobalt carbonate as necessary to obtain a Curie temperature of greater than or equal to 100°C [12]. A list of other important piezoceramic sensor materials and their properties is given in Table 4.

Pure lead titanate is often used as a hydrophone material when it is doped with either calcium or strontium [15]. This is because of its strong piezoelectric anisotropy. When doped with other elements, it is used as a knock sensor in automobiles. The higher operating temperature range of lead titanate allows it to be mounted closer to the combustion chamber, thus giving it a faster response time as compared to PZT [13].

Three component ceramics (or PCMs) consist of lead zirconate and lead titanate along with a third component, typically lead magnesium niobate, $Pb(Mg_{1/3}Nb_{2/3})O_3$ [17]. These piezoelectric ceramics offer several of the same advantages as do the PZT and they are quite competitive with the PZT's in terms of the piezoelectric properties.

Turner et al., reviewed a number of other piezoelectric ceramic materials that can be used for sensor applications, especially at high temperatures [13]. A synopsis of the findings is presented here. Modified bismuth titanate, with the composition $Na_{0.5}Bi_{4.5}Ti_4O_{15}$, has a layered structure and can be used for accelerometers at temperatures

up to 400°C. Lead metaniobate, $PbNb_2O_6$, a member of the tungsten bronze family, is often used in nondestructive testing, medical diagnostic imaging, and for deep submergence hydrophones [12]. However, problems such as a high level of porosity and relatively low mechanical strength are often encountered in its use. Another niobate - sodium potassium niobate $(NaK)Nb_2O_6$ has seen use for high frequency transducer applications (10-200 MHz) [17]. Antimony sulfur iodide (SbSI) has a very high g_h coefficient, especially when it is modified with 4-8% oxygen, making it attractive for hydrophone applications. Unfortunately, its Curie temperature is only about 34 °C, above which it loses its piezoelectric properties [12].

SENSOR CONFIGURATIONS

When operated in a hydrostatic environment, bulk piezoelectric ceramics are typically poor choices as underwater acoustic sensors in the audio to low ultrasonic frequency range (i.e. < 100 kHz). As receivers, the sensitivity is low because of the crystal symmetry of the poled ceramic. The piezoelectric charge coefficient in the hydrostatic mode, d_h, is equal to the sum $d_{31}+d_{32}+d_{33}$ of the ceramic. However, $d_{31}=d_{32}$, and for the various PZT compositions, $d_{33} \approx -2d_{31}$; therefore, d_h is nearly zero. As mentioned before, the piezoelectric voltage coefficient, g_h, is equal to d_h/ε, where ε is the permittivity ($K\varepsilon_o$). Since ε for most ferroelectric ceramics is very large (>1000), the g_h coefficient subsequently small. As a consequence, the voltage generated by an incoming pressure wave is very low. In order to improve the electroacoustic performance of a poled ceramic, it must be configured in such a way so that the effect of the hydrostatic pressure is minimized. This usually takes the form of air backing one side of the ceramic element, encapsulating part of the ceramic in a soft polymer to absorb a portion of the hydrostatic stress, or incorporating air spaces into the transducer itself. The primary piezoelectric sensor configurations are described below and are shown in Figure 3.

Bars, disks, and cylinders

Bars, disks, and cylinders (free-flooded rings) are the simplest practical structures for electroacoustic transducers. They can be manufactured either as continuous units or as a compilation of segments, where the segmented cylinder is called a barrel-stave or a ring-stave transducer. The fundamental resonance of these structures is dictated mainly by their dimensions. In order to obtain a resonance in the audio to low ultrasonic frequency range, these transducers are required to be on the order of several meters long or in diameter and consequently weigh hundreds to thousands of kilograms. Since hydrophones are operated well below their fundamental resonance, these configurations can be used as underwater receivers, provided a portion of the transducer is acoustically shielded from the effects of a hydrostatic pressure wave.

Spheres

Spherical designs are most often used when omnidirectional reception is required. Macro-spheres can be constructed by adhering two radially poled hemispheres back-to-back or by gluing triangular-shaped ceramic plates together into a quasi-spherical shape where the plates are poled through their thickness direction [19].

Miniature piezoelectric hollow sphere transducers, also known as BBs due to their similarity in size to the pellets used in buckshot, have a nominal diameter of 2.76 mm and a wall thickness of 80μm [20]. They are made by the patented Torobin process. A fine slurry of PZT is prepared and injected through a coaxial nozzle to form a hollow cylinder. The bottom later closes due to surface tension and hydrostatic pressure. The closed cylinder is inflated into a bubble by the inner air pressure until this pressure equals the surface tension of the cylinder. At this critical pressure, the bubble closes and the sphere breaks free. By changing the viscosity of the slurry and the air jet velocity, the sphere diameter and wall thickness can be tailored between 1 to 6 mm and 12-150 μm, respectively [21].

Two poling configurations have been studied: radial and top-to-bottom. In the radial poling configuration, the electrodes are located on the inner and outer walls of the sphere. Two principal modes of vibration were measured in this case - a volumetric expansion and contraction of the sphere at 633 kHz and a wall thickness mode at 13.4 MHz. For top-to-bottom poling, two external cap electrodes are located on the upper and lower surfaces of the sphere. In this case, the principal mode of vibration is an elliptical distortion of the sphere at 230 kHz. In both instances, the permittivity is quite high, approximately 1000.

When subject to a hydrostatic stress, this transducer exhibits a very large $d_h \cdot g_h$ product (figure of merit), on the order of 324,000 fm^2/N for radial poling and 100,000 fm^2/N for top-to-bottom poling. The amplification of d_h and figure of merit in BBs result purely from the spherical geometry. An applied hydrostatic pressure is transformed into radial and tangential stress components and amplified by a factor, which can be defined as the ratio of radius to wall thickness (r/t). The properties are reported to remain stable up to 7 MPa.

Flexors/Benders

The traditional flexor transducer consists of two piezoceramic plates (poled in opposing directions) which are cemented on each side of a central metal plate, or elastic shim. An enhanced voltage response comes from the sum of the contributions of the bending of the disk and the compression of the ceramic itself. Flexural piezoelectric elements are widely employed as ultrasonic sensors and accelerometers. Because of their dimensions, they are generally best suited for applications in the low ultrasonic frequency range. The conventional bender-type transducers are the bimorph and the unimorph [22]. The bimorph consists of two thin ceramic elements sandwiching a thin metal shim, whereas the unimorph is simply one thin ceramic element bonded to a thin metal plate.

A new type of flexural disk transducer is the monomorph, which consists of only a single flexible ceramic plate. An example of a monomorph is the RAINBOW. The rainbow

transducer shows excellent promise as a low pressure (<100 kPa) sensor and/or acoustic transmitter. RAINBOW is an acronym for Reduced And INternally Biased Oxide Wafer. It consists of an electromechanically active layer, such as PZT, PMN, PLZT (lead lanthanum zirconate titanate), PBZT (lead barium zirconate titanate), or PSZT (lead stannate zirconate titanate), in direct contact with a lead-rich constraining layer [23]. This constraining layer is formed by exposing one side of a lead-containing ceramic to a reducing atmosphere at high temperature produced by placing a ceramic in contact with a carbon block. The reduction of the active layer occurs as a result of oxidation of the solid carbon block, first to CO(g) then to CO_2(g). This reduced layer is no longer piezoelectric, and is in fact, a good electrical conductor. Because of the thermal expansion mismatch between the reduced and oxide layer, a curvature develops in the structure, giving it a dome (or rainbow) shape, with the oxide layer in compression throughout its volume.

The RAINBOW disks are typically 0.5 mm thick and can range in diameter from one to tens of centimeters. When used as a pressure sensor, the dome needs to be fixed to a base plate; otherwise, the voltage response will only be equal to that of the bulk ceramic. Rainbows exhibit highly pressure-dependent properties but are extremely robust. As pressure increases, the dome gradually flattens, decreasing the bending contribution to g_h until it reaches the bulk value. For a 1 cm diameter sample bonded to a 1 mm thick plate base plate, a $d_h \cdot g_h$ product of 400 fm^2/N was measured at 2 MPa. A 3.16 cm diameter rainbow exhibited a $d_h \cdot g_h$ product of 10^7 fm^2/N (g_h=800 mV•m/N) at pressures below about 100 kPa. At 1 MPa, it dropped to around 1000 fm^2/N, and beyond 2 MPa, it approached that of the bulk [24].

PIEZOELECTRIC COMPOSITE SENSORS

Due to the low hydrostatic sensitivity of poled PZT, new approaches need to be taken to improve its performance. One such approach was the development of the RAINBOW, as discussed in the previous section. An older and more time-tested approach

has been the incorporation of piezoceramics into composites. Composites provide the capability of utilizing the best aspects of each component in the composite while minimizing the poorest features. Most composite hydrophones consist of two phases - a stiff piezoceramic and a soft polymer. Newnham, et al., established the notation for describing the number of dimensions each phase is physically in contact with itself [25]. There are only ten ways in which two distinct components can be incorporated into a single composite. They are given the notation of 0-0, 1-0, 2-0, 3-0, 1-1, 2-1, 3-1, 2-2, 3-2, or 3-3 [26]. To date, eight different connectivity types of two-phase piezoelectric composites (piezocomposites) have been studied: 0-3, 1-3, 2-2, 2-3, 3-0, 3-1, 3-2, and 3-3. In the case of piezocomposites, the first number in the notation denotes the physical connectivity of the active phase and the second number refers to the physical connectivity of the passive phase. A schematic of these different connectivities is shown in Figure 4.

Most ceramic-polymer composite sensors have been used as hydrophones. The purpose of the polymer is to absorb a portion the hydrostatic stress in either the transverse or longitudinal direction, effectively eliminating either the g_{33} and g_{31} contribution to the g_h of the poled ceramic. Extensive investigations have been performed to determine which ceramic-polymer connectivity configuration will provide the optimum hydrophone performance.

PIEZOELECTRIC CERAMIC-POLYMER COMPOSITES

• *Composites with 3-3 connectivity*

Composites with 3-3 connectivity were the first of the two phase composites to be investigated. Composites with this connectivity have reinforcement in the lateral directions which serves to further decouple negative contributions from lateral stresses [27]. They were initially fabricated by a technique known as the replamine process [28] which is the lost wax replication of a coral skeleton. Since then, additional technologies have been developed such as the fugitive phase, or BURPS (BURned out Polymer Spheres), process

[29] which produces a porous three-dimensionally interconnected ceramic structure by sintering a compacted mixture of volatilizable plastic spheres and PZT powder. Mitsubishi Mining and Cement has developed several techniques for introducing connected porosity in PZT ceramics: reactive sintering, foaming agents, organic additives, and careful control of particle size and firing conditions [26]. A reticulated ceramic technology has recently been used to produce 3-3 composites [27]. Reticulated ceramics are created by coating an organic foam substrate (i.e. polyurethane) with a ceramic slurry, pyrolyzing the foam, and then sintering the ceramic. This group reports that by distorting, or elongating, the foam, it is possible to create a pseudo 1-3 interconnected configuration. They claim the advantages of enhanced hydrostatic response by the decoupling of the d_{31} and d_{32} responses as well as straightened ceramic pathways between electrodes, allowing for an increased level of poling and lateral reinforcement. A comparison of the properties from different fabrication techniques is listed in Table 5.

• *Composites with 0-3 and 3-0 connectivity*

Composites with 0-3 connectivity consist of a random array of piezoelectric particles dispersed in a 3-D polymer matrix [30]. The primary advantage of these composites is their ability to be formed into shapes while remaining piezoelectrically active. These composites are manufactured commercially by NTK Technical Ceramic Division of the NGK Spark Plugs Corporation in Japan under the name *PiezoRubber* (NTK-306). PiezoRubber was developed by Banno and Saito and utilizes PT (lead titanate) rather than PZT in order to take advantage of the large piezoelectric anisotropy in PT [31].

The composite consists of fine $PbTiO_3$ particles of a very narrow size distribution (centered around 20 μm) embedded in a chloroprene polymer matrix [32]. A typical thickness of a 0-3 composite sheet is 500 μm. Good bonding between the particles and the rubber is necessary to achieve successful poling and subsequent good piezoelectric properties [33]. The use of a polymer with a high thermal coefficient of resistivity makes it

possible to pole the composite at elevated temperatures by using the improved ceramic/polymer resistivity balance to give saturation poling while still retaining the high resistance and low loss at typical operating temperatures [30]. The g_h value reported by NTK for their *PiezoRubber* depends on the volume fraction of ceramic present and can be pressure insensitive up to 35 MPa [32-35].

The first 3-0 composites were fabricated by a tape casting technique. Fugitive ink was screen printed onto green PZT sheets which were subsequently stacked. When the ink and binder were burned out and the ceramic sintered, the resultant PZT block contained pores where the ink originally was. A second method for fabricating 3-0 composites consisted of hot pressing a mixture of large polymer spheres and PZT powder [26]. Table 6 compares the properties of these types of composites. One interesting application of 0-3 composites is a potential use as piezoelectric paint for use as a 'built-in' vibration modal sensor [36].

• *Composites with 3-1, 3-2, and 2-3 connectivity*

Conventional composites exhibiting 3-1 and 3-2 connectivity consist of a PZT block with holes drilled through either one side (3-1) or both sides (3-2) in a direction perpendicular to the poled direction of the PZT. The holes are subsequently backfilled with polymer. The one dimensional or two dimensional interconnected polymeric phases in the transverse direction reduce the g_{31} and g_{32} contributions to the hydrostatic voltage response by decreasing the stress coupling in the plane normal to the poled direction [37]. A negligible change in properties occurs up to 7 MPa. In 3-1 and 3-2 composites manufactured in this way, the dielectric constant, as well as the d_h and g_h coefficients are all functions of hole size, PZT thickness, poling technique, and center-to-center distance between adjacent holes [29].

The relic process, in combination with a weaving technique, has been developed to easily manufacture large area composites consisting of fine PZT fibers interconnected in

two dimensions and embedded in a 3-D interconnected polymer matrix (2-3 connectivity). The relic process, reported by Rutgers University, starts with approximately 370 carbon fabric fibers 10 μm to 20 μm in diameter woven into yarns 37 picks per inch by 36 ends per inch [38]. The fabrics are soaked in a PZT slurry before being arranged into the desired structure. The carbon is then burned out and the resulting PZT relic is sintered to leave a structure similar to the original carbon template. A piezoelectric/polymer composite is subsequently formed by infiltrating this structure with epoxy. The weave and shell configurations both exhibit 2-3 connectivity. The weave has an interconnected checkerboard pattern. The shell consists of fibers rolled in a helical fashion around a center point.

Another type of 3-1 composite configuration utilizes a thin-walled 3-D interconnected piezoceramic frame (also known as a honeycomb). The first honeycombs were poled in directions either parallel or perpendicular (transverse) to the extrusion direction with the epoxy and PZT phases connected mechanically in parallel and series, respectively [26]. Recently, a configuration has been devised where the poling direction of the piezoceramic is parallel to the frame direction [39]. Thus, the composite operates in the d_{31} mode. The high hydrostatic response comes from the sum of the individual responses of the three orthogonal directions of the frame. That makes this composite better than a capped cylinder, in which only the axial direction contributes to the hydrostatic response.

Two configurations of this composite have been fabricated. The first had the top and bottom of the frame covered with flat caps, leaving the empty space inside filled only with air. In this particular case, the d_{33} response of the piezoceramic is completely eliminated because the stress component perpendicular to the wall is zero.

The second configuration simply had the space within the frame infiltrated with a soft epoxy. Now, the d_{33} component is no longer suppressed because the stress component perpendicular to the wall is no longer zero. Nevertheless, since the frame is three dimensionally interconnected, the Poisson's ratio effect in the polymer phase (which is

quite detrimental for 1-3 composites) is still greatly reduced. A complete listing of properties for these composites is shown in Table 7.

• *Composites with 1-3 connectivity*

Unquestionably, the composites with 1-3 connectivity are the most extensively studied, understood, and utilized of all the two-phase connectivity types. This type of composite consists of individual PZT rods, or fibers, aligned in a direction parallel to the poling direction and surrounded by a polymer matrix. A decoupling of the d_{33} and d_{31} coefficients of the composite enhances the d_h. The rod diameter, rod spacing, composite thickness, volume percent of rods, and polymer compliance all influence the composite performance.

The first 1-3's were made from extruded PZT rods, ranging in diameter from 254 μm to 840 μm, which were aligned in a specially designed fixture which allowed for the epoxy to be poured around the rods [40]. Because of the labor intensive procedure, this technique does not lend itself well to mass production. The dice and fill technique [41] lends itself better to the mass production of smaller samples, but is too costly to meet the needs of large area coverage [32]. This technology involves the cutting of deep grooves into a solid block of PZT using a diamond saw. Square rods with sides of length down to 50 μm are achievable with aspect ratios approaching twenty [42].

Cao, Zheng, and Cross [43] have shown that the stress transfer in 1-3 composites is accomplished through shear coupling at the interface between the ceramic and the polymer. The effectiveness of the stress transfer can be characterized by a stress amplification factor which depends upon the elastic properties of both phases, the ceramic content, and most importantly, the aspect ratio (radius/length) of the ceramic rods. These same parameters also affect the displacement uniformity over the surface of the composite [44]. When subject to a hydrostatic pressure, the stress applied in the transverse direction reduces the stress enhancement effect in the axial direction. This is due to the Poisson's

ratio effect. When squeezed from both sides, the polymer bulges, pulling on the ceramic rods and trying to lengthen them. Hence, under hydrostatic pressure, the stress amplification factor is practically reduced by a factor of $(1-2\sigma)$, where σ is Poisson's ratio. Essentially, this produces a contribution to the d_{31} of the composite from the d_{33} of the ceramic [45], which in turn lowers the d_h of the structure.

A number of design modifications have been investigated to alleviate this problem. The incorporation of air pockets into the composite to absorb the lateral strain seems to be the preferred solution. This has been done by drilling air holes through the epoxy matrix in a direction parallel to the PZT rods [46], eliminating the interface between the PZT and the polymer matrix, allowing the stress transfer to instead be realized by armature plates located on the upper and lower surfaces of the composite [47], introducing pores or hollow glass spheres into the polymer matrix [48], and lastly, utilizing hollow, radially poled PZT tubes, which operate in the d_{31} mode instead of the d_{33} mode as in the case of rods [49,50]. Introducing a softer polymer matrix between the PZT rod and the harder epoxy has also been investigated [51] as well as incorporating glass fibers in the lateral direction to support the transverse direction stress [48]. Capping the rods serves to distribute the stress more uniformly over the active PZT surface and further decreases coupling of the Poisson stress components in the plane normal to the poled direction [52].

Square rods can give rise to undesirable inter-post resonant activity. This problem can be alleviated if circular or irregularly shaped rods are used instead [46]. By dicing a honeycomb configuration, "+", "L", and "T" shapes were easily fabricated [38]. Materials Systems Inc. has developed new technology for the mass production of large area 1-3 composites using an injection molding process [53]. This process is capable of producing arrays with rod diameters <100 μm. It is also possible to easily vary the PZT element type, layout, and shape. A comparison of the properties of various 1-3 composite designs is provided in Table 8.

• *Composites with 2-2 connectivity*

For large area acoustic projectors, it is necessary to generate large surface displacements while operating at a moderate driving voltage to get high radiative power over a wide frequency range. The 1-3 type composites often cannot meet these requirements. In addition, the d_h coefficient is limited by the longitudinal piezoelectric strain coefficient d_{33}. This can be alleviated by increasing the thickness, but at the cost of a higher electrical impedance. As in the case of the 1-3 composites, the strain profile across the surface of a 2-2 composite with a lamellar configuration is inhomogeneous due to the different elastic stiffnesses of the two components. The stress transfer between the two phases depends on the volume percent of active component as well as the aspect ratio of the two components [54]. Pressure induced depolarization can also become serious in a composite with low piezoelectric content. The 1-3 tubular composites operate in the d_{31} mode and do not depole under high pressures. Unfortunately, their manufacturing cost is high. The 2-2 piezocomposite operating in the transverse d_{31} mode possesses the advantages of the PZT tubular composite but with lower manufacturing costs and a simpler fabrication process [55]. This composite has thin piezoelectric plates forming a parallel array imbedded in a polymer matrix. The ceramic plates are electroded over the side faces with the polarization direction parallel to the acoustic radiation plane, i.e. they are transversely poled (TP). From Table 9, it can be seen that this new transverse operating mode 2-2 composite exhibits much better performance than the conventional longitudinal mode 2-2 designs, which are simply layers of PZT sandwiched between layers of polymer [55, 38].

PIEZOELECTRIC CERAMIC-METAL COMPOSITES

Ceramic-metal composites are generally characterized by their simple designs and robustness. In these composites, metal faceplates, shells, or caps are coupled to both the

active ceramic as well as the surrounding medium and are the means by which the incident stress is transferred to the ceramic. The best ceramic-metal composite sensors are the flextensional-type transducers. The term 'flextensional' is in fact derived from a combination of the two words describing how the transducer works: the flexural vibration of the metal shell causes an extensional (or contractional) vibration of the piezoelectric element [56]. Flextensional transducers are typically quite large, in terms of both size and weight. The 'moonie' and 'cymbal' type transducers are miniaturized versions of flextensionals.

The moonie and cymbal transducers possess 2-(0)-2 connectivity. These transducers consist of a poled piezoelectric disk (fully electroded on each face) which is sandwiched between two metal endcaps, each containing a shallow air-filled cavity on their inner surface. In the case of the moonie, the cavities are in the shape of a half moon, whereas the cymbal has a truncated cone-shaped cavity (Figure 5). The presence of these cavities allows the metal caps to serve as mechanical transformers for transforming and amplifying a portion of the incident axial-direction stress into tangential and radial stresses of opposite sign. Thus, the d_{31} and d_{33} contributions of the PZT now add together (rather than subtracting) in the effective d_h of the device [57]. For a moonie transducer 12.7 mm in diameter with a brass cap thickness of 0.3 mm, cavity diameter of 9 mm, and maximum cavity depth of 200 μm, an effective d_{33} coefficient of about 9000 pC/N has been reported [58]. In addition, a $d_h \cdot g_h$ product exceeding 50000 m^2/N is achievable [59]. A cymbal transducer, on the other hand, with brass caps 0.20 mm thick, cavity diameter of 9 mm, and maximum cavity depth of 200 μm will exhibit an effective d_{33} coefficient of at least 15000 pC/N [60] and a $d_h \cdot g_h$ product upwards of 100,000 m^2/N [57]. The higher sensitivity in the case of the cymbal as compared to the moonie is at a cost of an increase in pressure dependence on its performance [57].

FUTURE TRENDS

Since the 1950's, lead oxide based compounds have been the leading materials for piezoelectric transducers due to their excellent dielectric and piezoelectric properties. However, with the increased public awareness on health concerns associated with lead and the recent changes in environmental policies, lead containing materials are now perceived as a health hazard. Therefore, increased research activity on Pb-free piezoelectric materials, in addition to the current intense efforts, are expected in the future. Additionally, research on piezoelectric single crystals in which very high strains can be induced, as in the recent example of PZN-PT and PMN-PT [61], and other lead-based as well as lead-free morphotropic phase boundary materials would be expected to continue yielding commercially available materials. An additional application which is gaining importance is the need for and the use of piezoelectric materials at cryogenic temperatures in outer space. Deep ocean exploration will also require highly sensitive piezoelectric materials which can operate at low temperatures (~4°C) and under high hydrostatic pressures (20 MPa). Most importantly, ferroelectric thin films are expected to form a major part of piezoelectric device applications.

SUMMARY

Beginning with the discovery of ferroelectricity in $BaTiO_3$ and with the development of applications such as, electroacoustic transformers, signal processing devices, actuators and sensors piezoelectric materials have became an important part of engineering applications, as well as daily life. This is evidenced by a review of piezoelectric sensors and sensors materials and an examination of the properties of the most common piezoelectric ceramic material: PZT, as well as other piezoelectric ceramics and single crystals. Several sensor configurations can be prepared from bulk ceramics as can piezoelectric ceramic - polymer composite sensors described by the connectivity of their constituent phases. A wide range of hydrophone figure of merit ($d_h \cdot g_h$) can be engineered

through these sensor configurations. Recent examples of piezoelectric ceramic - metal composite sensors, and the future trends in the area of piezoelectric sensors show that piezoelectric sensors have established a solid presence in our daily life from ultrasound applications in medicine, to underwater ultrasound in military and civilian applications, to smart sensor systems in automobiles, to non-destructive testing in industry. They will continue to increase their impact even further with emerging technologies, improved material properties, and with an increased understanding of piezoelectric and ferroelectric phenomena.

ACKNOWLEDGMENTS

A major part of the research on piezoelectric sensors and sensor materials at Materials Research Laboratory at The Pennsylvania State University has been supported by the Office of Naval Research (ONR) and National Science Foundation (NSF). The authors would like to thank for their financial support.

REFERENCES

1. R. Maines, *Sensors*, **6**, 26 (1989).

2. D. Damjanovic and R.E. Newnham, *J. Intell. Mater. Struct.*, **3**, 190 (1992).

3. R. Barrett and F. Wilcoxon, *Sensors*, **10**, 16 (1993).

4. R.E. Newnham, *MRS Bulletin*, **22**, 20 (1997).

5. A.J. Moulson and J.M. Herbert, *Electroceramics* (Chapman & Hall, New York, 1992), p. 266.

6. H. Jaffe and D. Berlincourt, *Proc. IEEE*, **53**, 1372 (1965).

7. G.H. Haertling, in *Ceramic Materials for Electronics, Processing, Properties, and Applications*, edited by R.C. Buchanan (Marcel Dekkar, New York, 1986) p. 165.

8. B. Jaffe, W.R. Cook, and H. Jaffe, *Piezoelectric Ceramics* (Academic Press, New York, 1971), p. 148.

9. D. Berlincourt, *J. Acoust. Soc. Am.*, **70**, 1586 (1981).

10. A.S. Bhalla and R.Y. Ting, *Sensors and Materials*, **4**, 181 (1988).

11. T.B. Gabrielson, Presented at tha 1997 ONR Transducer Materials and Transducers Workshop, The Pennsylvania State University, April 1997.

12. O.B. Wilson, *Introduction to the Theory and Design of Sonar Transducers* (Peninsula Publishing, Los Altos, CA, 1988), p. 65.

13. R.C. Turner, P.A. Fuirer, R.E. Newnham, and T.R. Shrout, *Appl. Acoustics*, **41**, 1 (1993).

14. T. Ikeda, *Fundamentals of Piezoelectricity* (Oxford University Press, New York, NY, 1990), p. 209.

15. Morgan Matroc company product literature.

16. K.M. Rittenmyer and R.Y. Ting, in *Electronic Materials: Technology, Here and Now*, edited by R. Keyson, D. Basiulis, and B. Woon (Society for the Advancement of Material & Process Engineering, 1991), p.24.

17. J.A. Gallego-Juarez, *J. Phys. E: Sci. Instrum.*, **22**, 804 (1989).

18. R.G. Seippel, *Transducers, Sensors, and Detectors* (Reston Publishing Co., Reston, VA, 1983), p. 115.

19. O.B. Wilson, *Introduction to the Theory and Design of Sonar Transducers* (Peninsula Publishing, Los Altos, CA, 1988), p. 124.

20. J.T. Fielding, Jr., D. Smith, R.J. Meyer, Jr., S. Trolier-McKinstry, and R.E. Newnham, in *Proc. 9th IEEE Intl. Symp. Apps. Ferroelectrics*, edited by R.K. Pandey, M. Liu, and A. Safari (IEEE, New York, 1995), p. 202.

21. S. Alkoy, A. Dogan, A-C. Hladky, P. Langlet, J.K. Cochran, and R.E. Newnham, *IEEE Trans. UFFC*, **44**, 1067 (1997)

22. K. Uchino, *Piezoelectric Actuators and Ultrasonic Motors* (Klewer Academic Publishers, Boston, 1997)

23. G.H. Haertling, *Am. Ceram. Soc. Bull.*, **73**, 93 (1994).

24. S. Sherrit, H.D. Wiederick, B.K. Mukherjee, and G.H. Haertling, in *Proc. 9th IEEE Intl. Symp. Apps. Ferroelectrics*, edited by R.K. Pandey, M. Liu, and A. Safari (IEEE, New York, 1995), p. 390.

25. R.E. Newnham, D.P. Skinner and L.E. Cross, *Mat. Res. Bull.*, **13**, 525 (1978)

26. T.R. Gururaja, A. Safari, R.E. Newnham, and L.E. Cross, in *Electronic Ceramics: Properties, Devices, and Applications*, edited by L.M. Levinson (Marcel Dekkar, New York, 1988) p 92.

27. M.J. Creedon, S. Gopalakrishnan, and W.A. Schulze, in *Proc. 9th IEEE Intl. Symp. Apps. Ferroelectrics*, edited by R.K. Pandey, M. Liu, and A. Safari (IEEE, New York, 1995) p. 299.

28. D.P. Skinner, R.E. Newnham, and L.E. Cross, *Mat. Res. Bull.*, **13**, 599 (1978).

29. A. Safari, R.E. Newnham, L.E. Cross, and W.A. Schulze, *Ferroelectrics*, **41**, 197 (1982).

30. R.C. Twiney, *Adv. Mater.*, **4**, 819 (1992).

31. H. Banno, *Ferroelectrics*, **50**, 3 (1983).

32. R.Y. Ting, *Ferroelectrics*, **102**, 215 (1990).

33. R.Y. Ting, *Appl. Acoustics*, **41**, 325 (1994).

34. R.Y. Ting, and F.G. Geil, in *1990 IEEE 7th Intl. Symp. App. Ferroelectrics* (IEEE, New York, 1991) p. 14.

35. R.Y. Ting, *IEEE Trans. Inst. Msmt.*, **41**, 64 (1992).

36. S. Egusa and N. Iwasawa, *J. Intell. Mater. Sys. Struct.*, **5**, 140 (1994).

37. R.E. Newnham, J.F. Fernandez, K.A. Markowski, J.T. Fielding, A. Dogan, and J. Wallis, *Mat. Res. Soc. Proc.*, **360**, 33, 1995.

38. V.F. Janas, S.M. Ting, S.S. Livneh, F.R. Walker, R. Schaeffer, T.F. McNulty, and A. Safari, in *Proc. 9th IEEE Intl. Symp. Apps. Ferroelectrics*, edited by R.K. Pandey, M. Liu, and A. Safari (IEEE, New York, 1995) p 295.

39. Q.M. Zhang, H. Wang, J. Zhao, J.T. Fielding, R.E. Newnham, and L.E. Cross, *IEEE Trans. UFFC*, **43**, 36 (1996).

40. K.A. Klicker, J.V. Biggers, and R.E. Newnham, *J. Am. Ceram. Soc.*, **64**, 5 (1981).

41. W.A. Smith, *SPIE*, **1733**, 3 (1992).

42. W.A. Smith and A.A. Shaulov, *Ferroelectrics*, **87**, 309 (1992).

43. W. Cao, Q.M. Zhang, and L.E. Cross, *J. Appl. Phys.*, **72**, 5814 (1992).

44. W. Cao, *Ceramic Engineering and Science Proc.*, **17**, 83 (1996).

45. W.A. Smith. in *1990 IEEE 7th Intl. Symp. Apps. Ferroelectrics*, (IEEE, New York, 1990) p. 145.

46. J.A. Hossack, and R.L. Bedi, *Key Engr. Mater.*, **92-93**, 301 (1994).

47. L. Eyraud, C. Richardand D. Guyomar, *in 1994 Ultrasonic Symposium Proceedings*, edited by M. Levy, S.C. Schneider, and B.R. McAvoy (IEEE, New York, 1994) p. 929.

48. M.J. Haun, R.E. Newnham, and W.A. Schulze, *Adv. Ceram. Mater.*, **1**, 361 (1986).

49. Q.M. Zhang, H. Wang, and L.E. Cross, *J. Mater. Sci.*, **28**, 3962 (1993).

50. J. Chen, Q.M. Zhang, L.E. Cross, and M. Trottier, in *Proc. 9th IEEE Intl. Symp. Apps. Ferroelectrics*, edited by R.K. Pandey, M. Liu, and A. Safari (IEEE, New York, 1995) p. 746.

51. C. Kim, K.M. Rittenmyer, and M. Kahn, *Ferroelectrics*, **156**, 19 (1994).

52. R.Y. Ting, *Ferroelectrics*, **67**, 143 (1986).

53. L. Bowen, R. Gentilman, D. Fiore, H. Pham, W. Serwatka, C. Near, and B. Pazol, *Ferroelectrics*, **187**, 109 (1996).

54. W. Cao, Q.M. Zhang, and L.E. Cross, *IEEE Trans. UFFC* , **40**, 103 (1993).

55. Q.M. Zhang, J. Chen, H. Wang, J. Zhao, L.E. Cross, and M.C. Trottier, *IEEE Trans. UFFC*, **42**, 774 (1995).

56. K.D. Rolt, *J. Acoust. Soc. Am.*, **87**, 1340 (1990).

57. J.F. Tressler, A. Dogan, J.F. Fernandez, J.T. Fielding, Jr., K. Uchino, and R.E. Newnham, in *1995 IEEE Ultrasonics Symposium Proceedings*, edited by M. Levy, S.C. Schneider, and B.R. McAvoy (IEEE, Piscataway, NJ, 1995), p. 897.

58. K. Onitsuka, A. Dogan, J.F. Tressler, Q.C. Xu, S. Yoshikawa, and R.E. Newnham, *J. Intell. Mat. Sys. Struct.*, **6**, 447 (1995).

59. Q.C. Xu, S. Yoshikawa, J.R. Belsick, and R.E. Newnham, *IEEE Trans. UFFC*, **38**, 634 (1991).

60. A. Dogan, K. Uchino, and R.E. Newnham, *IEEE Trans. UFFC*, **44**, 597 (1997).

61. S.-E. Park and T. R. Shrout, *J. Appl. Phys.*, **82**, No.4, 1804 (1997)

62. Y. Xu, *Ferroelectric Materials and Their Applications* (North-Holland, Amsterdam, The Netherlands, 1991), p. 217, 277

63. M.M. Choy, W.R. Cook, R.F.S. Hearmon, H. Jaffe, J. Jerphagnon, S.K. Kurtz, S.T. Liu and *Landolt-Börnstein Numerical Data and Functional Relationships in Science and Technology*, edited by K.-H. Hellwege and A.M. Hellwege, (Springer-Verlag, Heidelberg, New York, 1979), Vol. 11, p. 328

LIST OF FIGURES

LIST OF TABLES

Table 1. Listing of common ion substitutions in PZT [7,62]

Pb-site donors :	La^{3+}, Bi^{3+}, Nd^{3+}, Sb^{3+}, Th^{4+}
(Ti-Zr)-site donors:	Nb^{5+}, Ta^{5+}, Sb^{5+}, W^{6+}
Pb-site acceptors:	K^{+}, Na^{+}, Rb^{+}
(Ti-Zr)-site acceptors:	Fe^{3+}, Al^{3+}, Sc^{3+}, In^{3+}, Cr^{3+}, Co^{3+}, Ga^{3+}, Mn^{3+}, Mn^{2+}, Mg^{2+}, Cu^{2+}
isovalent substitutions:	Sr^{2+}, Ca^{2+}, Ba^{2+} (for Pb^{2+}), Sn^{4+} (for Ti^{4+} or Zr^{4+})
multivalent ions:	Cr, U

Table 2. Room temperature properties of common piezoelectric crystals

crystal name	chemical formula	point group	max. piezoelec. charge coef. (pC/N)		Dielectric Constant K_{11}^T	Dielectric Constant K_{33}^T	Ref.
Amonium Dihydrogen Phosphate (ADP)	$NH_4H_2PO_4$	42m	50.0	(d_{36})	55.0	15.0	[63]
Barium Sodium Niobate (BNN)	$Ba_2NaNb_5O_{15}$	mm2	52.0	(d_{24})	246.0	51.0	[62,63]
Barium Titanate	$BaTiO_3$	4mm	392.0	(d_{15})	2920.0	168.0	[63]
Ethylene Diamine Tartrate (EDT)	$C_6H_{14}N_2O_6$	2	-12.3	(d_{23})	5.0	6.0	[63]
Lead Barium Niobate (PBN)	$Pb_{0.37}Ba_{0.63}Nb_2O_6$	4mm	108.0	(d_{15})	600.0	135.0	[62]
Lead Potassium Niobate (PKN)	$Pb_2KNb_5O_{15}$	mm2	470.0	(d_{15})	1550.0	129.0	[63]
Lead Niobate	$PbNb_2O_6$	mm2	45.0	(d_{33})	-	180.0	[63]
Lithium Niobate	$LiNbO_3$	3m	68.0	(d_{15})	84.0	30.0	[14,62]
Lithium Sulfate	$LiSO_4 \cdot H_2O$	2	16.2	(d_{22})	5.6	6.5	[63]
Lithium Tantalate	$LiTaO_3$	3m	26.0	(d_{15})	51.0	45.0	[14,62]
Quartz	SiO_2	32	2.3	(d_{11})	4.6	4.7	[63]
Potassium Dihydrogen Phosphate (KDP)	KH_2PO_4	42m	23.2	(d_{36})	44.0	21.0	[62,63]
Rochelle Salt	$NaKC_4H_4O_6 \cdot 4H_2O$	222	2300.0	(d_{14})	1100.0	9.2	[62,63]

Table 2. Room temperature properties of common piezoelectric crystals [continued]

crystal name	chemical formula	point group	max. piezoelec. charge coef. (pC/N)		Dielectric Constant K_{11}^T	Dielectric Constant K_{33}^T	Ref.
Sodium Chlorate	$NaClO_3$	23	1.7	(d_{14})	5.8		[63]
Triglycine Sulfide (TGS)	$(NH_2CH_2COOH)_3.H_2SO_4$	2	25.3	(d_{23})	8.6	5.7	[62,63]
Tourmaline	$CaAl_3Mn_6(BO_3)_3(SiO_3)_6(OH)_4$	3m	3.6	(d_{15})	8.2	7.5	[63]
Zinc Sulfide	ZnS	6mm	3.2	(d_{33})	8.6	8.0	[63]

Table 3. Properties of Lead Zirconate Titanate (PZT) ceramics ['d' coeff. in (pC/N)]

Designation	T_c(°C)	d_{33}	d_{31}	d_{15}	K_{33}^T	k_{33}	k_{31}	k_{15}	Ref
PZT-2	370	152	-60	440	450	0.63	-0.28	0.70	[63]
PZT-4	325	285	-122	495	1300	0.70	-0.33	0.71	[15]
PZT-4D	320	315	-135	n/a	1450	0.71	-0.34	n/a	[15]
PZT-5A	365	374	-171	585	1700	0.71	-0.34	0.69	[15]
PZT-5B	330	405	-185	564	2000	0.66	-0.34	0.63	[15]
PZT-5H	195	593	-274	741	3400	0.75	-0.39	0.68	[15]
PZT-5J	250	500	-220	670	2600	0.69	-0.36	0.63	[15]
PZT-5R	350	450	-195	n/a	1950	n/a	-0.35	n/a	[15]
PZT-6A	335	189	-80	n/a	1050	0.54	-0.23	n/a	[63]
PZT-6B	350	71	-27	130	460	0.37	-0.15	0.38	[63]
PZT-7A	350	153	-60	360	425	0.67	-0.30	0.68	[15]
PZT-7D	325	225	-100	n/a	1200	n/a	-0.28	n/a	[15]
PZT-8	300	225	-97	330	1000	0.64	-0.30	0.55	[15]

Table 4. Properties of other common piezoelectric ceramics

Chemical Formula	Cryst. Struct.*	T_c (°C)	K_{33}^T	d_{33} (pC/N)	d_{31} (pC/N)	d_{15} (pC/N)	k_{33}	k_{31}	k_{15}	Ref.
$BaTiO_3$	P	115	1700	190	-78	260	0.50	0.21	0.48	[63]
$PbTiO_3$	P	470	190	56	-	68	0.45	-	-	[13]
$PbNb_2O_6$	TB	570	225	85	9	-	0.38	>0.045	-	[17,63]
$KNaNb_2O_6$	TB	420	495	127	-51	306	0.60	-0.27	-0.46	[63]
$Ba_{0.4}Pb_{0.6}Nb_2O_6$	TB	260	1500	~220	-90	-	~0.55	~0.22	-	[63]
$LiNbO_3$	C	1150	25	6	-	69	0.23	-	0.60	[13]
$Na_{0.5}Bi_{0.5}Ti_2O_5$	B	320	300	~70	~15	-	~0.40	~0.10	-	[63]

* P : Perovskite, TB : Tungsten Bronze, C : Corundum, B : Bismuth

Table 5. Comparison of hydrostatic properties of composites with 3-3 connectivity

technique	d_h	g_h	$d_h \cdot g_h$	K^T	matrix	reference
replamine	36	140	5040	50	silicone rubber	[27]
BURPS	260	100	26000	300	silicone rubber	[26]
BURPS	120	27	3200	500	epoxy	[26]
Mitsubishi	90	50	4500	200	epoxy	[27]
reticulated	30	25	750	135	epoxy	[28]

Table 6. Comparison of hydrostatic properties of composites with 0-3 and 3-0 connectivity

technique	d_h	g_h	$d_h \cdot g_h$	K^T	matrix	reference
3-0 macrovoid	150	30	4500	560	air	[27]
0-3 PZT/polymer	28.3	32	900	100	silicone rubber	[26]
0-3 *PiezoRubber*	44	111	4884	45	elastomer	[37]

Table 7. Comparison of hydrostatic properties of composites with 3-1, 3-2, and 2-3 connectivity

technique	d_h	g_h	$d_h \cdot g_h$	K^T	matrix	reference
perforated 3-1	222	56	12300	450	epoxy	[26]
parallel h-comb	20	5	100	450	polymer	[27]
transverse h-comb	100	30	3000	400	polymer	[27]
d_{31} honeycomb	4700	1.02	4800	520	air	[39]
d_{31} honeycomb	4666	0.92	4316	570	polymer	[39]
perforated 3-2	329	128	42000	290	epoxy	[26]
2-3 weave	80	65	5200	140	epoxy	[38]
2-3 shell	80	60	4800	150	epoxy	[38]

Table 8. Comparison of hydrostatic properties of composites with 1-3 connectivity

technique	d_h	g_h	$d_h \cdot g_h$	K^T	matrix	reference
PZT particles	29	32	900	100	polymer	[27]
PZT spheres	23	4	96	410	polymer	[27]
extruded rods	176	239	42064	83	polymer	[26]
dice & fill	52	18	935	330	polymer	[52]
w/ armature plate	160				air/epoxy	[47]
w/ glass rods	203	220	44700	104	epoxy	[48]
w/ 2 polymers	288	78	22464	416	epoxy	[51]
diced honeycomb	75	15	1125	660	epoxy	[38]
PZT tubes	5502	1.2	6389	2922	epoxy	[39]
sonopanel	268	66	17688	460	polyurethane	[53]

Table 9. Comparison of hydrostatic properties of composites with 2-2 connectivity

technique	d_h	g_h	$d_h \cdot g_h$	K^T	matrix	reference
2-2 laminate	50	16.6	830	340	epoxy	[55]
2-2 (TP)	6000	5	30000	136	polyurethane	[55]
2-2 tape cast	25	10	250	300	epoxy	[38]

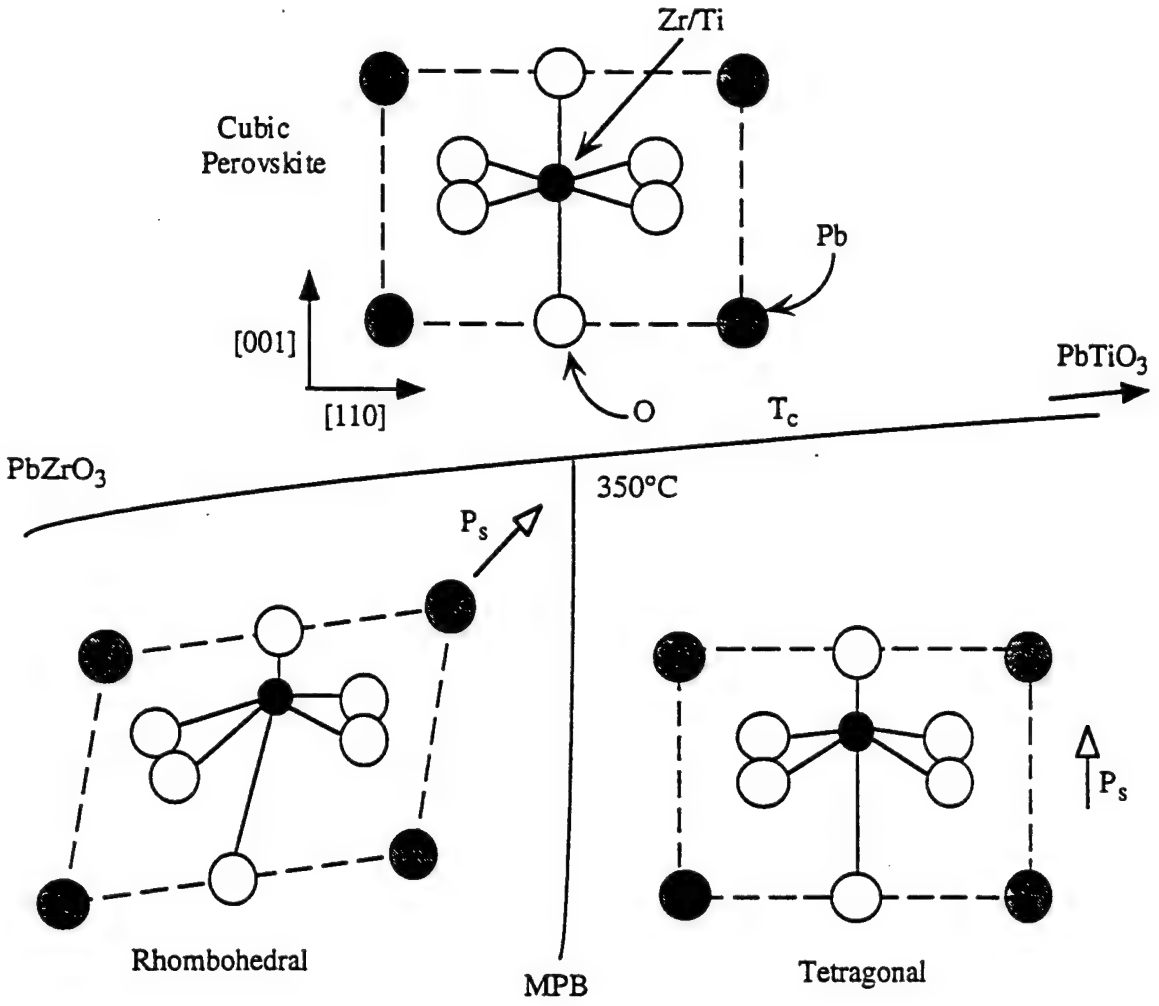

Figure 1. A portion of the $PbZrO_3$ - $PbTiO_3$ phase diagram showing the structural changes at the Curie temperature and the morphotropic phase boundary (MPB). Compositions near the morphotropic phase boundary have 14 possible poling directions [4]

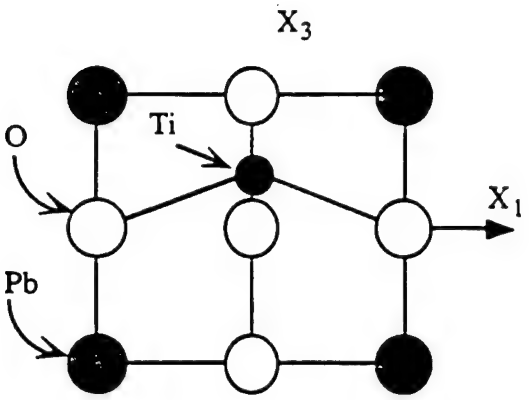

(a) $PbTiO_3$ - Symmetry 4mm

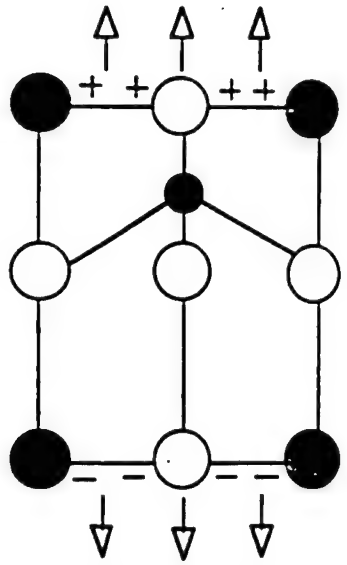

(b) $\Delta P_3 = d_{33}\,\sigma_3$ (d_{33} ~ 120 pC/N)

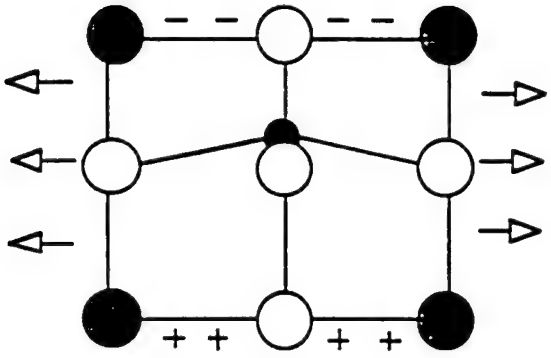

(c) $\Delta P_3 = d_{31}\,\sigma_1$ (d_{31} ~ 50 pC/N)

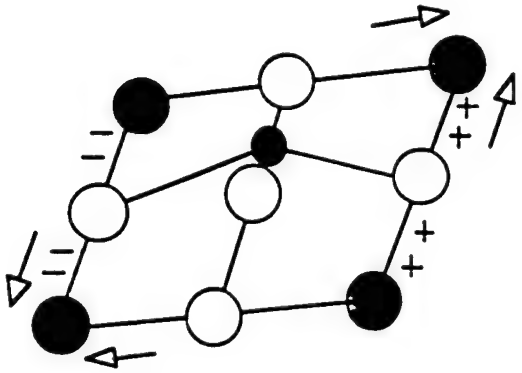

(c) $\Delta P_3 = d_{15}\,\sigma_5$ (d_{15} ~ 300 pC/N)

Figure 2. Intrinsic piezoelectric effect in polar lead titanate [4].

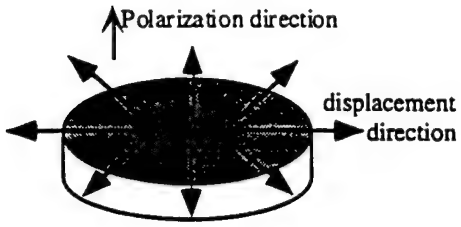

Thin disc radial mode

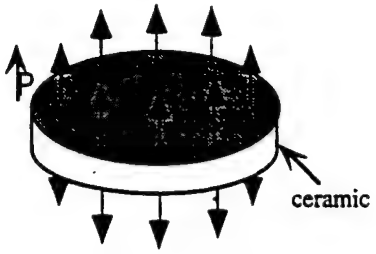

Thin disc thickness mode

Long thin bar length mode

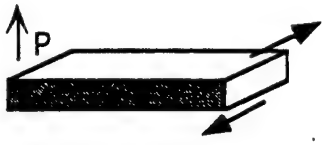

Shear plate (d_{15} mode)

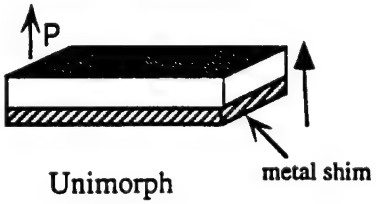

Unimorph

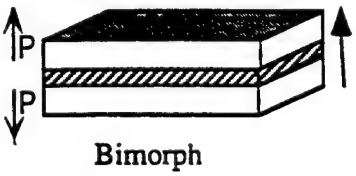

Bimorph

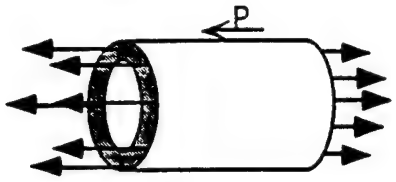

Thin wall tube length mode

Thin wall tube thickness mode

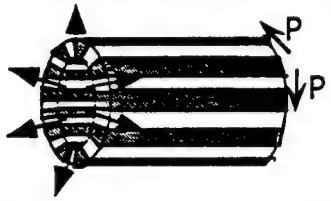

Thin wall tube radial (hoop) mode

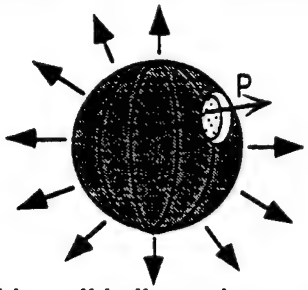

Thin wall hollow sphere, radially poled,breathing mode

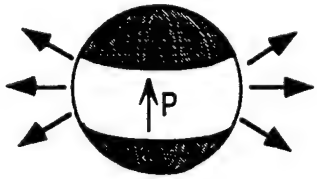

Thin wall hollow sphere tangentially poled, ellipsoidal mode

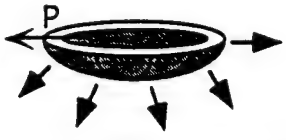

RAINBOW (monomorph)

Figure 3. Sensor configurations

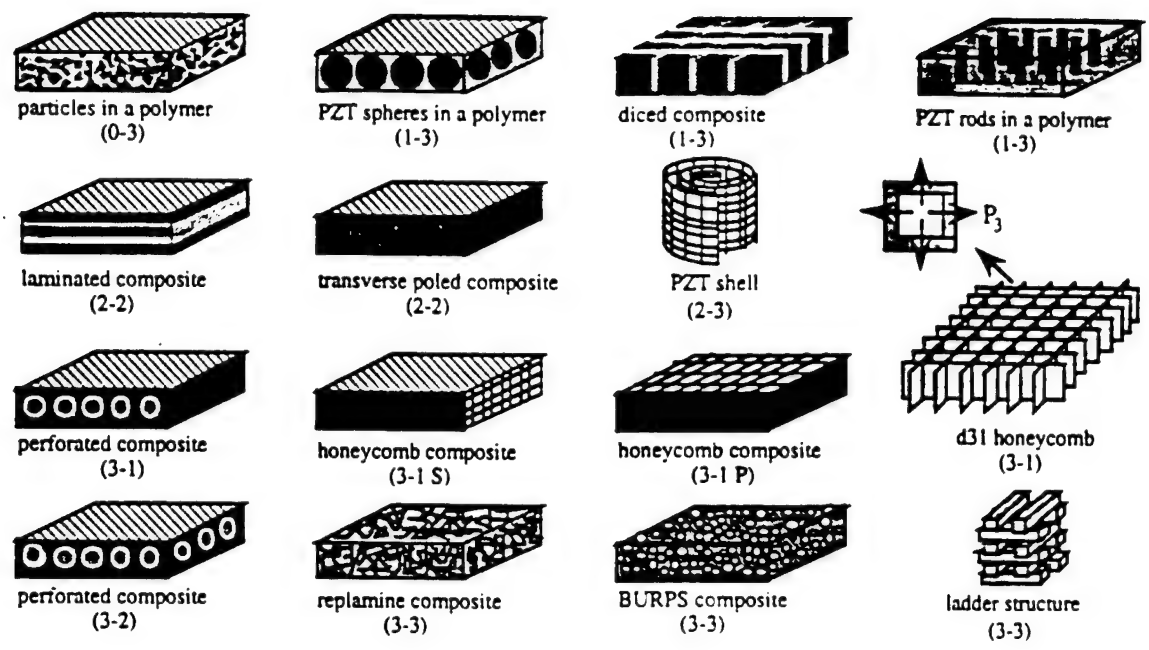

Figure 4. Connectivity of constituent phases in piezoelectric ceramic - polymer composites

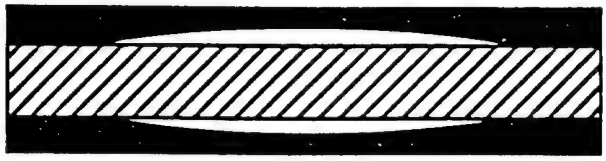

(a) Moonie Structure

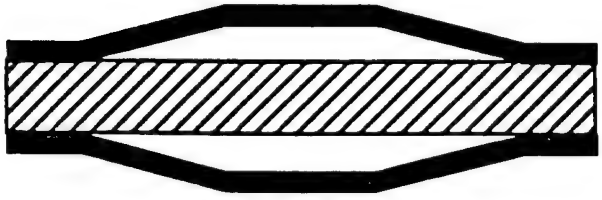

(b) Cymbal structure

Figure 5. Cross-sectional views of the (a) moonie and (b) cymbal transducers. The dark areas represent the caps, and the hatched areas the PZT disk.

APPENDIX 37

FUNCTIONAL COMPOSITES FOR SENSORS, ACTUATORS, AND TRANSDUCERS

J.F. Tressler, S. Alkoy, A. Dogan[a], and R.E. Newnham

Materials Research Laboratory, Pennsylvania State University, University Park, PA 16802

ABSTRACT

Following the trend in structural applications, composite structures are being used more commonly in transducer applications to improve acoustic, mechanical and electrical performance of piezoelectric devices. Functional composite transducers for actuators and sensors generally consist of an active ceramic phase incorporated with a passive polymer phase, each of which has a phase transition associated with it. In this paper, several polymer-piezoelectric ceramic composite transducers, mostly designed for sensing hydrostatic waves, are discussed based on the connectivity of the constituent phases. Also discussed are some recent examples of metal-ceramic composites, and single element ceramic transducers with modified shapes for improved performance. A comparison of these designs are given based on their hydrophone figure of merit ($d_h \cdot g_h$).

INTRODUCTION

Composite materials have found use in a number of structural applications, but their use in the electronics industry has been relatively limited. As the advantages of composites, sensors, and actuators become more clear, this picture is expected to change.

Functional composites make use of a number of underlying ideas, including the following: connectivity patterns leading to field and force concentration; the use of periodicity and scale in resonant structures; the symmetry of a composite structure and its influence on physical properties; polychromatic percolation and coupled conduction paths; varistor action and other interfacial effects; sum, combination, and other product properties; coupled phase-transformation phenomena; and the important role that porosity and inner surface play in many functional composite materials. These ideas provide a basic understanding of functional composite sensors and actuators.

An important approach to making functional composites is to bring together two or more different materials, each of which has a phase transition associated with it. As an example, polymeric materials having phase transitions in which the elastic properties undergo large changes are combined with ferroelectric materials in which the dielectric properties have an associated instability. The two materials have different types of instability, allowing for the building up of structures especially good for sensing and actuating.

When constructing functional composites, one is generally not trying to optimize all of the tensor coefficients but only those appearing in the figure of merit. Combining a mechanically soft but electrically hard (with a low dielectric constant) polymer with a mechanically stiff but electrically soft ferroelectric ceramic in various connectivity schemes allows for the build-up of parallel and series connections that optimize particular combinations of tensor coefficients.

In addition to the ceramic polymer composites, other novel approaches in sensor and actuator design for improved performance and amplified sensing and/or actuation response include incorporating metals and ceramics into a composite structure, as well as modifying the geometry of the ceramic. One example of a metal-ceramic composite sensor configuration is the flextensional-type transducer, in which metal endcaps are used to transfer stress to the piezoelectric ceramic. Recent examples of flextensional transducers, namely the 'moonie' and the 'cymbal' type miniaturized versions will be discussed in the proceeding sections. Improving transducer performance through modified geometry will also be discussed using the shell shape monomorph 'rainbow' and the hollow spherical 'BB' transducers as examples.

CERAMIC-POLYMER COMPOSITES

Newnham, et al. [1], established the notation for describing the number of dimensions each phase is physically in contact with itself. To date, eight different types of two-phase piezoelectric composites (piezocomposites) have been studied: 0-3, 1-3, 2-2, 2-3, 3-0, 3-1, 3-2, and 3-3. In the case of piezocomposites, the first number in the notation denotes the physical connectivity of the active phase and the second number refers to the physical connectivity of the passive phase. A schematic of these different connectivities is shown in Figure 1.

Most ceramic-polymer composites have been used as hydrophones and as biomedical transducers. The purpose of the polymer is to detect a portion the hydrostatic stress in either the transverse or longitudinal direction, effectively eliminating either the g_{33} or g_{31} contribution to the g_h of the poled ceramic. Extensive investigations have been performed to determine which ceramic-polymer connectivity configuration will provide the optimum hydrophone performance. The optimum performance is associated with maximizing the figure-of-merit, which in this case is $d_h \cdot g_h$ product.

---

[a] Current address: Dept. of Ceramic Science, Eskisehir Anadolu University, Eskisehir, TURKEY

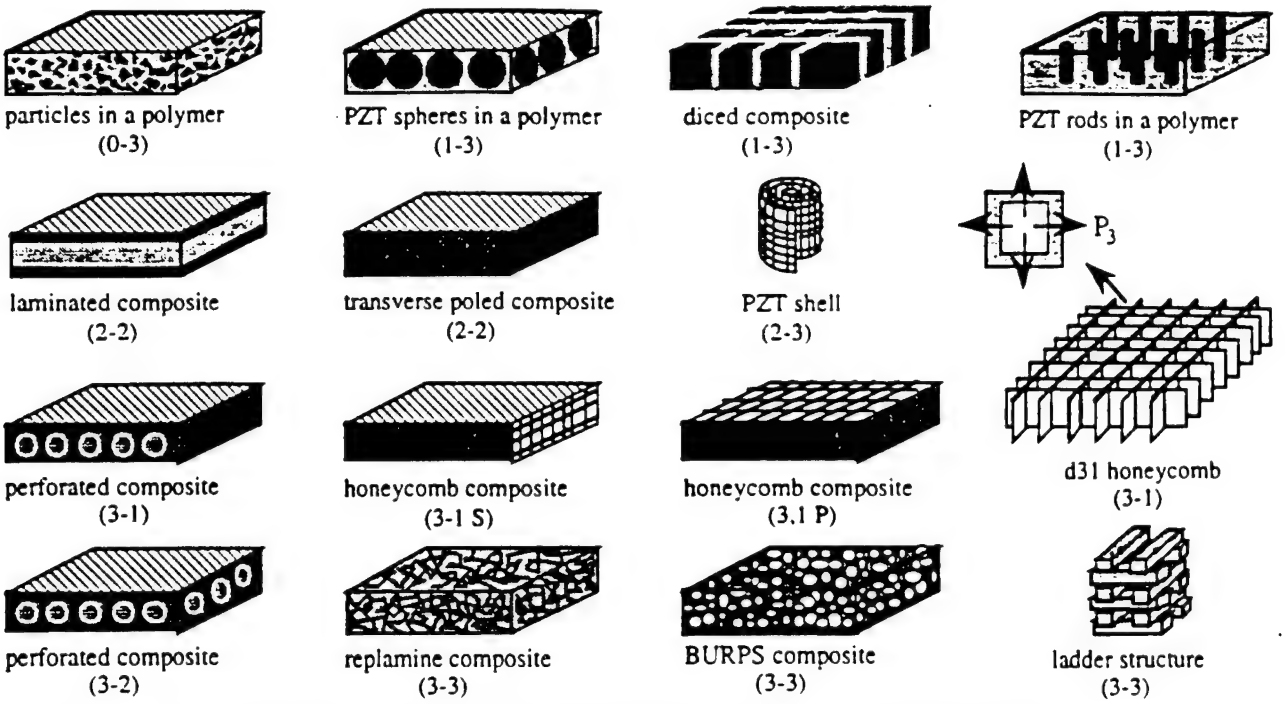

Figure 1. Connectivity of constituent phases in piezoelectric ceramics - polymer composites

The d_h coefficient is called the hydrostatic piezoelectric charge coefficient and is reported in terms of 10^{-12} Coulombs per Newton (pC/N). The g_h coefficient is the hydrostatic piezoelectric voltage coefficient and is reported in terms of 10^{-3} Volt•meters per Newton (mV•m/N).Thus, the figure of merit has units of 10^{-15} meters squared per Newton, or fm^2/N. In the proceeding sections examples of ceramic polymer composites with various connectivities are discussed.

Composites with 3-3 connectivity

Composites with 3-3 connectivity were the first of the two phase composites to be investigated. Composites with this connectivity have unpoled reinforcement in the lateral directions which serves to further decouple negative contributions from lateral stresses [2]. They were initially fabricated by a technique known as the replamine process [3] which involves the lost wax replication of a coral skeleton. Since then, additional technologies have been developed such as the fugitive phase, or BURPS, process [4] which produces a porous three-dimensionally interconnected ceramic structure by sintering a compacted mixture of volatilizable plastic spheres and PZT powder. Mitsubishi Mining and Cement has developed several techniques for introducing connected porosity into PZT ceramics: reactive sintering, foaming agents, organic additives, and careful control of particle size and firing conditions [5]. A reticulated ceramic technology has recently been used to produce 3-3 composites [2]. Reticulated ceramics are created by coating an organic foam substrate (i.e. polyurethane) with a ceramic slurry, pyrolyzing the foam, and then sintering the ceramic.

Composites with 0-3 and 3-0 connectivity

Composites with 0-3 connectivity consist of a random array of piezoelectric particles dispersed in a 3-D polymer matrix [6]. The primary advantage of these composites is their ability to be formed into shapes while remaining piezoelectrically active. These composites are manufactured commercially by NTK Technical Ceramic Division of the NGK Spark Plugs Corporation in Japan under the name *PiezoRubber* (NTK-306). PiezoRubber was developed by Banno and Saito and utilizes PT (lead titanate) rather than PZT in order to take advantage of the large piezoelectric anisotropy in PT [7]. The g_h value reported by NTK for their *PiezoRubber* depends on the volume fraction of ceramic present and can be pressure insensitive up to 35 MPa [8-11].

The first 3-0 composites were fabricated by a tape casting technique. Fugitive ink was screen printed onto green PZT sheets which were subsequently stacked. When the ink and binder were burned out and the ceramic sintered, the resultant PZT block contained pores where the ink was originally located. A second method for fabricating 3-0 composites consisted of hot pressing a mixture of large polymer spheres and PZT powder [5].

Composites with 3-1, 3-2, 2-3 connectivity

Conventional composites exhibiting 3-1 and 3-2 connectivity consist of a PZT block with holes drilled through either one side (3-1) or both sides (3-2) in a direction perpendicular to the poled direction of the PZT. The holes are subsequently backfilled with polymer. The one dimensional or two dimensional

interconnected polymeric phases in the transverse direction reduce the g_{31} and g_{32} contributions to the hydrostatic voltage response by decreasing the stress coupling in the plane normal to the poled direction [12]. A negligible change in properties occurs up to 7 MPa. In 3-1 and 3-2 composites manufactured in this way, the dielectric constant, as well as the d_h and g_h coefficients are all functions of hole size, PZT thickness, poling technique, and center-to-center distance between adjacent holes [5].

The relic process [13], in combination with a weaving technique, has been developed at the Rutgers University to easily manufacture large area composites consisting of fine PZT fibers interconnected in two dimensions and embedded in a 3-D interconnected polymer matrix (2-3 connectivity). In this process, carbon fabric fibers of 10 μm to 20 μm in diameter are soaked in PZT slurry and then woven into yarns with the desired structure. The carbon is then burned out and the resulting PZT relic is sintered to leave a structure similar to the original carbon template. A piezoelectric/polymer composite is subsequently formed by infiltrating with epoxy.

Another type of 3-1 composite configuration utilizes a thin-walled 3-D interconnected piezoceramic frame (also known as a honeycomb). The first honeycombs were poled in directions either parallel or perpendicular (transverse) to the extrusion direction with the epoxy phase and PZT connected mechanically in parallel and series, respectively [5]. Recently, a configuration has been devised where the poling direction of the piezoceramic is parallel to the frame direction [14]. Thus, it operates in the d_{31} mode. The high hydrostatic response comes from the sum of the individual responses of the three orthogonal directions of the frame. That makes this composite better than a capped cylinder, in which only the axial direction contributes to the hydrostatic response.

Composites with 1-3 connectivity

Unquestionably, the composites with 1-3 connectivity are the most studied, understood, and utilized of all the two-phase connectivity types. This composite consists of individual PZT rods or fibers aligned in a direction parallel to the poling direction and surrounded by a polymer matrix. A decoupling of the d_{33} and d_{31} coefficients of the composite enhances the d_h. The rod diameter, rod spacing, composite thickness, volume percent of rods, and polymer compliance all influence the composite performance.

The first 1-3's were made from extruded PZT rods, ranging in diameter from 254 μm to 840 μm, which were aligned in a specially designed fixture which allowed for the epoxy to be poured around the rods [15]. Because of the labor intensive procedure, this technique does not lend itself well to mass production. The dice and fill technique [16] is more easily adapted to the mass production of smaller samples, but is too costly to meet the needs of large area coverage [8]. This technology involves the cutting of deep grooves into a solid block of PZT using a diamond saw. Square rods with sides of length down to 50 μm are achievable with aspect ratios approaching twenty [17]. Square rods can give rise to undesirable inter-post resonant activity. This problem can be alleviated if circular or irregularly shaped rods are used instead [18]. By dicing a honeycomb configuration, "+", "L", and "T" shapes were easily fabricated [13]. Materials Systems Inc. has developed a new technology for the mass production of large area 1-3 composites using an injection molding process [19]. This process is capable of producing arrays with rod diameters <100 μm. It is also possible to easily vary the PZT element type, layout, and shape.

Cao, Zheng, and Cross [20] have shown that the stress transfer in 1-3 composites is accomplished through shear coupling at the interface between the ceramic and the polymer. The effectiveness of the stress transfer can be characterized by a stress amplification factor which depends upon the elastic properties of both phases, the ceramic content, and most importantly, the aspect ratio (radius/length) of the ceramic rods. These same parameters also affect the displacement uniformity over the surface of the composite [21]. When subject to a hydrostatic pressure, the stress applied in the transverse direction reduces the stress enhancement effect in the axial direction. This is due to the Poisson's ratio effect. When squeezed from both sides, the polymer bulges, pulling on the ceramic rods and trying to lengthen them. Hence, under hydrostatic pressure, the stress amplification factor is practically reduced by a factor of $(1\text{-}2\sigma)$, where σ is Poisson's ratio. Essentially, this produces a contribution to the d_{31} of the composite from the d_{33} of the ceramic [22], which in turn lowers the d_h of the structure.

Preparing a 1-3 composite using thin-wall piezoelectric hollow spheres as the active ceramic phase is also feasible. The resultant structure has a good acoustic matching with water due to the low acoustic impedance of polymer and the air-filled space in the ceramic part. Hollow spheres are discussed in more detail in the 'single element transducers' section.

Composites with 2-2 connectivity

For large area acoustic projectors, it is necessary to generate large surface displacements while operating at a moderate driving voltage to get high radiative power over a wide frequency range. The 1-3 type composites often cannot meet these requirements. In addition, the d_h coefficient is limited by the longitudinal piezoelectric strain coefficient d_{33}. The 2-2 piezocomposites might be an answer to these problems. In a 2-2 composite the stress transfer between the two phases depends on the volume percent of active component as well as the aspect ratio of the two components [23]. There are two different configurations for 2-2 composites: laminated 2-2 which consists of layers of PZT sandwiched between layers of polymer and poled through the layers, and 2-2 piezocomposites poled over the side faces,

parallel to the layers. The latter operates in the transverse d_{31} mode and possesses the advantages of the PZT 1-3 tubular composite but with lower manufacturing costs and a simpler fabrication process [24]. This transverse operating mode 2-2 composite also exhibits much better performance than the conventional longitudinal mode 2-2 laminated [13,24].

CERAMIC-METAL COMPOSITES

Ceramic -metal composites generally have a simple design with a metal faceplate, shell, or cap that couples to both the ceramic as well as the surrounding medium. The metal component transfers the incident stress to the ceramic or the displacement to the medium. Flextensional transducer are good examples of ceramic-metal composites. In flextensional transducers, the flexural vibration of the metal shell causes an extensional (or contractional) vibration of the piezoelectric element [25]. The miniaturized versions of flextensionals, the moonie and cymbal transducers possess 2-(0)-2 connectivity. These transducers, shown in Figure 2, consist of a poled piezoelectric disk (fully electroded on both faces) which is sandwiched between two metal endcaps, each containing a shallow air-filled cavity on their inner surface.

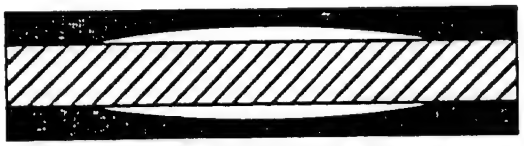

(a) Moonie Structure

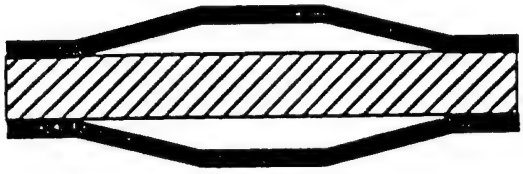

(b) Cymbal structure

Figure 2. Cross-sectional views of the (a) moonie and (b) cymbal transducers. The dark areas represent the caps, and the hatched areas the PZT disk

In the case of the moonie, the cavities are in the shape of a half moon, whereas the cymbal has a truncated cone-shaped cavity. The presence of these cavities allow the metal caps to serve as mechanical transformers for transforming and amplifying a portion of the incident axial-direction stress into tangential and radial stresses of opposite sign. Thus, the d_{31} and d_{31} contributions of the PZT now add together (rather than substracting) in the effective d_h of the device [26].

SINGLE ELEMENT TRANSDUCERS

A single piezoelectric ceramic element with electroded surfaces is the most basic and simple transducer, but this type of transducers have severe limitations such as, low d_h, high acoustic impedance. As a result composite structures which have good acoustic matching to water, and with their designs to amplify externally applied stress became the main transducer configuration. However, composite structures are not the only avenue to an improved transducer performance. In the recent years, several single element ceramic transducers with specially designed geometries were shown to display a performance comparable to composite transducers. Among these two of them, miniature hollow sphere transducers (BBs) and monomorph 'rainbow' transducers will be discussed in this section.

Directional characteristics are important in designing a transducer for underwater applications and when omnidirectional reception is required a spherical design is most often used. Miniature piezoelectric hollow spheres, also known as BBs due to their similarity in size to the pellets used in buckshot, are made using a coaxial nozzle slurry technique with a diameter of 1-6 mm and a wall thickness of 40 to 150μm [27]. Spheres with both tangential and radial poling configurations, shown in Figure 3, exhibit a very large hydrophone figure of merit ($d_h \cdot g_h$). The amplification of d_h and figure of merit in BBs result purely from the spherical geometry. An applied hydrostatic pressure is transformed into radial and tangential stress components, and are amplified by a factor, which can be defined as the ratio of radius to wall thickness (r/t). Properties of the BBs are reported to remain stable up to 7 MPa.

Another novel design exploiting the geometry of a single ceramic element is the monomorph flexural disk transducer 'rainbow'. The rainbow transducer shows excellent promise as a low pressure (<100 kPa) sensor and/or acoustic transmitter. It consists of an electromechanically active layer, such as PZT in direct contact with a lead-rich constraining layer [28]. This constraining layer is formed by exposing on side of a the ceramic to a reducing atmosphere at high temperature by placing the ceramic in contact with a carbon block. Due to the thermal expansion mismatch between the reduced non-piezoelectric layer and the oxide piezoelectric layer, a curvature develops in the structure, giving it a dome shape, with the oxide layer in compression throughout its volume. The dome needs to be fixed on a base plate when it is used as a pressure sensor;otherwise, the voltage response will only be equal to that of the bulk ceramic. Rainbows exhibit highly pressure dependent properties but are extremely robust. As pressure increases, the dome gradually flattens, decreasing the bending contribution to g_h until it reaches the bulk value. Hydrophone figure of merit ($d_h \cdot g_h$) of all the composite and single element transducers discussed so far are compared in the plot in Figure 4.

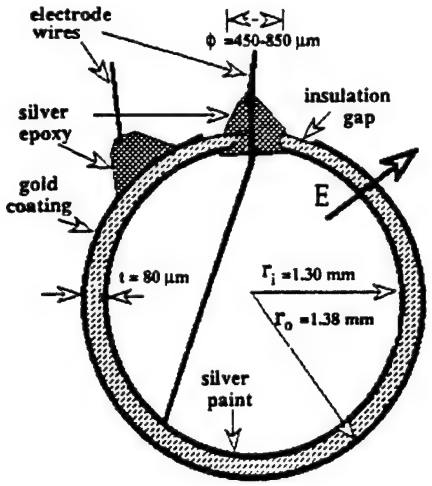

(a) Radial poling configuration

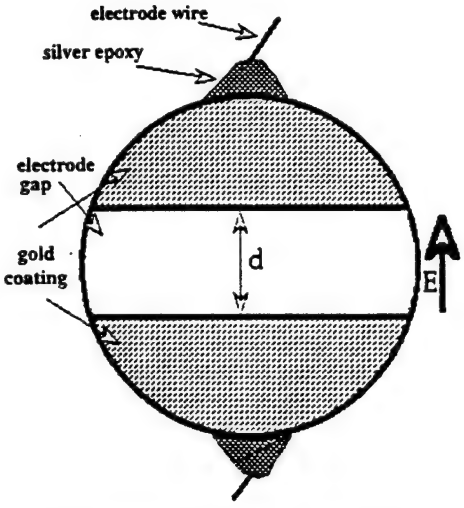

(b) Tangential poling configuration

Figure 3. Poling configurations of BB transducers

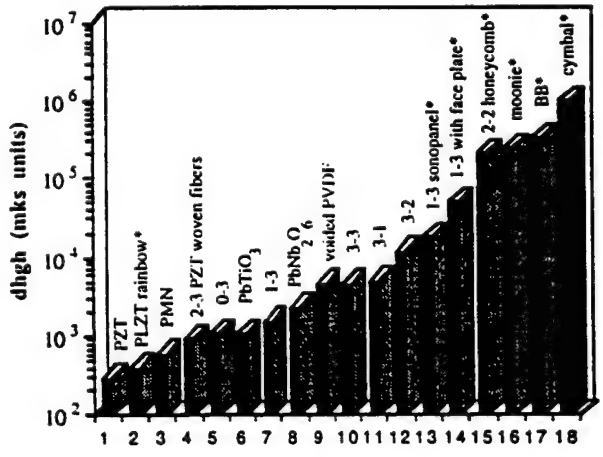

Figure 4. Comparison of hydrophone figure of merit of several piezoelectric ceramics and transducer designs.

In this figure, the figure of merit of the transducers marked with '*' is size dependent. Therefore, the figure of merit is calculated for a 1 cm^2 transducer for a valid comparison.

CONCLUSIONS

Some important goals in composite transducer research include: improved acoustic impedance - better coupling to air, to fluids, and to metals; lower drive voltage through the use of internal electrodes; improved sensitivity to hydrostatic waves; strain amplification to produce enlarged displacements; acoustic isolation of adjacent sound sources; passive and active vibration suppression; enhanced high-frequency performance through mode control; mechanical strength and flexibility; backing layers to absorb unwanted vibrations; reduced hysteresis; internal stress and field rearrangement; improved breakdown strength; tuned coupling coefficients, including permittivity, and elasticity; beam-forming capability; and rapid ringdown.

Integration and miniaturization of electroceramic components is an ongoing process in the automotive and consumer electronics areas. Multilayer packages containing signal processing layers made up of low permittivity dielectrics and printed metal interconnections are in widespread production. Further integration with embedded resistors and capacitors are under development and it seems likely that sensor and actuator systems will make use of the same processing technology. Tape casting and screen printing are processes used most often, and varistors, chemical sensors, thermistors, and piezoelectric transducers can all be fabricated this way, opening up the possibility of multicomponent multifunction integrated ceramics.

ACKNOWLEDGMENT

The authors wish to thank the Office of Naval Research (ONR) for its financial support.

REFERENCES

(1) Newnham, R.E., Skinner, D.P. and Cross, L.E. Connectivity and Piezoelectric- Pyroelectric Composites. *Mat. Res. Bull.* 1978, **13**, 525

(2) Creedon, M.J., Gopalakrishnan, S., and Schulze, W.A. 3-3 composite hydrophones from distorted reticulated ceramics. in 'Proc. 9th IEEE Intl. Symp. Apps. Ferroelectrics' (Eds. R.K. Pandey, M. Liu, and A. Safari), IEEE, New York, 1995, pp. 299-302

(3) Skinner, D.P., Newnham, R.E., and Cross, L.E. Flexible composite transducers. *Mat. Res. Bull.* 1978, **13**, 599

(4) Safari, A., Newnham, R.E., Cross, L.E., and Schulze, W.A. Perforamted PZT-polymer composites for piezoelectric transducer applications. *Ferroelectrics* 1982, **41**, 197

(5) Gururaja, T.R., Safari, A., Newnham, R.E., and Cross, L.E. Piezoelectric ceramic- polymer composites for transducer applications. in 'Electronic Ceramics: Properties, Devices, and Applications' (Ed. L.M. Levinson), Marcel Dekkar, New York, 1988, pp. 92-1435

(6) Twiney, R.C. Novel piezoelectric materials. *Adv. Mater.* 1992, **4**, 819

(7) Banno, H. Recent developments of piezoelecric ceramic products and composites of synthetic rubber and piezoelectric ceramic particles. *Ferroelectrics* 1983, **50**, 3

(8) Ting, R.Y. The hydroacoustic behavior of piezoelecric composite materials. *Ferroelectrics* 1990, **102**, 215

(9) Ting, R.Y. Composite piezoelectric materials for transduction. *Appl. Acoustics* 1994, **41**, 325

(10) Ting, R.Y. and Geil, F.G. Recent development in the application of 0-3 piezoelectric composites for hydrophone arrays. in '1990 IEEE 7th Intl. Symp. App. Ferroelec.' IEEE, New York, 1991, pp.14-17

(11) Ting, R.Y. A review on the development of piezoelectric composites for underwater acoustic applications. *IEEE Trans. Inst. Msmt.* 1992,**41**,64

(12) Newnham, R.E., Fernandez, J.F., Markowski, K.A., Fielding, J.T., Dogan, A., and Wallis, J. Composite piezoelectric sensors and actuators. *Mat. Res. Soc. Proc.* 1995, **360**, 33

(13) Janas, V.F., Ting, S.M., Livneh, S.S., Walker, F.R., Schaeffer, R., McNulty, T.F., and Safari, A. Fine-scale, large area piezoelectric fiber/polymer composites for transducer applications. in 'Proc. 9th IEEE Intl. Symp. Apps. Ferroelectrics' (Ed. R.K. Pandey, M. Liu, and A. Safari) IEEE, New York, 1995, pp. 295-298

(14) Zhang, Q.M., Wang, H., Zhao, J., Fielding, J.T., Newnham, R.E., and Cross, L.E. A high sensitivity hydrostatic piezoelectric transducer based on transverse piezoelectric mode honeycomb ceramic composites. *IEEE Trans. UFFC* 1996, **43**, 36

(15) Klicker, K.A., Biggers, J.V., and Newnham, R.E. Composites of PZT and epoxy for hydrostatic transducer applications. *J. Am. Ceram. Soc.* 1981, **64**, 5

(16) Smith, W.A. New opportunities in ultrasonic transducers emerging from innovations in piezoelectric materials. *SPIE* 1992, **1733**, 3

(17) Smith, W.A. and Shaulov, A.A. Composite piezoelecrics: basic research to a practical device. *Ferroelectrics* 1992, **87**, 309

(18) Hossack, J.A., and Bedi, R.L. Design of composite piezoelectric transducers. *Key Engr. Mater.* 1994, **92-93**, 301

(19) Bowen, L., Gentilman, R., Fiore, D., Pham, H., Serwatka, W., Near, C., and Pazol,B. design, fabrication, and properties of sonopanel™ 1-3 piezocomposite transducers. *Ferroelectrics* 1996, **187**, 109

(20) Cao, W., Zhang, Q.M. and Cross, L.E. Theoretical study on the static performance of piezoelectric ceramic-polymer composites with 1-3 connectivity. *J. Appl. Phys.* 1992, **72**, 5814

(21) Cao, W. Simulation of the dynamical behavior of 1-3 piezocomposite using finite element method. *Ceramic Eng. and Sci. Proc.* 1996, **17**, 83

(22) Smith, W.A. The application of 1-3 piezocomposites in acoustic transducers. in '1990 IEEE 7th Intl. Symp. Apps. Ferroelectrics' IEEE, New York, 1990, pp. 145-152

(23) Cao, W., Zhang, Q.M. and Cross, L.E. Theoretical study on the static performance of piezoelectric ceramic-polymer composites with 2-2 connectivity. *IEEE Trans. UFFC* 1993, **40**, 103

(24) Zhang, Q.M., Chen, J., Wang, H., Zhao, J., Cross, L.E., and Trottier, M.C. A new transverse piezoelectric mode 2-2 piezocomposite for underwater transducer applications. *IEEE Trans. UFFC* 1995, **42**, 774

(25) Rolt, K.D., *J. Acoust. Soc. Am.* 1990, **87**, 1340

(26) Tressler, J.F., Dogan, A., Fernandez, J.F., Fielding, J.T. , Jr., Uchino K. and Newnham,R.E. Capped ceramic hydrophones. in '1995 *IEEE Ultrasonics Symposium Proceedings* ', edited by M. Levy, S.C. Schneider and B.R. McAvoy, IEEE Piscataway, NJ, 1995, pp. 987

(27) Alkoy, S., Dogan, A., Hladky, A.-C., Langlet, P., Cochran, J.K., and Newnham, R.E. Miniature piezoelectric hollow sphere transducers (BBs). *IEEE Trans. UFFC* 1997, **44**, 1067

(28) Haertling,G.H., *Am. Ceram. Soc. Bull.* 1994, **73**, 93

APPENDIX 38

Composite Piezoelectric Transducer with Truncated Conical Endcaps "Cymbal"

Aydin Dogan, Kenji Uchino, *Member, IEEE*, and Robert E. Newnham, *Member, IEEE*

Abstract—**This paper presents original results obtained in the development of the moonie-type transducers for actuator applications. The moonie-type actuators fill the gap between multilayer and bimorph actuators, but its position-dependent displacement and low generative force are unacceptable for certain applications. The moonie transducers were modified systematically by using finite element analysis combined with experimental techniques. A new transducer design, named "cymbal transducer", was developed with larger displacement, larger generative forces, and more cost-effective manufacturing. The cymbal transducers consist of a cylindrical ceramic element sandwiched between two truncated conical metal endcaps and can be used as both sensors and actuators. The cymbal actuator exhibits almost 40 times higher displacement than the same size of ceramic element. Effective piezoelectric charge coefficient. Eff. d_{33}, of cymbal is roughly 40 times higher than PZT itself.**

I. Introduction

Recently, a number of capped ceramic actuators have been developed for various applications [1]–[6]. Central to the development of these actuators has been the combination of high displacements and moderate generative forces which fill the gap between multilayer actuators and bimorph actuators. Multilayer actuators with internal electrodes exhibit high generative force, but only small displacement. Cantilever bimorph actuators exhibit large displacement, but very small generative force. These two actuators have already been commercialized [7]–[10].

This paper describes a new composite transducer, the "cymbal", with a large displacement and relatively high generative (blocking) force. The design and construction of a 12.7 mm diameter actuator with 2 mm total thickness is described, along with the displacement, generative force, and effective coupling factor. The cymbal composite actuator is then compared with other actuator designs.

II. The Method of Designing Endcaps

A. Effect of Endcap Design on Displacement

The cymbal actuator is a second generation moonie-type composite developed using FEA analysis in collaboration with experiment. Finite element analysis has identified high stress concentration in the metal endcaps just above the edge of the ceramic metal bonding layer near the edge of cavity [11]. Stress distribution diagrams in the longitudinal z-direction and in the tangential direction are shown in Figs. 1 and 2, respectively, for a moonie hydrophone, subjected to a unit hydrostatic pressure. The compressive stress concentration (13–15 units) at the inner edge of the bonding is marked with "−−" symbols. The tensile stresses appear in the region marked with "++" symbols near the outer edge of the piezoelectric ceramic.

The stress concentration on the brass endcap just above the bonding layer reduces the effective force transfer from the ceramic to the cap. It is possible to eliminate part of the stress concentration by removing a portion of the endcap just above the bonding region where the maximum stress concentration is observed. An enhancement in properties has been observed by introducing a ring-shaped groove on the exterior surface of the endcaps [12].

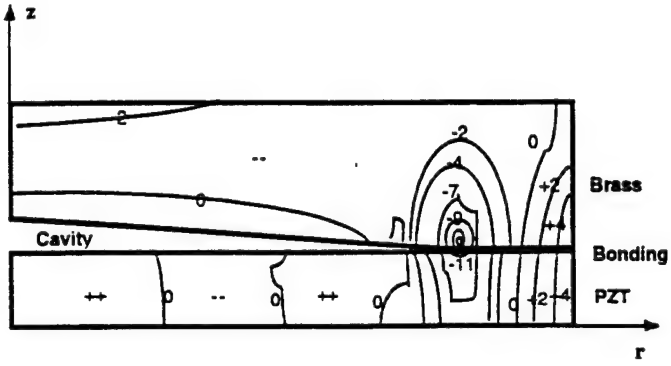

Fig. 1. Longitudinal z-directional stress distribution under hydrostatic pressure.

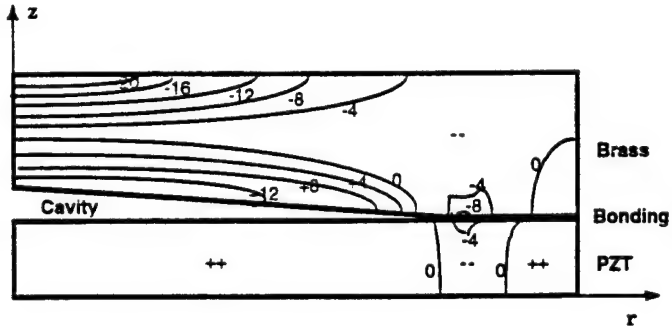

Fig. 2. Radial r-directional stress distribution under unit hydrostatic pressure. (−−) indicates compressive stresses and (++) indicates tensile stresses.

Manuscript received December 11, 1995; accepted October 30, 1996.

The authors are with Materials Research Laboratory, International Center for Actuators and Transducers, The Pennsylvania State University, University Park, PA 16802 (e-mail: kxu1@alpha.mrl.psu.edu).

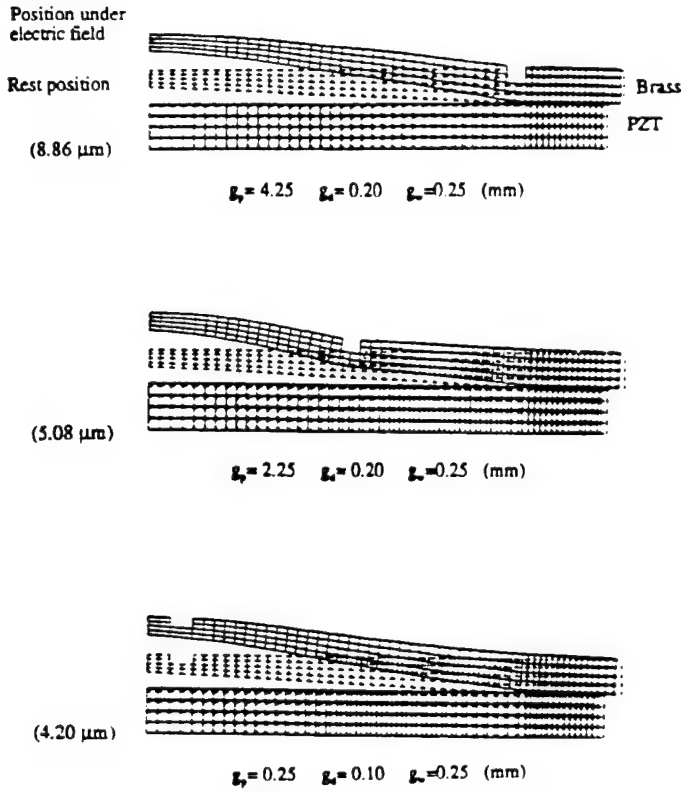

Dimensions: Groove position (radius), g_r ; Groove depth, g_s ; Groove width, g_w

Fig. 3. Effect of the groove introduced to the endcap on the displacement characteristics of the moonie actuator. Displacements are shown in parenthesis.

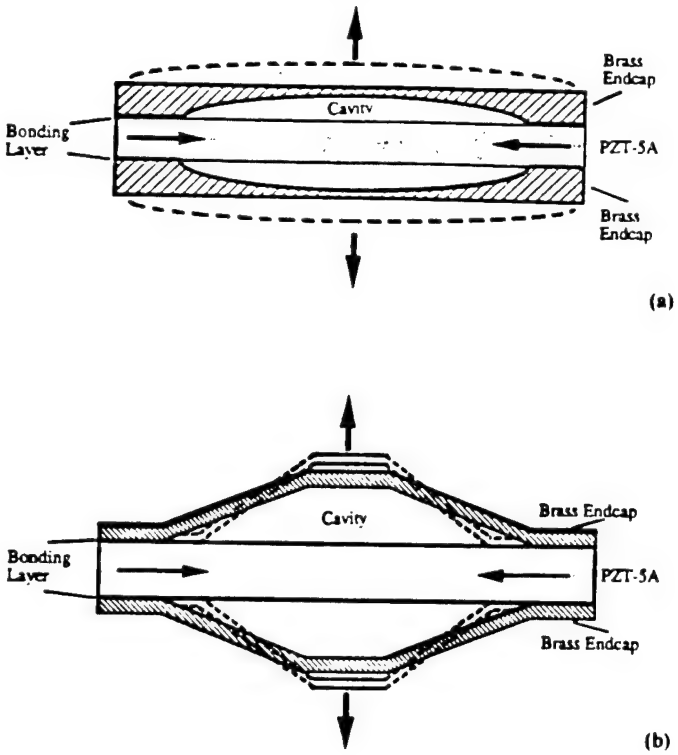

Fig. 4. (a) Displacement motion of the moonie design (side view of disk shape). (b) Displacement motion of the cymbal design. Arrows show the displacement direction under positive bias and dashed lines show the displacement motion (side view of disk shape). Dimensions (in mm): Metal endcap diameter, d_m = 12.7; thickness, t_m = 0.3. Sheet thickness of cymbal t_s = 0.2. PZT ceramic diameter, d_p = 12.7; thickness t_p = 1.0. Cavity diameter, d_c = 9.0; height, h = 0.20. Bonding layer thickness, t_b = 0.015

By moving the groove toward the edge of the actuator, the displacement increases. The highest displacement was achieved when the groove was above the bonding layer. It is found that the deeper and wider the groove, the higher the displacement [13]. Fig. 3 shows the effect of the ring-shaped groove position on the displacement values.

In reality, placing a ring-shaped groove on the endcap does not eliminate the stress but further concentrates it into a very narrow region. Stress concentrations at the groove edges are a potential source of fatigue and may eventually produce failure under long term usage. Moreover, additional labor is required to machine the groove into the endcaps. Measurements on grooved endcaps are described later in this paper.

B. New Endcap Design "Cymbals"

A new endcap has been designed to remove much of the stress concentration and to produce higher and more reproducible displacements. Displacement motions of moonie and cymbal actuators are illustrated graphically in Figs. 4a and 4b. Although this new design looks similar to the earlier moonie design, it has a different displacement mechanism. Displacement is primarily a flexural motion of the endcap for the original moonie design; but, for the cymbal, the displacement is created by the combination of flexural and rotational motions. Moreover, the endcaps are easily fabricated from sheet metal by punching, resulting in identical endcaps with minimal labor. Fig. 5 shows the displacement values of the different endcap designs with a fixed cavity depth (0.20 mm) and diameter (9.0 mm).

A moonie actuator with 0.30 mm thick brass endcaps provides a 22 μm displacement. Using the ring-shaped groove design, the displacement was increased to 32 μm with a groove 9.0 mm in diameter, 0.2 mm in depth, and 1.0 mm in width machined into the brass endcaps of the same actuator. With the new design, a cymbal actuator with uniformly thick punched endcaps exhibits around 40 μm displacement, about twice the moonie displacement.

C. Fabrication of "Cymbal" Transducer and Characterization

A punch die was designed to rapidly fabricate truncated conical shape "cymbal" endcaps at minimal cost. The die was manufactured from cutting tool steel for punching cymbal endcaps 12.7 mm in diameter with a 0.2 mm conical cavity depth and a 9.0 mm cavity diameter. Shaping and cutting operations are carried out simultaneously during processing. The final product requires only surface treatment for good bonding. The cymbal endcaps were fabricated from 0.2 mm thick brass (70% Cu-30% Zn) sheets.

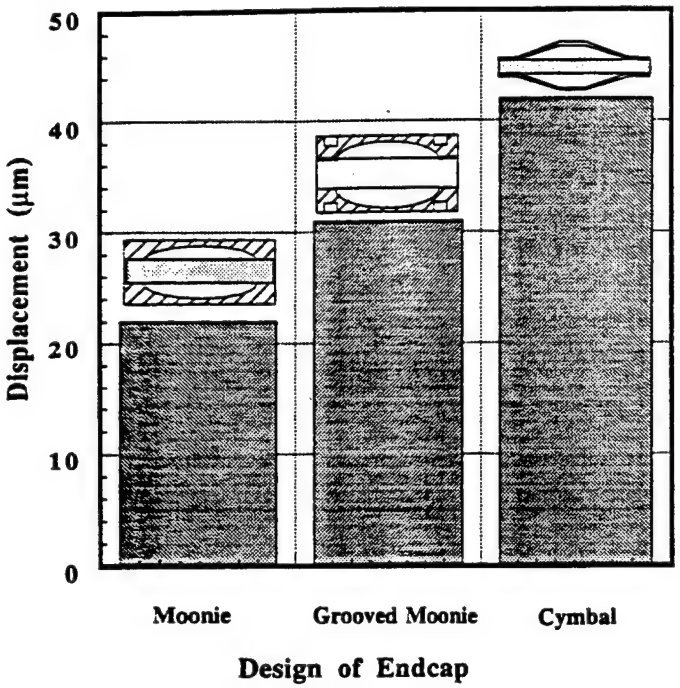

Fig. 5. Comparison of the displacement values of different endcap designs.

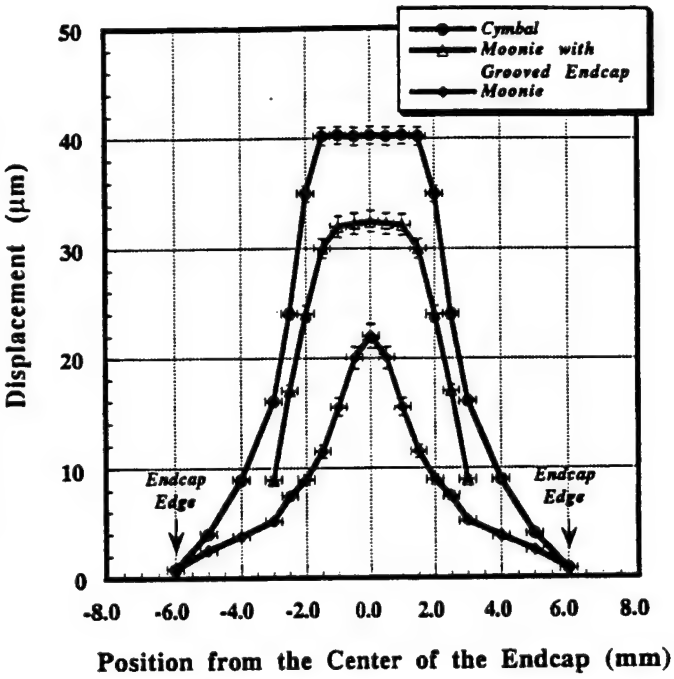

Fig. 6. The position dependence of displacement of the different endcap designs.

The moonie endcaps were fabricated from brass disks 12.7 mm in diameter and 0.3 mm thick. Shallow cavities 9.0 mm in diameter with a 0.2 mm center depth were machined into the inner surface of each of the caps.

The moonie and cymbal endcaps were bonded to the electroded niobium doped piezoelectric, PZT-5A, disks (12.7 mm in diameter and 1.0 mm thickness provided by PiezoKinetics Co. PA) around the circumference using Eccobond epoxy resin from Emerson & Cuming, taking special care not to fill the cavity. The thickness of the epoxy bonding layer was approximately 20 μm.

The displacement of the composite actuator at 0.1 Hz under 1 kV/mm electric field was measured with a linear voltage differential transducer (LVDT) having a resolution of approximately 0.05 μm. Generative (blocking) force measurements were done under static loading conditions, again using the LVDT system. Resonance characteristics were obtained with an Impedance/Gain Phase Analyzer HP-4194A to calculate the response speed and to evaluate the bonding layer.

III. Experimental Results

A. Position Dependence of Capped Composite Actuators

Flexural motion of the endcaps is the principal displacement mechanism of the original moonie actuator. For this reason, displacement of the moonie actuator is highly dependent on position. Displacement decreases dramatically away from the center of the endcap, where the maximum displacement is observed, to the edge, where displacement is equal to that of PZT-5A without the endcap. Fig. 6 shows the position dependence of the displacement for moonie and cymbal actuators. Position-dependent displacement is a disadvantage of the original moonie design since there is only a small contact area with the highest displacement makes stacked moonies impractical. In earlier studies it was suggested that bonding a disk to the center of the endcap's outer surface would provide a uniform displacement over the surface of the actuator [12]. However, adding an extra disk also makes the design more complex and unstable. Moonies with grooved endcaps show significantly less position-dependent displacement. The cymbal design delivers a homogeneous displacement with deviations of < 1 μm over a wide section of the center of the endcap. The large flat contact surface of the new endcap design makes it more practical for stacking the individual actuators together to reach higher displacements. Additionally, the new multistacked structure is more stable under uniaxial axisymmetric loading. The basic design of a multistacked cymbal is shown in Fig. 7. Five cymbal actuators stacked in series produce a 175 μm displacement, as shown in Fig. 8.

B. Degree of Hysteresis

The degree of hysteresis is an important criteria for actuators that provides information about the thermal and mechanical losses. Reproducibility in the displacement for an actuator is an essential property for some applications. Uchino [8] has defined the degree of hysteresis as:

$$\text{Hysteresis } \% = \frac{\Delta x}{X_{\max}} \times 100 \qquad (1)$$

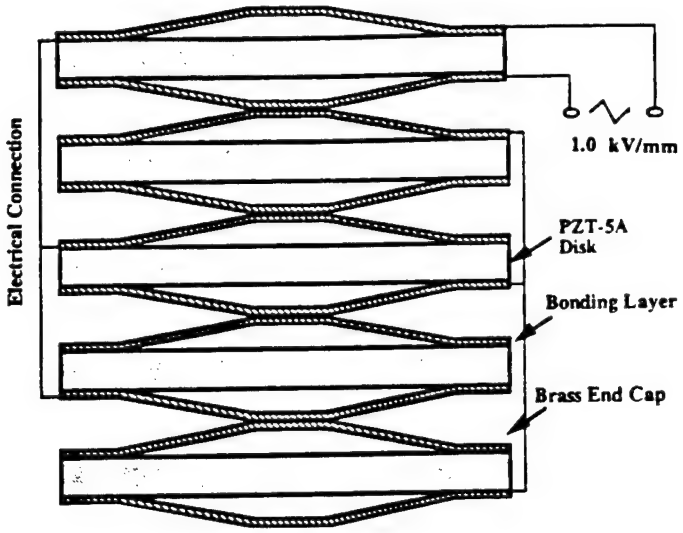

Fig. 7. The basic design of the multistacked cymbal actuator for more displacement amplification.

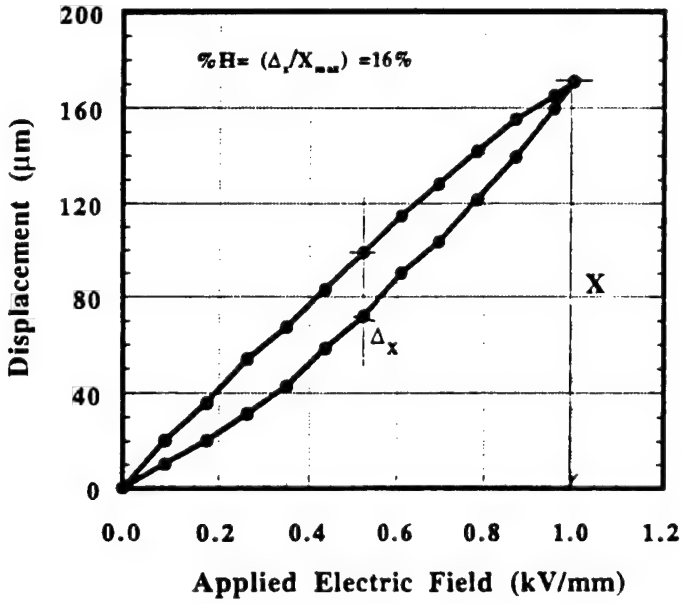

Fig. 8. Displacement hysteresis of the multistacked cymbal actuator.

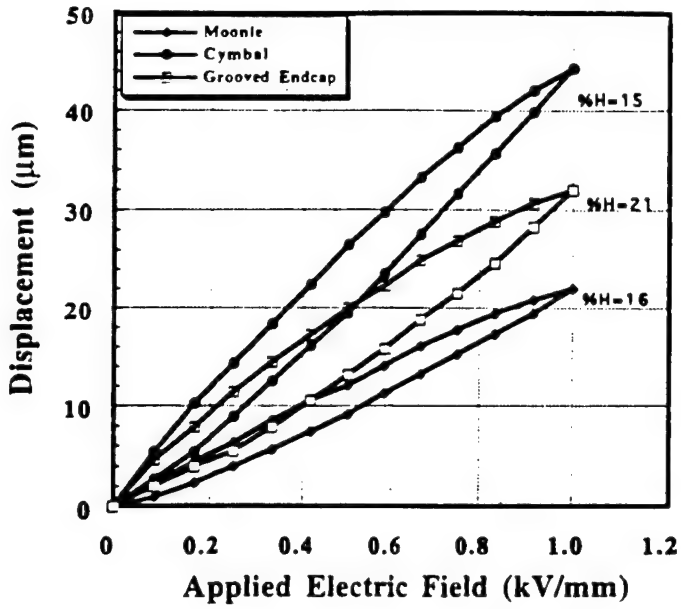

Fig. 9. Displacement hysteresis of different endcap designs.

where X_{max} is the displacement at the maximum electric field, E_{max}. E_{max} is fixed at 1.0 kV/mm in our calculations and strain hysteresis is obtained under the same field at 0.1 Hz for a triangular wave form. Δx is the difference in displacement for increasing and decreasing paths at half maximum of the electric field, $(E_{max})/2$, (0.5 kV/mm).

In Fig. 9 the degree of hysteresis for different moonie designs have been compared. Hysteresis curves are plotted after 10 cycles to eliminate zero-point drift. PZT-5A ceramic disks show 5–8% hysteretic losses. The main cause of these losses in the piezoelectric ceramic element are domain reversal mechanisms [14]. In general, all moonie designs show substantial hysteresis. Most probably, the losses in the epoxy bonding layer between ceramic and endcaps and mechanical losses on the endcaps are the reason for the increase in hysteric behavior. The degree of hysteresis increases for a brass-capped (0.3 mm thick) moonie to about 16%. Grooving the endcaps also increases the degree of hysteresis. A 21% degree of hysteresis has been observed for a moonie actuator with 0.3 mm thick grooved endcaps. A possible reason for the increase may be mechanical losses associated with the grooves. Cymbals show a degree of hysteresis of 15%. It can be concluded that cymbal endcaps transfer the stresses more efficiently with less mechanical loss.

C. Maximum Generative (Blocking) Force

The displacement-applied force relation of the cymbal actuator is shown in Fig. 10. The maximum generative force of the cymbal actuator is around 15 N (this corresponds to the intercept on the force axis at the point corresponding to the blocking force for which the displacement is equal to zero). Displacement curves under zero electric field and 1.0 kV/mm are parallel to one another up to 20 N. The difference in displacement of the samples between zero electric field and 1.0 kV/mm decreases for blocking forces over 20 N. The experiment was terminated at an applied force of 27 N to prevent permanent deformation of the endcaps. The elasticity of the endcap material is a key parameter for the cymbal actuator since the endcaps tend to act like a spring under an applied force.

Stiffness of the metal endcaps and force application area are the two important parameters defining maximum generative force of the moonie. Even though the flexural motion and displacement are largest at the center of the moonie, the generative force is small at this point [3]. The maximum generative force (also called the blocking force) of a moonie actuator with a 0.30 mm thick brass endcap is approximately 3.0 N. The main reason for this behavior is the small contact area and the very thin membrane ($\approx$ 100 μm) at the contact point.

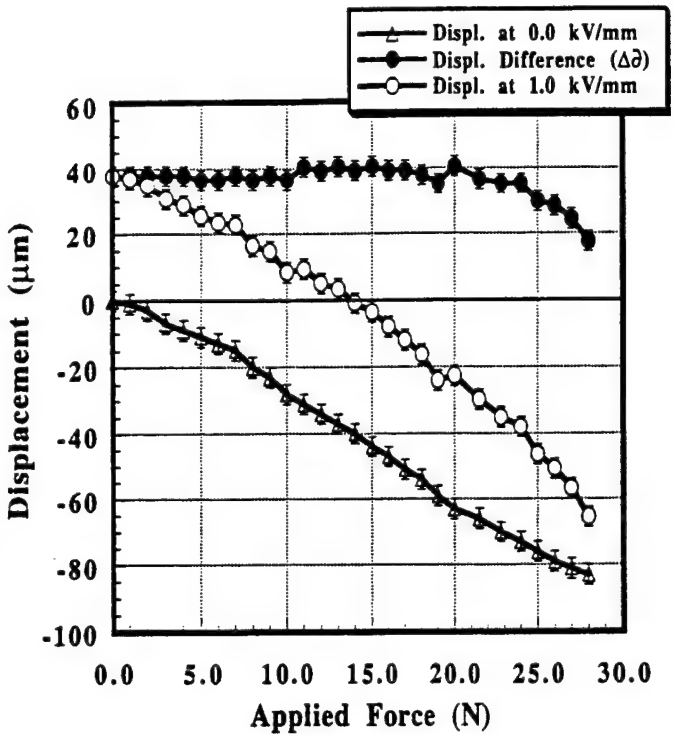

Fig. 10. Displacement-applied force relation of cymbal actuator.

The force range for the cymbal actuator is appreciably greater than that of the moonie actuator. Cymbals have a force limit of about 20 N, which is mainly controlled by the elasticity of the endcap material. By using a stiff metal for the endcap, the force limit can be increased markedly [15].

D. Electromechanical Coupling Factor and Transmission Coefficient

The electromechanical coupling factor, k, is an important parameter for piezoelectric transducers and is defined as the square root of the ratio of stored mechanical energy over input electrical energy [14]. The energy transmission coefficient, λ, is the ratio between mechanical output energy over input electrical energy, and it is a key parameter used in comparing of actuators. The relation between the electromechanical coupling factor and the maximum energy transmission coefficient is given by:

$$\lambda_{\max} = \left(\frac{1}{k} - \sqrt{\frac{1}{k^2} - 1}\right)^2. \tag{2}$$

Taking account of the maximum mechanical energy output, the energy transmission coefficient is expressed as follows:

$$\lambda = \frac{1}{2\left(\frac{2}{k^2} - 1\right)}. \tag{3}$$

which is slightly smaller than the $\lambda_{\max}$, but almost the same for the k values around 0.5.

Electromechanical coupling factors for piezoelectric ceramics are normally calculated from resonance and antiresonance frequencies. However, for the composite designs, because of their complex structure and different electrical equivalent circuits, the resonance technique is not adequate for all cases. For this reason, the input and output energy were measured, and the electromechanical coupling factors of the composite structures were calculated. To distinguish it from the materials coupling factor, the coupling factor of the composite structure is referred to as an effective electromechanical coupling factor. The energy transmission coefficient of the cymbal actuator with the dimensions given in the fabrication section was calculated as follows:

The input electrical energy, E_E, is estimated from the expression:

$$E_E = \int iV dt = \int \frac{dQ}{dt} V dt = \int CV dV = \frac{1}{2} CV^2 \approx 1.1 \times 10^{-3} j. \tag{4}$$

The dielectric constant of the PZT decreases as the applied voltage increases. As a result of this decrease, the actual capacitance is less than the low voltage capacitance value. Therefore, the electrical input energy must be less than the calculated value given by (4). For a precise calculation, the dielectric constant of PZT should be measured under an applied field up to 1.0 kV/mm. However, for simplicity the low voltage capacitance is used in these calculations. The maximum mechanical output energy, E_M, is calculated from the displacement versus applied force relation of the cymbal actuator (Fig. 10) using following equation:

$$E_M = \left(\frac{1}{2} d_{\max}\right)\left(\frac{1}{2} F_{\max}\right) = 1.3 \times 10^{-4} j \tag{5}$$

where $d_{\max}$ is the maximum displacement and $F_{\max}$ is the maximum generative force.

Therefore the energy transmission coefficient of the cymbal is equal to:

$$\lambda \approx \frac{E_M}{E_E} = 0.12. \tag{6}$$

Using (3), the effective electromechanical coupling factor, k_{eff}, of the cymbal actuator was calculated as 0.62.

As mentioned earlier, a moonie's characteristics depend on both load position (centered vs. non-centered) and contact surface (point vs. surface). For this reason the electromechanical coupling factor calculations must be completed taking both positional and contact surface dependence into consideration.

The energy transmission coefficient of a moonie actuator was calculated in a manner similar to the cymbal actuator. For a moonie actuator with the dimensions given earlier, the energy transmission factor and effective electromechanical coupling factor were calculated for a point contact at the center of the endcaps as $\lambda = 0.015$ and $k_{\text{eff}} = 0.26$, respectively. The electromechanical coupling

TABLE I
COMPARISON OF THE ENERGY TRANSMISSION COEFFICIENT AND ELECTROMECHANICAL COUPLING FACTOR OF DIFFERENT ACTUATOR MATERIALS AND DESIGNS

	Energy Transmission Coefficient (λ)		Effective Electromechanical Coupling Factor (k_{eff})	
	Experimental	FEA	Experimental	FEA
Moonie	0.015	0.0123	0.26	0.22
Cymbal	0.121	-	0.62	-
PZT-5A*	0.134 (0.2)	-	0.65 (0.75-0.80)	-
Multilayer † Ceramic	0.28	-	0.83	-

* Calculated from the admittance spectrum of the PZT-5A disk. It is assumed to be higher under higher electric field conditions. Numbers in parentheses shows expected high electric field values
† Calculated from the displacement-applied force graph in the Tokin Co. actuator product catalog [9].

factor and energy transmission coefficient of the moonie, cymbal, PZT-5A disk, and a multilayer ceramic plate are listed in Table I for comparison. With the cymbal endcap design, a remarkably high electromechanical coupling factor is obtained.

The efficiency is determined by the mechanical and electrical losses. Even though the transmission factors for piezoelectric ceramics, the composite moonie, and cymbal actuator designs look very low, they actually have higher efficiencies more than 95%. It can be determined by calculation of the P-E hysteresis loss, which is around 5%. This can also be explained in terms of stored energy as follows: The efficiency can be defined as:

$$\eta = \frac{\text{Output Mechanical Energy}}{\text{Consumed Electrical Energy}}. \tag{7}$$

In a work cycle (e.g., an electric field cycle), the input electrical energy is transformed partially into the mechanical energy, and the remainder is stored as electrical energy. The unconsumed energy is ultimately returned to the power source as reactive loading [8].

E. Effective Piezoelectric Coefficient of the Moonie and Cymbal

The piezoelectric charge coefficient is a material parameter. The direct piezoelectric effect is important for sensors and the converse piezoelectric effect is important for actuators. Because of the composite design of moonie and cymbal, the effective piezoelectric coefficient is used to distinguish it from a material constant. The piezoelectric coefficient of the moonie and cymbal transducers were measured with a modified Berlincourt d_{33} meter. Fig. 11 shows the position dependence of effective d_{33} coefficients for three different endcap designs. The moonie shows highly position-dependent behavior for the effective piezoelectric coefficient. For samples with 0.30 mm thick brass endcaps, a piezoelectric coefficient of approximately 10,000 pC/N was measured at the center. Moving from the center to the edge of the sample, the effective d_{33} coefficient decreases drastically, until it reaches a value similar to the PZT ceramic itself. The cavity beneath the endcap of the moonie actuator plays a crucial role on the characteristics of the moonie [16]. The effective piezoelectric coefficient increases with increasing cavity diameter and cavity depth. The effective piezoelectric coefficient of the moonie transducer decreases rapidly with increasing endcap thickness. The piezoelectric charge coefficient of moonie transducers also shows position-dependent behavior similar to that of the displacement.

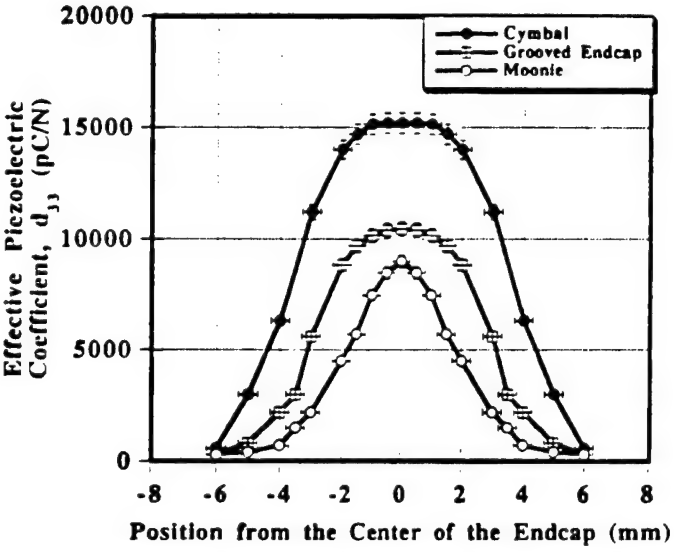

Fig. 11. Effective piezoelectric charge coefficient of different endcap designs

Placing a groove 9.0 mm in diameter, 0.2 mm in depth, and 1.0 mm in width in the brass endcaps increased the effective piezoelectric coefficient almost 20%. The piezoelectric charge coefficient is simply the ratio of the applied stress and the induced charge. Thus we can say that the groove on the endcaps increases the stress transformation ratio and therefore the generated charge. The moonies

with grooved endcaps also showed less position-dependent behavior. For the 2 mm diameter section at the center of the samples. the effective piezoelectric coefficient is about 12.000 pC/N.

With the cymbal endcaps, the piezoelectric coefficients increased almost 60%. For a cymbal 12.7 mm in diameter and 1.7 mm in total thickness, an effective piezoelectric coefficient of more than 15,000 pC/N was measured over the 3 mm diameter center section of the cymbal transducer. We have concluded that the thick metal region near the edge of the moonie metal endcaps is a passive region which does not assist stress transfer, and acts to decrease the total efficiency. Cymbal endcaps transfer the stress more efficiently and improve the energy transfer markedly.

F. Resonance Characteristics of the Cymbal

The resonance spectrum of the cymbal transducer (12.7 mm in diameter and 1.7 mm thick) is shown in Fig. 12. The first resonance peak at 20.30 kHz corresponds to the flextensional mode of the composite transducer. Resonances between 150 and 160 kHz comes from the coupling between the radial mode of the PZT disc and higher order flextensional modes. Sharp resonance peaks, combined with an absence of any spurious mode, are indicative of a high quality bond between metal and ceramic. The fastest response time is an important criteria for the actuators and it can be defined as the time to achieve the quick and precise response of the actuator without overshoot and ringing. The mechanical resonance of the systems limits the practical actuation range. Actuators should be used in linear range of their resonance spectrum [17]. The fastest response time of the cymbal transducer was evaluated from: $t_{(\text{sec})} = (1/f_{\text{ft}})$, where f_{ft} is the flextensional resonance frequency. The fastest response time of the cymbal actuator is about 50 μsec.

The response time of the moonie actuator depends on the geometry of the cavity beneath the endcaps, but normally increases with increasing cavity diameter and changes only slightly with cavity depth [16]. The fastest response time is inversely proportional to the endcap thickness, and increases further with increasing compliance of the endcap material. The fastest response time of the moonie actuator is in the range of 5 to 50 μsec depending on the cavity size and endcap thickness.

IV. Discussion

A. Comparison of the Solid State Actuator Designs

Several features of the various solid state actuator designs are listed in Table II. It is rather difficult to compare the different actuators because of differences in geometry and various operating conditions for specific applications. To make a fair comparison, similar dimensions for each actuator were selected, and the measurement conditions are those specified in Table II. Flextensional moonie and cymbal actuators with their moderate generative force and displacement values fill the gap between multilayer and bimorph actuators. Each solid state actuator design has attractive features that can be exploited for certain applications. Advantages of the moonie and cymbal actuators are the easy tailoring of the desired actuator properties by altering the cavity size and endcap dimensions. Easy fabrication is another advantage. The rainbow actuator also partially covers this gap [5]. For that type of actuator a reduction step during processing of the ceramic element at high temperature results in a semiconducting layer and stress-bias. Even though it shows flexural motion, the rainbow can be categorized as a monomorph or a unimorph type of actuator. The effective coupling factor of rainbow is theoretically smaller than the moonie and cymbal. High applied field, position-dependent displacement and cost are the main disadvantages of the rainbow actuator in comparison with the cymbal. In the moonie and cymbal design, a multilayer piezoelectric ceramic can be used as driving element to reduce the drive voltage.

B. Potential Applications for Moonie and Cymbal Transducers

Moonie and cymbal actuators have great potential in the automotive industry, where they can be utilized as sensing and vibration suppression elements [18], [19]. Moonie and cymbal actuators can also be utilized as the switching element in valve designs. There is a volume change inside the moonie and cymbal transducers during cycling. This volume change can be utilized in minipump applications.

The moonie actuator can be used as a micropositioner for applications requiring small size with relatively quick response. OMRON corporation has already succeeded in using the multilayer moonie actuator for an optical scanner [20]. The high density memory storage driver such as CD-ROM driver and magneto-optic memory storage driver are other possible applications for moonie actuators capable of delivering precise positioning.

Because of their very high piezoelectric charge coefficients, moonie and cymbal transducers can be used as hydrophones, accelerometers, and air acoustic transducers. Cymbal accelerometers have more than two order of magnitude higher sensitivity than PZT ceramics at low frequencies [21]. The advantages of the cymbal type of hydrophone are very large d_h (hydrostatic charge) and g_h (hydrostatic voltage) coefficients along with lightweight and inexpensive fabrication [22].

V. Conclusion

The goals of this study were to evaluate the actuator performance of the moonie transducer. and to develop a new endcap design called the "cymbal". Displacement, generative force, and electromechanical coupling factor were used to compare the composite actuators. A die punch was designed to fabricate cymbal endcaps at min-

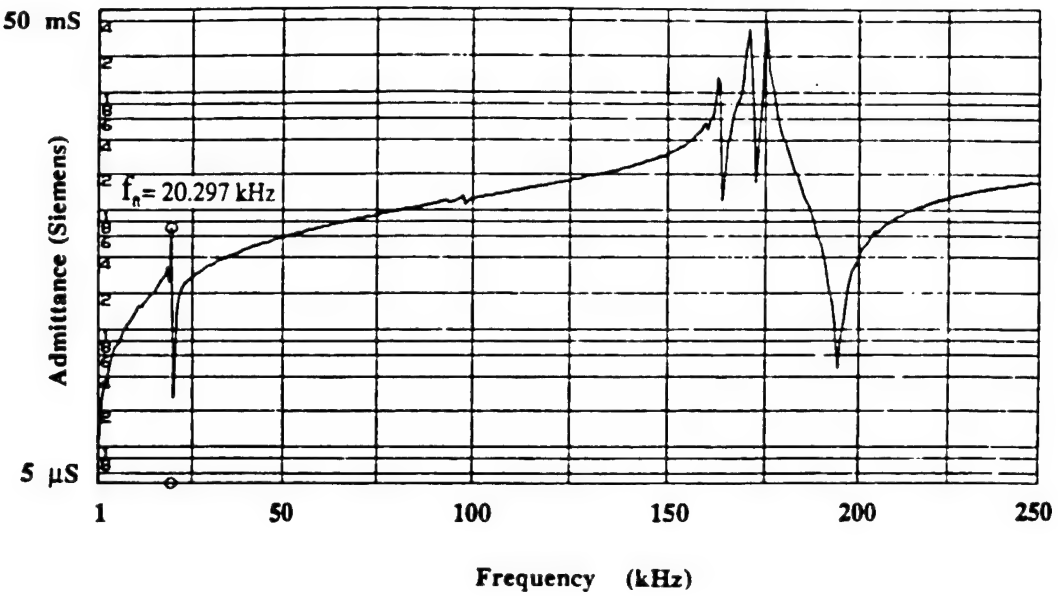

Fig. 12. Resonance spectrum of the cymbal transducer.

TABLE II
COMPARISON OF THE SOLID STATE ACTUATOR DESIGNS

Features	Multilayer [9]	Bimorph [9]	Rainbow [5]	Cymbal	Moonie [3], [16]
Dimensions	5 × 5 × 12.7 (L × W × T)	12.7 × 10 × 0.6 (L × W × T)	F 12.7 mm T = 0.5 mm	F 12.7 mm T = 1.7 mm	F 12.7 mm T = 1.7 mm
Driving Voltage (V)	100	100	450	100	100
Displacement (μm)	10	35	20	40	20
Contact surface (mm^2)	25	1	1	3	1
Generative Force (N)	900	0.5–1	1–3	15	3
Position dependent of displacement	None	Maximum at the tip	Maximum at the center	Maximum at the center but more diffuse	Maximum at the center
Stability under loading	very high	very low	low	high	low
Fastest Response Time (μsec)	1–5	100	100	5–50	5–50
Fabrication method	Type casting and cofiring at 1200°C	Bonding ceramic element with metal shim	Reducing ceramic element at 950°C	Bonding ceramic element with metal endcaps	Bonding ceramic element with metal endcaps
Cost	high	low	medium	low	medium

imal cost. Cymbal actuators 12.7 mm in diameter and 1.7 mm in total thickness can generate a 40 μm displacement at 1 kV/mm. Cymbal actuators have higher generative force than moonie actuators because of the enlarged active surface areas on the endcap: the observed forces are 15 N compared to 3 N for the standard moonie design. The cymbal actuator also shows less position-dependent behavior.

ACKNOWLEDGMENT

The authors wish to thank Drs. L. E. Cross, Q. C. Xu, K. Onitsuka, and M. Megherhi of PiezoKinetics Inc.; J. F. Fernandez and Mr. J. F. Tressler for their advice and assistance. The following agencies and organizations provided support for this project: Office of Naval Research Contract no. N00014-92 J 1510, National Science Foundation Grant no. DMR-9223847, Turkish Science and Technology Council (TUBITAK).

REFERENCES

[1] R. E. Newnham, Q. C. Xu, and S. Yoshikawa, "Metal-electroactive ceramic composite actuators," U.S. Patent, 5,276,657, Jan. 4, 1994.

[2] Y. Sugawara, K. Onitsuka, S. Yoshikawa, Q. C. Xu, R. E. Newnham and K. Uchino, "Metal-ceramic composite actuators," *J. Am. Ceram. Soc.*, vol. 75, no. 1, pp. 996–998, 1992.

[3] A. Dogan, Q. C. Xu, K. Onitsuka, S. Yoshikawa, K. Uchino, and R. E. Newnham "High displacement ceramic-metal composite actuator," *Ferroelectrics*, vol. 156, pp. 1–6, 1994.

[4] Q. C. Xu, A. Dogan, J. F. Tressler, S. Yoshikawa, and R. E. Newnham, "Ceramic-metal composite actuator," *Ferroelectrics*, vol. 160, pp. 337–346, 1994.

[5] G. Haertling, "Rainbow ceramics, a new type of ultra high dis-

placement actuator," *Bull. Amer. Ceramic Soc.*, vol. 73, no. 1, pp. 93–96, Jan. 1994.
[6] PCB-AVC, in *Active Vibration Control Instrumentation Catalog 701*, New York: Piezoelectric Inertial Actuator, 1995.
[7] K. Uchino, "Ceramic actuators principles and applications," *MRS Bull.*, vol. 18, no. 4, pp. 42–48, 1993.
[8] ——, *Piezoelectric/Electrostrictive Actuators*, Tokyo: Morikita, 1986.
[9] Multilayer Piezoelectric Actuator, Technical Documents, Tokin Co., Tokyo, Japan, 1988.
[10] Ceramic Multilayer Actuators, Technical Documents, Philips Co., Reomond, The Netherlands, 1994.
[11] Q. C. Xu, S. Yoshikawa, J. R. Belsick, and R. E. Newnham, "Piezoelectric composites with high sensitivity and capacitance for use at high pressure," *IEEE Trans. Ultrason., Ferroelect., Freq. Contr.*, vol. 38, pp. 634–639, 1991.
[12] Y. Sugawara, "Development of metal-ceramic composite piezoelectric actuators and their applications," M.S. Thesis, Phys. Dept., Sophia University, Tokyo Japan, 1991.
[13] K. Onitsuka, A. Dogan, Q. C. Xu, S. Yoshikawa, and R. E. Newnham, "Design optimization for metal-ceramic composite ceramic composite actuator," *Ferroelectrics*, vol. 156, pp. 37–42, 1994.
[14] B. Jaffe, W. R. Cook, Jr., and H. Jaffe, *Piezoelectric Ceramics*, New York: Academic, 1971.
[15] J. F. Fernandez, A. Dogan, J. F. Fielding, K. Uchino, and R. E. Newnham, "Temperature dependence of new design ceramic-metal composite actuators," *Proc. IV EuCers*, vol. 5, pp. 133–138, Italy, 1995.
[16] A. Dogan, S. Yoshikawa, K. Uchino, and R. E. Newnham, "The effect of geometry on the characteristics of the moonie transducer and reliability issue," *IEEE Ultrason. Symp. Proc.*, vol. II, 1994, pp. 935–939.
[17] S. Sugiyama and K. Uchino, "Pulse Driving Method of Piezoelectric Actuators" in *Proc. 6th IEEE Int. Symp. Appl. Ferroelec.*, 1986, p. 637.
[18] J. F. Tressler, "Smart ceramic-metal composites for active vibration control," M.S. thesis, Ceramic Science Dept., Pennsylvania State Univ., 1993.
[19] K. Onitsuka, A. Dogan, J. F. Tressler, Q. C. Xu, S. Yoshikawa, and R. E. Newnham, "Metal-ceramic composite transducer, the moonie," *J. Int. Mater. Syst. Struct.*, vol. 6, pp. 447–455, 1995.
[20] H. Goto and K. Imanaka, "Super compact dual axis optical scanning unit applying a tortional spring resonator driven by a piezoelectric actuator," *Proc. SPIE-Int. Soc. Opt. Eng.*, vol. 1544, pp. 272–281, 1991.
[21] B. Koc, A. Dogan, J. F. Fernandez, R. E. Newnham, and K. Uchino "Accelerometer application of the moonie and cymbal transducers," *Jap. J. Appl. Phys.*, vol. 35, Part 1, no. 8, pp. 65–67, 1996.
[22] J. F. Tressler, A. Dogan, J. F. Fernandez, J. T. Fielding, K. Uchino, and R. E. Newnham "Capped Ceramic Hydrophone," in *IEEE-UFFC Ultrason. Symp. Proc.*, Seattle, WA, 1995, pp. 897–900.

Aydin Dogan was born in Ankara, Turkey, on February 22, 1966. He received the B.S. degree in materials science and metallurgical engineering in 1988 and the M.S. degree in 1990, both from Middle East Technical University in Ankara, Turkey. He received the Ph.D. degree in materials program (Solid State Science) in 1994 from the Pennsylvania State University, University Park, PA. His research interests include electronic ceramics, sensors and actuators, smart materials and systems, and ferroelectrics.

He is currently a post-doctoral research associate in the Materials Research Laboratory at the Pennsylvania State University, University Park, PA. He was a NATO-TUBITAK science fellowship recipient.

Kenji Uchino (M'89) was born on April 3, 1950, in Tokyo, Japan. He received the B.S. degree in physics in 1973, the M.S. and Ph.D. degrees in physical electronics in 1975 and 1981, respectively, from Tokyo Institute of Technology, Tokyo, Japan.

He is presently Director of the International Center for Actuators and Transducers and Professor of Electrical Engineering at the Pennsylvania State University, University Park, PA, and is vice-president of NF Electronic Instruments, Inc., State College, PA. Previously, he was a faculty member at Tokyo Institute of Technology and Sophia University, Tokyo, Japan. His research interests are in dielectrics, ferroelectrics, and piezoelectrics, including basic research on materials, device design and fabrication processes, as well as applicational development of solid state actuators to precision positioners, ultrasonic motors, etc.

Robert E. Newnham (M'85) was born in Amsterdam, NY, on March 28, 1929. He received the B.S. degree in mathematics in 1950 from Harrwick College, Oneonta, NY, the M.S. degree in physics from the Colorado State University, Fort Collins, CO, a Ph.D. in physics and mineralogy from The Pennsylvania State University, and a second doctorate in crystallography from Cambridge University in 1960.

He is ALCOA Professor of Solid State Science and Associate Director of the Materials Research Laboratory at the Pennsylvania State University, University Park, PA. Previously, he was a staff member of the Laboratory for Insulation Research at the Massachusetts Institute of Technology, Cambridge, MA. His research interests are in structure-property relations, electroceramics, and composite materials for electronic applications.

APPENDIX 39

THE "CYMBAL" ELECTROMECHANICAL ACTUATOR

Aydin Dogan, Jose F. Fernandez, Kenji Uchino, and Robert E. Newnham,
ICAT-Materials Research Laboratory-The Pennsylvania State University
University Park, PA 16802

Abstract- **A new transducer design was developed named the "Cymbal Transducer" with larger displacement, larger generative forces and more cost effective manufacturing. The cymbal transducers consist of a cylindrical ceramic element sandwiched between two truncated conical metal endcaps, and can be used as both sensors and actuators. The cymbal actuator exhibits almost 40 times higher displacement than the same size of ceramic element. Effective piezoelectric charge coefficient, eff. d_{33}, of a cymbal is roughly 40 times higher than PZT itself.**

I. INTRODUCTION

This paper describes a new composite transducer, the "Cymbal", with a large displacement and relatively high generative (blocking) force. The design and construction of a 12.7 mm diameter actuator with 2 mm total thickness is described, along with the displacement, generative force, and fastest response time. The cymbal actuator is a second generation moonie-type composite developed using FEA analysis in collaboration with experiment[1-5]. Displacement is primarily a flexural motion of the endcap for the original moonie design, but for the cymbal, the displacement is created by the combination of flexural and rotational motions [5]. Moreover, the endcaps are easily fabricated from sheet metal by punching, resulting in identical endcaps with minimal labor. The cymbal composite actuator is compared with other actuator designs in the discussion part of this paper.

II. FABRICATION AND CHARACTERIZATION METHOD

A punch die was designed to rapidly fabricate truncated conical shape "cymbal " endcaps at minimal cost. The die was manufactured from cutting tool steel for punching cymbal endcaps 12.7 mm in diameter with a 0.2 conical cavity depth and a 9.0 mm cavity diameter. Shaping and cutting operations are carried out simultaneously during processing. The final product requires only surface treatment for good bonding. The cymbal endcaps were fabricated from 0.25 and 0.20 mm thick sheets of various metals whose properties are listed in table I. The basic schematic of the cymbal transducer is shown in Fig. 1.

The cymbal endcaps were bonded to the piezoelectric, electrostrictive, or antiferroelectric-ferroelectric switching type of ceramic disk (12.7 mm in diameter and 1.0 mm thickness) around the circumference using Eccobond epoxy resin from Emerson & Cuming, taking special care not to fill the cavity. The thickness of the epoxy bonding layer was approximately 20 μm.

TABLE I PHYSICAL PROPERTIES OF ENDCAP MATERIALS

METAL ENDCAP	DENSITY (g/cm^3)	v_s (km/s)	α ($10^{-6} K^{-1}$)	E (GPa)
ZIRCONIUM	6.49	3.44	5.90	77
BRASS	8.53	3.59	19.9	110
KOVAR	8.36	4.00	5.50	138
LC STEEL	7.86	5.13	11.7	207
MOLYBDENUM	10.22	5.63	5.10	324
TUNGSTEN	19.30	4.58	4.60	405

The displacement of the composite actuator at 0.1 Hz under 1kV/mm electric field was measured with a Linear Voltage Differential Transducer (LVDT) having a resolution of approximately 0.05 μm. Generative (blocking) force measurements were done under static loading conditions, again using the LVDT system. Resonance characteristics were obtained with an Impedance/Gain Phase Analyzer HP-4194A to calculate the response speed and to evaluate the bonding layer.

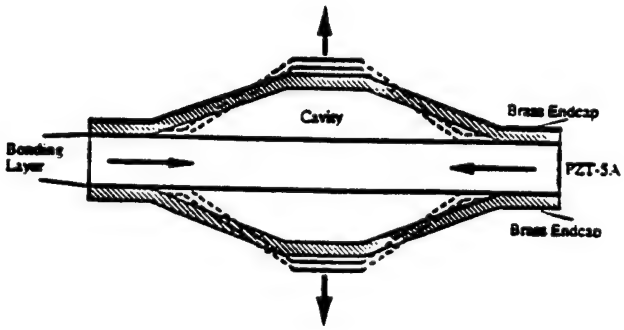

Fig. 1 Schematic of the cymbal transducer.

III. EXPERIMENTAL RESULTS

A) Displacement characteristics of the cymbal actuator

Fig. 2 shows the position dependence of the displacement cymbal actuators (0.2 mm thick endcaps) in comparison with earlier designs. Position-dependent displacement is a disadvantage of the original moonie. Moonies with grooved endcaps show significantly less position-dependent displacement. The cymbal design delivers a homogeneous displacement with deviations of <1 μm over a wide section of the center of the endcap. The large flat contact surface of the new endcap design makes it more practical for stacking the individual actuators together to reach higher displacements. Additionally, the new multistacked struc-

0-7803-3355-1/96/$5.00 © 1996 IEEE.

ture is more stable under axisymmetric loading. A displacement value of 175 μm has been achieved for the stacked cymbal actuator (five cymbals stacked in series) [5].

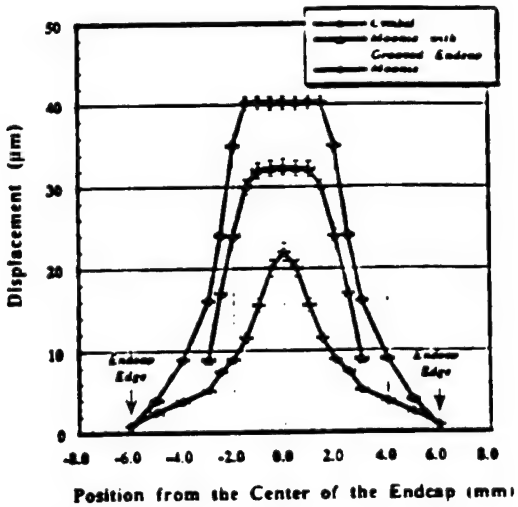

Fig. 2 Position dependence of the displacement of cymbal actuator

Fig. 3 shows the effect of Young's modulus of the metal endcaps and type of ceramic materials on the displacement of composite cymbal actuators (0.25 mm thick endcaps). For the same metal endcap, there is dependence of the displacement on the d_{31} piezoelectric coefficient of the ceramic. The higher the contraction of the PZT in the radial direction, and thereafter the contraction of the cavity, the higher the axial displacement of the cap. The decrease of the displacement with the increase in the stiffness of the metal endcap is related to higher mechanical losses in the roto-flextensional motion (monolithic hinge type plus flextensional motion) of the endcap. The displacement of the stiffest metal is approximately 52-57% of that achieved using less stiff metal endcaps, and it is practically independent of the ceramic type.

Piezoelectric, electrostrictive and antiferroelectric-ferroelectric switching type of electro-active ceramic elements can be used as the driving element in the cymbal design. Even though they exibit linear displacement characteristics, cymbals with piezoelectric ceramics show high hysteresis. By using PMN-PT type of electrostrictive ceramics, hysteric losses can be decreased drastically. However cymbal actuators with electrostrictive driving elements exhibit non-linear displacement according with the relaxor characteristics of the PMN-PT. Very interesting results can be obtained with antiferroelectric-ferroelectric switching type of PNZST ceramic driving element. The unique property of this material is its volumetric expansion under applied electric field. With the cymbal endcap design this volumetric expansion is converted to negative axial displacement. Fig. 4 shows the displacement hysteresis of the cymbal actuator with PNZST driving element.

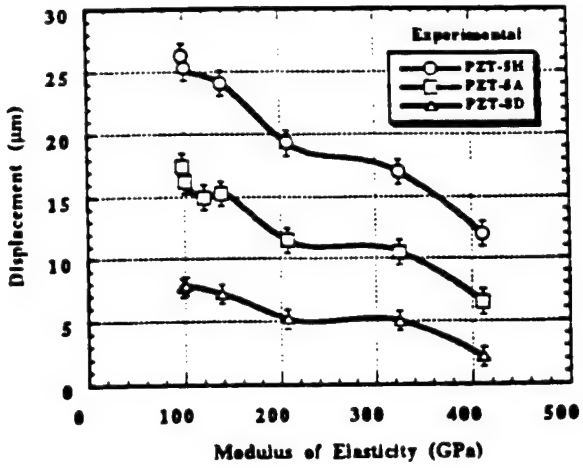

Fig. 3 Displacement of the cymbal actuators for various ceramics and metal endcaps

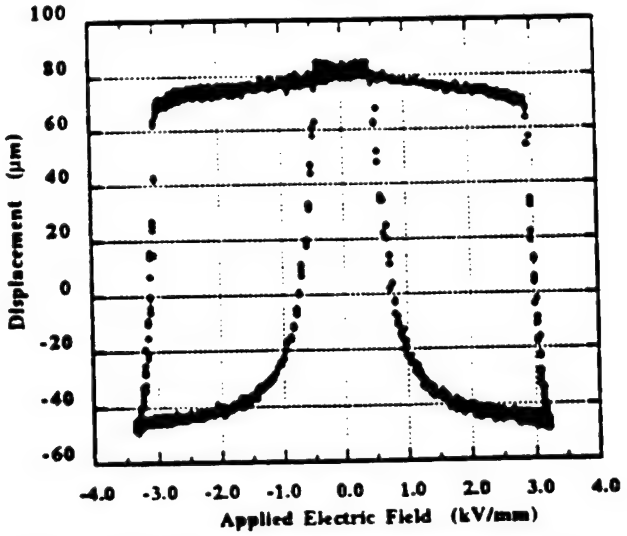

Fig. 4 Displacement hysteresis of the cymbal with PNZST driving element

B) Maximum Generative (Blocking) Force

The maximum generative force of the cymbal actuator with brass endcaps is around 15 N. (This corresponds to the intercept on the force axis at the point corresponding to the blocking force for which the displacement is equal to zero). The elasticity of the endcap material is a key parameter for the cymbal actuator since the endcaps tend to act like a spring under an applied force. The force range for the cymbal actuator is appreciably greater than that of the moonie actuator. By using a stiff metal for the endcap, the force limit can be increased markedly. The cymbal actuator with tungsten endcaps exhibits a generative force of more than 100 N. Fig. 5 shows the effect of modules of elasticity on the displacement and generative force performance of the cymbal actuator.

C) Fastest response time of the cymbal actuator

The fastest response time is an important criteria for the actuators and it can be defined as the time to achieve the quick and precise response of the actuator without overshoot and ringing [6]. The mechanical resonance of the system limits the practical actuation range. Actuators should be used in the linear range of their resonance spectrum. The fastest response time (FRT) of the cymbal transducer was evaluated from: $t_{(res)} = (1/f_n)$, where f_n is the flextensional resonance frequency. Fig. 6 shows the FRT of the various cymbal actuators with different piezoelectric driving element as a function of sound velocity of metal endcaps. The fastest response time of the cymbal actuator is about 50 μsec for the given dimensions.

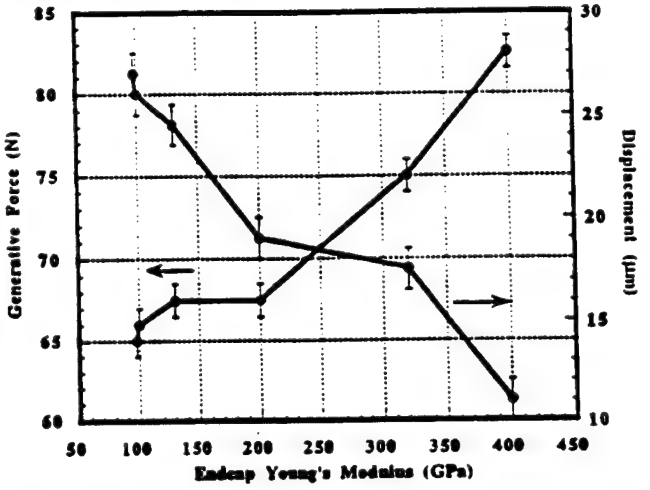

Fig. 5 Effect of modules of elasticity on the displacement and generative force performance of the cymbal actuator

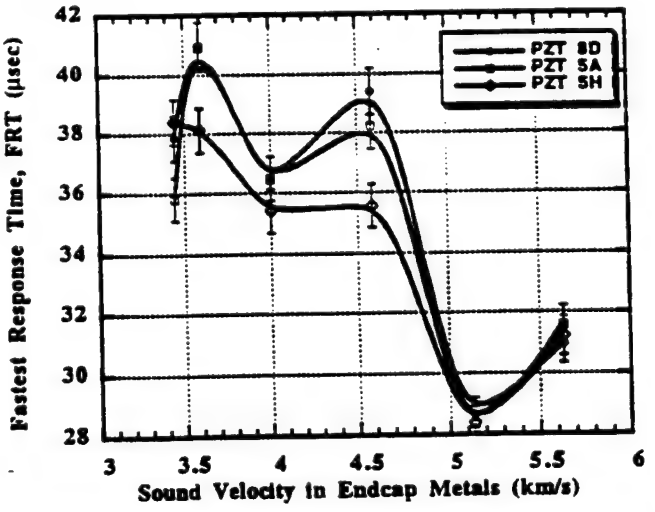

Fig. 6 FRT of the cymbal actuator as a function of sound velocity of the endcap materials

D) Effective Piezoelectric Coefficient of the Cymbal

The piezoelectric charge coefficient is a material parameter. The direct piezoelectric effect is important for sensors and the converse piezoelectric effect is important for actuators. Because of the composite design of moonie and cymbal, the effective piezoelectric coefficient is used to distinguish it from a material constant. The piezoelectric coefficient of the moonie and cymbal transducers were measured with a modified Berlincourt d_{33} meter. For samples with 0.30 mm thick brass endcaps, a piezoelectric coefficient of approximately 10,000 pC/N was measured at the center. The cavity beneath the endcap of the moonie actuator plays a crucial role on the characteristics of the moonie [3]. The piezoelectric charge coefficient of moonie transducers also shows position dependent behavior similar to that of the displacement.

With the cymbal endcaps the piezoelectric coefficients increased almost 60%. For a cymbal 12.7 mm in diameter and 1.7 mm in total thickness, an effective piezoelectric coefficient of more than 15,000 pC/N was measured over the 3 mm diameter center section of the cymbal transducer. We have concluded that the thick metal region near the edge of the moonie metal endcaps is a passive region which does not assist stress transfer, and acts to decrease the total efficiency. Cymbal endcaps transfer the stress more efficiently and improve the energy transfer markedly.

IV. DISCUSSION

A. Comparison of the Solid State Actuator Designs

Several features of the various solid state actuator designs are listed in Table II. It is rather difficult to compare the different actuators because of differences in geometry and various operating conditions for specific applications. To make a fair comparison, similar dimensions for each actuator were selected, and the measurement conditions are those specified in Table II. Flextensional moonie and cymbal actuators with their moderate generative force and displacement values fill the gap between multilayer and bimorph actuators. Each solid state actuator design has attractive features that can be exploited for certain applications. Advantages of the moonie and cymbal actuators are the easy tailoring of the desired actuator properties by altering the cavity size and endcap dimensions. Easy fabrication is another advantage. The rainbow actuator also partially covers this gap [7]. For that type of actuator a reduction step during processing of the ceramic element at high temperature results in a semiconducting layer and stress-bias. Even though it shows flexural motion, the rainbow can be categorized as a monomorph or a unimorph type of actuator. The effective coupling factor of rainbow is theoretically smaller than the moonie and cymbal. High applied field, position-dependent displacement and cost are

TABLE II. COMPARISON OF THE SOLID STATE ACTUATOR DESIGNS

FEATURES	MULTILAYER [10]	BIMORPH [10]	RAINBOW [7]	CYMBAL	MOONIE [3],[4]
Dimensions	5x5x12.7 (lxwxt)	12.7x10x0.6 (lxwxt)	ϕ 12.7 mm, t= 0.5 mm	ϕ 12.7 mm, t= 1.7 mm	ϕ 12.7 mm, t= 1.7 mm
Driving Voltage (V)	100	100	450	100	100
Displacement (μm)	10	35	20	40	20
Contact Surface (mm^2)	25	1	1	3	1
Generative Force (N)	900	0.5-1	1-3	15	3
Position Dependent of Displacement	None	Maximum at the tip	Maximum at the center	Maximum at the center but More diffuse	Maximum at the center
Stability Under Loading	Very high	Very low	Low	High	Low
Fastest Response Time (μSec)	1- 5	100	100	5-50	5-50
Fabrication Method	Type casting and cofiring at 1200 °C	Bonding ceramic element with metal shim	Reducing ceramic element At 950 °C	Bonding ceramic element with metal endcaps	Bonding ceramic element with metal endcaps
COST	HIGH	LOW	MEDIUM	LOW	MEDIUM

the main disadvantages of the rainbow actuator in comparison with the cymbal. In the moonie and cymbal design, a multilayer piezoelectric ceramic can be used as driving element to reduce the drive voltage. In this study, we kept the dimensions constant to investigate the effect of endcap materials and driving elements. Moreover, it is possible to reach higher displacement by scaling the structure. For the sample of 35 mm diameter, a displacement value of 150μm has been achieved. FEA and scaling studies of the cymbal transducer will be presented in some other publications.

B) Potential Applications for The Cymbal Transducers

The cymbal actuators have great potential in the automotive industry where they can be utilized as sensing and vibration suppression elements. The cymbal actuators can also be utilized as the switching element in valve designs. There is a volume change inside the moonie and cymbal transducers during cycling. This volume change can be utilized in minipump applications. The high density memory storage driver such as CD-ROM driver and magneto-optic memory storage driver are other possible applications for cymbal actuators capable of delivering precise positioning.

Because of their very high piezoelectric charge coefficients, moonie and cymbal transducers can be used as hydrophones, accelerometers and air acoustic transducers. Cymbal accelerometers have more than two order of magnitude higher sensitivity than PZT ceramics at low frequencies [8]. The advantages of the cymbal type of hydrophone are very large d_h (hydrostatic charge) and g_h (hydrostatic voltage) coefficients along with light weight and inexpensive fabrication [9].

ACKNOWLEDGMENT

The authors wish to thank Dr. M. Megherhi of PiezoKinetics Inc., and Mr. J.F. Tressler for their advice and assistance. The authors would like to express their gratitude for the support to the following agencies and organizations: ONR Contract no. N00014-92 J 1510, Turkish Science and Technology Council (TUBITAK), Spanish Science Ministry (CICYT MAT94-807 and DGICYT PR94-028.

REFERENCES

[1] R. E Newnham, Q. C. Xu, and S. Yoshikawa, "Metal-Electroactive Ceramic Composite Actuators," U.S. patent, 5,276,657, Jan 4, 1994.

[2] A. Dogan, Q.C. Xu, K. Onitsuka, S. Yoshikawa, K. Uchino, R.E. Newnham" High Displacement Ceramic-Metal Composite Actuator," *Ferroelectrics* Vol. 156, pp. 1-6, 1994.

[3] A.Dogan, S. Yoshikawa, K. Uchino, R.E. Newnham, "The Effect of Geometry on the Characteristics of the Moonie Transducer and Reliability Issue", IEEE Ultrasonic Symposium Proceedings, Vol. II, pp. 935-939, 1994.

[4] K. Onitsuka, A. Dogan, J.F. Tressler, Q.C. Xu, S. Yoshikawa, R.E. Newnham, " Metal-Ceramic Composite Transducer, The Moonie", *J. Int. Mat. Sys. & Struct.*, Vol. 6, pp. 447-455, 1995.

[5] A. Dogan, K.Uchino and R.E. Newnham, "Composite piezoelectric transducer with truncated conical endcaps, Cymbal", Transaction of IEEE/UFFC (accepted for publication 1996)

[6] Sugiyama and K. Uchino, Proc. of 6th IEEE Int'l Symposium of Applied Ferroelectrics, p 637 (1986)

[7] G. Haertling, "Rainbow ceramics, a new type of ultra high displacement actuator," Bull. of Am. Ceramic Soc., Vol. 73, No 1, pp. 93-96, 1994.

[8] B. Koc, A. Dogan J.F. Fernandez, R.E. Newnham, and K. Uchino "Accelerometer application of the moonie and cymbal transducers" *Japanese Journal of Applied Physics*, (Submitted), 1995

[9] J.F. Tressler, A. Dogan, J.F. Fernandez, J.T. Fielding, K. Uchino, R. E. Newnham "Capped Ceramic Hydrophone" IEEE-UFFC Ultrasonic Symposium Proceeding, Seattle 1995.

[10] Multilayer Piezoelectric Actuator, Technical Documents, TOKIN Co., Japan, 1988.

APPENDIX 40

Ceramic-Metal Composite Transducers for Underwater Acoustic Applications

James F. Tressler, Wenwu Cao, Kenji Uchino, and Robert E. Newnham
International Center for Actuators and Transducers, Materials Research Laboratory
Pennsylvania State University, University Park, PA 16802 USA

Abstract--A ceramic-metal composite electroacoustic transducer has been developed for use as an underwater projector or receiver. Its resonance frequency ranges from 10 kHz to 40 kHz and its effective coupling coefficient is around 20%. Finite element analysis has been performed to ascertain how the transducer dimensions and the materials that comprise it effect aforementioned parameters.

I. INTRODUCTION

A. The Cymbal Transducer

The new cymbal-type transducer [1], like the patented moonie transducer [2], is based on the concept of the flextensional transducer. Both the cymbal and moonie utilize either a poled piezoelectric, electrostrictive, or ferro- to antiferroelectric phase change material in the form of a ceramic disk (fully electroded on each face). This disk is sandwiched between two specially shaped metal electrode endcaps, each of which contains a shallow air-filled cavity on its inner surface. In the case of the moonie transducer, the cavities are in the shape of a half moon, whereas the cymbal contains a truncated cone-shaped cavity (see Fig. 1). The presence of these cavities allows the metal caps to serve as mechanical transformers for converting a portion of an incident axial direction stress into radial and tangential stresses of opposite sign. Alternatively, the caps can also couple an extensional vibration mode of the ceramic to a flexural vibration motion of the cap to produce a large displacement in the axial direction.

B. Finite Element Analysis

The finite element method is a powerful tool for the design and analysis of electroacoustic transducers. There are a host of high quality references that detail the theory of FEM so it will not be discussed here. A number of software packages are currently available which perform FEA. The two most common which have the capability to perform piezoelectric analysis are Atila® and ANSYS®. The latter can do static, harmonic, transient, or modal analyses [3]. Static analysis is used to determine displacements, stresses, etc., under static loading conditions. Harmonic analysis determines the steady state response of a structure under a sinusoidal external drive. Transient dynamic analysis ascertains the response due to arbitrarily time-varying loads, and modal analysis calculates the natural frequencies and mode shapes of the structure.

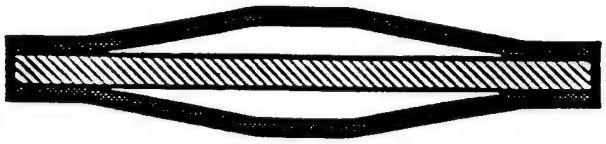

Fig. 1. Cross sectional view of the cymbal transducer (not to scale)

C. Transducer Characterization

When a transducer is used to detect sound underwater, it is commonly referred to as a source or projector. Conversely, when it is used to detect underwater sound, it is called a receiver or hydrophone. It is typically desirable to use a hydrophone at frequencies well below its fundamental resonance so that its response (i.e. output voltage per unit incident pressure) will be independent of frequency over a wide range. Projectors, on the other hand, are generally driven in the neighborhood of the resonance frequency in order to achieve the maximum volume velocity and output power.

The effective coupling coefficient, k_{eff}, is a measure of the transduction process. Its definition, based on energy conservation, is:

$$k_{eff} = \sqrt{\frac{\text{stored mechanical energy}}{\text{input electrical energy}}} \qquad (1)$$

This coefficient can be calculated easily from the resonance (f_r) and anti-resonance frequencies (f_a) as:

$$k_{eff} = \sqrt{1 - \left(\frac{f_r}{f_a}\right)^2} \qquad (2)$$

This paper will focus on how the geometry and materials affect the resonance frequency and effective coupling coefficient of the cymbal transducer.

0-7803-3355-1/96/$5.00

II. EXPERIMENTAL PROCEDURE

A. Cymbal Transducer Fabrication

Using metal foil between 120 μm and 380 μm thick, 12.7 mm diameter caps were simultaneously cut and shaped using a die punch. The cavity diameter was tapered from 3.0 mm at the top of the cap to 9.0 mm at the bottom. The depth of the cavity, as measured from the top of the cap, ranged from 120 μm to 470 μm. These caps were then adhered to 1.00 mm thick, 12.7 mm diameter poled PZT-552 disks (Piezokinetics) using Emerson and Cuming insulating epoxy. To ensure proper alignment of the caps, the entire assembly was kept under pressure in a special die during the 24 hour, room temperature curing step.

B. Finite Element Analysis

The ANSYS® software package version 5.1 (Swanson Analysis Systems, Inc.) was used to calculate the resonance and antiresonance frequencies, as well as the vibration modes of the cymbal transducer. A two-dimensional axisymmetric model was analyzed and it consisted of three parts: (1) a piezoelectric (PZT) disk, (2) two metal caps, and (3) epoxy layers between the cap and ceramic as well as surrounding the structure.

The PZT disk was fixed at a radius of 6.35 mm and a thickness of 1.0 mm. Equipotential surfaces were placed on both the top and bottom surfaces of the PZT disk to represent the electrodes. The epoxy layer between the cap and ceramic had a thickness of 20 μm and a width of 1.50 mm. The outer epoxy layer had a width of 0.20 mm and a height equal to that of the outer rim of the transducer. The radius of the cavity was fixed at 4.5 mm at the cap/PZT interface and was tapered to 1.5 mm at the top of the cap. Both the thickness of the cap as well as the maximum cavity depth were used as variables in the model.

The resonance frequencies of the transducer were obtained using the short circuit elastic stiffness matrix, $[c^E]$, in the model; whereas the antiresonance frequencies were calculated using the open circuit stiffnesses $[c^D]$. The coupling coefficients were then found by inserting the aforementioned values into Equation (2) [4]. Resonance and antiresonance frequencies were also obtained experimentally in air from the cymbal's admittance spectra using an HP 4194A Impedance Analyzer. The calculated values were then compared to those obtained experimentally.

III. EXPERIMENTAL RESULTS

The results presented in this paper will focus on the cymbal transducer as an underwater projector, as its pressure tolerance and performance as a hydrophone has been reported previously [5]. Fig. 2 shows the first vibration mode of the cymbal transducer as calculated by the ANSYS® program. This mode is the (0,1) or "umbrella" flexural mode of the caps. The dashed lines indicate the undeformed shape.

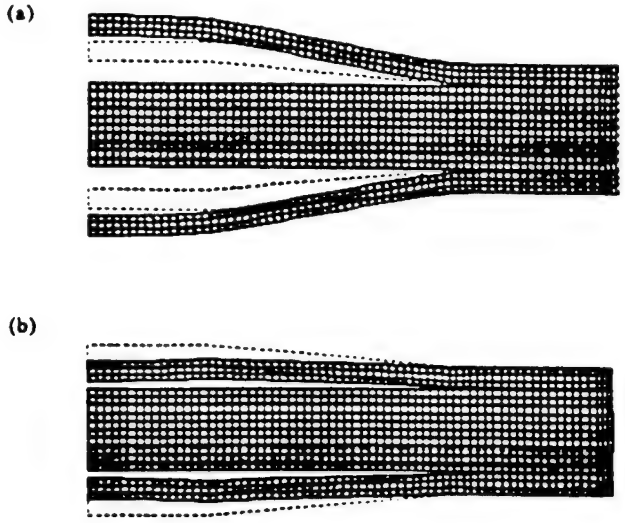

Fig. 2. First vibration mode of the cymbal transducer showing the cap deflection when (a) the ceramic is contracting, and (b) when the ceramic is expanding. The mesh size is also shown here.

Fig. 3 shows the experimentally measured admittance and phase as a function of frequency for a brass capped cymbal in the neighborhood of its fundamental resonance. The cap was 250 μm thick and had a maximum cavity depth of 320 μm. A sharp, smooth peak is indicative of a good quality metal-to-ceramic bond. The resonance at 21 kHz is due to the (0,1) vibration mode of the cap, as described above.

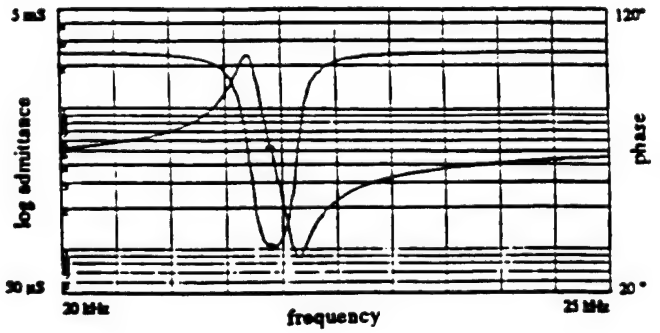

Fig. 3. Admittance and phase as a function of frequency for a brass capped cymbal transducer.

The first resonance frequency of a fixed size cymbal transducer but with different cap materials is shown in Fig. 4. It appears to be a linear function of the ultrasonic velocity of the cap material. The quantity $[E/\rho(1-\sigma^2)]^{1/2}$ is proportional to the resonance frequency of a thin circular plate clamped around its edge [6], which is approximately the boundary condition present in the cymbal. Experimentally obtained results are included for comparison. Discrepancies are attributed to the inability to precisely control the bonding layer width, cavity diameter, and cavity depth (all of which influence the resonance frequency) when fabricating the samples. These results do show, however, that for a given size cymbal transducer, the fundamental resonance frequency can be varied simply by changing the cap material.

The effective coupling coefficients for cymbals with different cap materials, both calculated and experimentally determined, are shown in Fig. 5. The coefficient is solely a function of the Young's modulus of the cap material, as opposed to the resonance frequency, which also depends upon the density and Poisson's ratio. The model underestimates the experimentally obtained value by as much as 20%. This is most likely due to the inability to adequately model the bonding layer. The experimentally determined coupling coefficients are probably more accurate because they are nearly equal to the reported value for a class V flextensional [4].

Fig. 6 shows how the cap thickness influences the resonance frequency of the cymbal transducer. These results show that as the cap thickness increases, the resonance frequency also increases. This is because the caps effectively become "stiffer" as they become thicker.

The effect of the cavity depth (i.e. the cap shape) on the resonance frequency is presented in Fig. 7. As the cavity depth increases, a corresponding increase in the resonance frequency is also observed. This is attributed to the fact that the nodal ring associated with the (0,1) vibration mode of the cap moves toward the center of the cap as the cavity depth increases, thus reducing the actively vibrating surface area.

Fig. 8 shows how the cap thickness and cavity depth affect the effective coupling coefficient (as calculated by the ANSYS® program). The data show that the cap thickness has relatively little effect on k_{eff}, whereas it is strongly influenced by the cavity depth.

Figs. 9 and 10 show the effect of PZT type on the resonance frequency and effective coupling coefficient, respectively. These calculated results show that the PZT type has little effect on the resonance frequency of the cymbal transducer. However, the transducers with softer PZT's exhibit slightly higher coupling coefficients than those which are made of hard PZT.

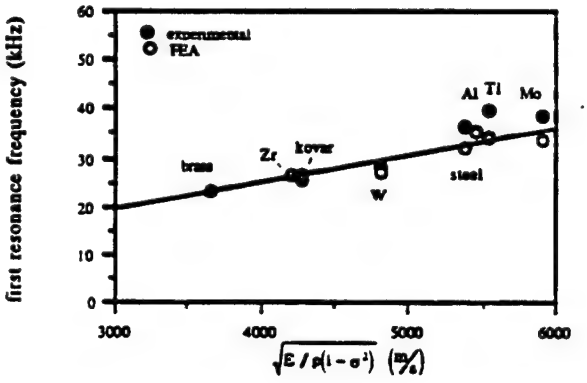

Fig. 4. Effect of cap materials on the first resonance frequency of the cymbal transducer. Metal names or elemental symbols are shown.

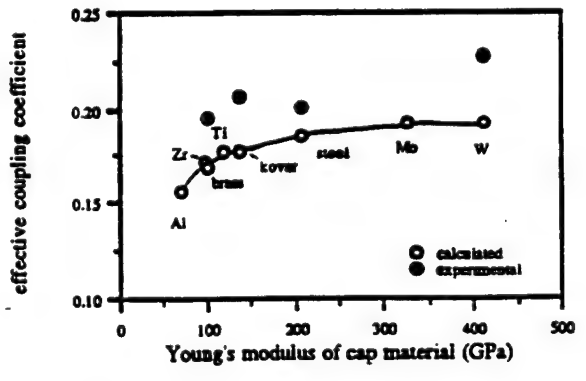

Fig. 5. Effect of cap materials on the effective coupling coefficient of the cymbal transducer. Metal names or elemental symbols are shown.

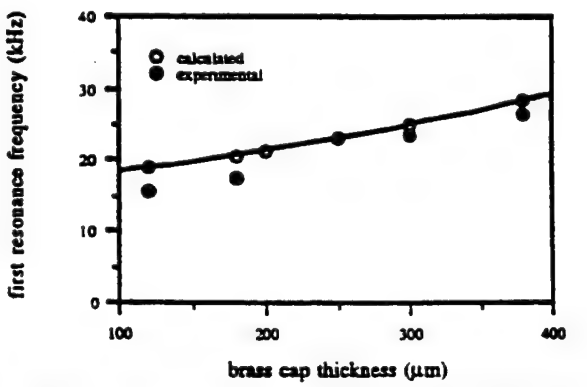

Fig. 6. Effect of brass cap thickness on the first resonance frequency of a cymbal transducer.

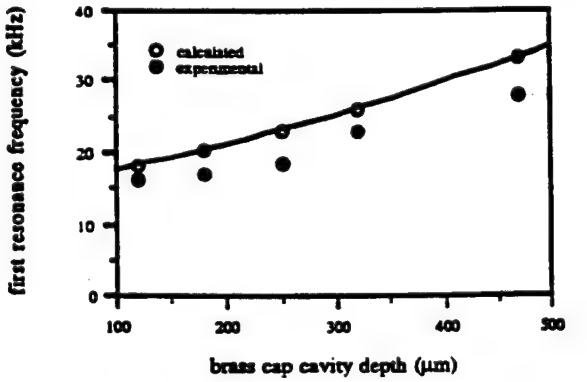

Fig. 7. Effect of brass cap cavity depth on the first resonance frequency of a cymbal transducer.

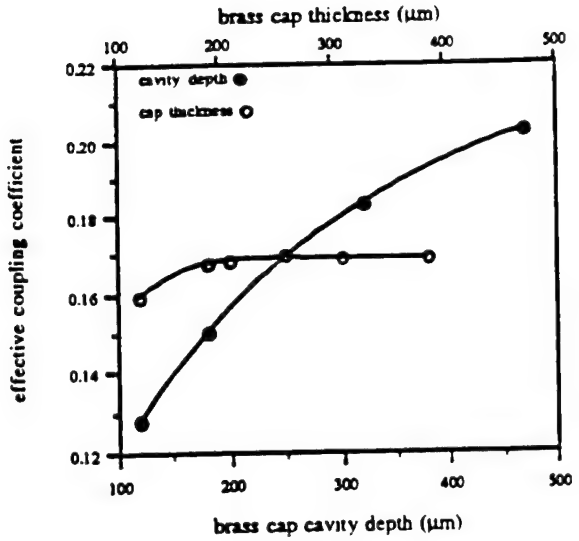

Fig. 8. Effect of brass cap thickness and cavity depth on the effective coupling coefficient of a cymbal transducer.

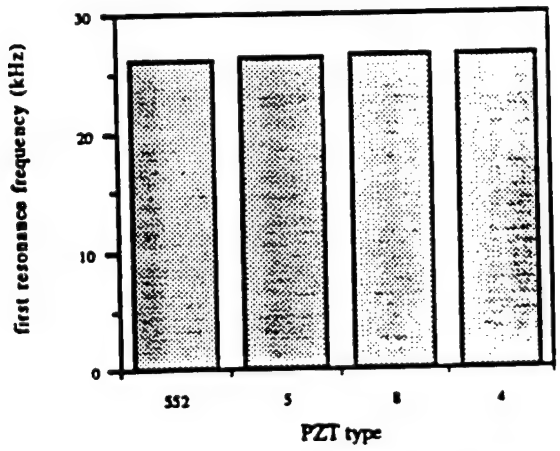

Fig. 9. Effect of PZT type on the resonance frequency of a cymbal transducer (with brass caps). Results are from FEA calculations.

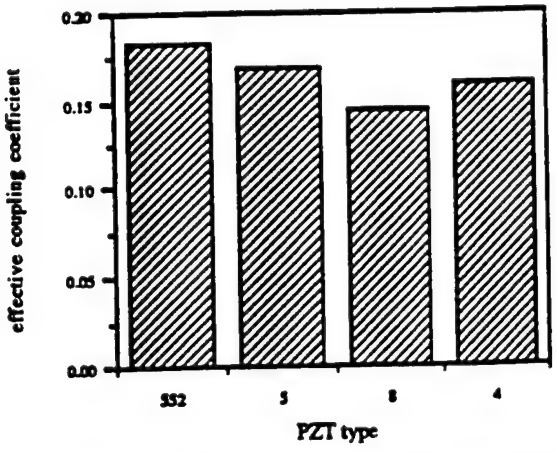

Fig. 10. Effect of PZT type on the effective coupling coefficient of a cymbal transducer (with brass caps). Results are from FEA calculations.

IV CONCLUSIONS

Both the fundamental resonance frequency and effective coupling coefficient of a cymbal transducer can be easily tailored either by changing its endcap material or varying the cap dimensions. This capability gives the transducer designer wider flexibility if constrained by size or materials limitations. Studies are currently underway to determine the effect of water loading on the performance and properties of the transducers.

ACKNOWLEDGMENT

This work was funded through the Office of Naval Research grant #N0001492J1510.

REFERENCES

[1] A. Dogan and R.E. Newnham, "Metal-electroactive ceramic composite actuator," United States Patent pending.

[2] R. E. Newnham, Q. C. Xu, and S. Yoshikawa, "Transformed Stress Direction Acoustic Transducer," United States Patent 4,999,819, March 12, 1991.

[3] *ANSYS User Manuals for revision 5.0*, Swanson Analysis Systems, Inc., Houston, PA, 1992.

[4] K. D. Rolt and J. L. Butler, "Finite element modulus substitution method for sonar transducer effective coupling coefficient," in *Proceedings of the Third International Workshop on Transducers for Sonics and Ultrasonics*, M. D. McCollum, B. F. Hamonic, and O. B. Wilson, Eds., Lancaster, PA: Technomic, 1993, pp. 344-352.

[5] J. F. Tressler, A. Dogan, J. F. Fernandez, J. T. Fielding, Jr., K. Uchino, and R. E. Newnham, "Capped ceramic hydrophones," in *1995 IEEE Ultrasonics Proceedings*, M. Levy, S. C. Schneider, B. R. McAvoy, Eds., Piscataway, NJ: Inst. Electrical and Electronics Engineers, 1995, pp. 897-900.

[6] L. E. Kinsler, A. R. Frey, A. B. Coppens, and J. V. Sanders, *Fundamentals of Acoustics*, 3rd ed., New York: John Wiley & Sons, 1982, ch. 4, pp. 92-95.

APPENDIX 41

Special Issue Correspondence

Doubly Resonant Cymbal-Type Transducers

James F. Tressler and
Robert E. Newnham, *Member, IEEE*

Abstract—**A doubly resonant cymbal-type transducer has been developed by capping a poled piezoceramic disk asymmetrically. It is intended for use in the frequency range between 10 and 50 kHz. The two resonance frequencies can be easily manipulated by selecting appropriate cap materials and/or geometry. The prominent feature of this device is the ability to obtain two resonances at desired frequencies without the need for electrical tuning. In addition, proper placement of the resonance frequencies may also allow for the broadening of the operational bandwidth as well as the generation of difference frequencies.**

I. Introduction

MULTIPLE RESONANT ACOUSTIC PROJECTORS can exhibit a number of advantages over their singly resonant counterparts, namely the potential for wider operational bandwidths and difference frequency generation. Typically, multiple resonances are generated through the use of electronics and/or the use of acoustic matching plates. Steel *et al.* [1] developed a continuously tunable two-plate high-frequency (240 kHz) transducer in which one piezoceramic disk was used as the driver and the second was used to control the resonance condition through the use of appropriate inductors and resistors in the electrical circuitry. Jain and Smith [2] applied this same concept to their low frequency (30 kHz) continuously tunable sandwich transducer, which consisted of four PZT rings (2 drive, 2 control) sandwiched between two metal masses. Loading the control ceramics with an inductive load made the structure resonate at two frequencies. Inouye *et al.* [3] achieved dual resonance conditions by attaching an acoustic matching plate to a tapered piezoceramic resonator. This configuration had resonances at 23 and 32 kHz. Similarly, a constant area Langevin transducer consisting of a quarter wave front (head) layer, a ceramic stack, and a steel tail was found to exhibit two distinct resonance peaks in its conduction response (at 73 and 119 kHz). This dual resonance behavior was only observed, though, when the characteristic impedance of the head material exceeded 4 MRayls [4]. Doubly resonant longitudinal vibrations have been obtained in tonpilz transducers by using three masses instead of the conventional two, where the additional mass is inserted within the piezoelectric stack [5]. This type of transducer has two mechanical resonances that can be used for both transmitting and receiving operations. By proper design, it is possible to use the entire frequency band from the lower resonance frequency to somewhat above the upper resonance frequency. Very high frequency dual mode transducers are also being investigated as ultrasonic probes for the carotid artery [6]. In this application, a dual frequency probe made from a multilayer ceramic is used to obtain a mode image simultaneously with a high resolution B mode scan. The ceramic consists of two layers of different thickness poled in opposite directions. A thickness ratio of 1 to 0.7 gave dual resonances at 3.75 and 7.5 MHz.

Manuscript received July 8, 1996; accepted April 2, 1997.

The authors are with the Materials Research Laboratory, The Pennsylvania State University, University Park, PA 16802 (e-mail: jft104@psu.edu).

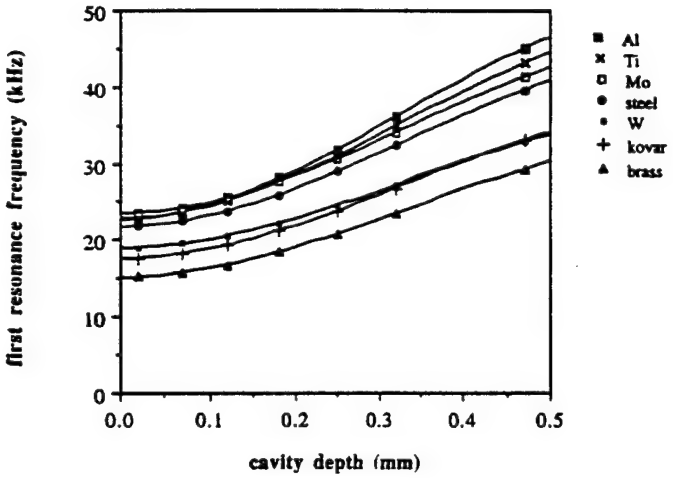

Fig. 1. Effect of cap material and cavity depth on the first resonance frequency of a standard size cymbal transducer (values calculated from Ansys® program). The key shows the element symbols or alloy names used as cap materials.

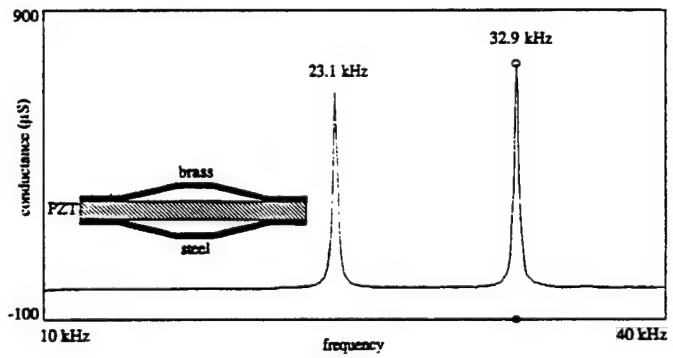

Fig. 2. Conductance vs. frequency for a cymbal transducer with a brass/steel endcap combination as measured in air.

The patented moonie and cymbal-type transducers [7], [8] have been shown to be excellent electroacoustic transducer candidates. Their operational principles have been reported previously [9], [10]. The cymbal design consists of a piezoelectric ceramic disk (typically PZT) poled in the thickness direction which is sandwiched between two thin metal endcaps, each of which contains a truncated cone-shaped cavity on its inner surface. The moonie style cap, on the other hand, consists of a metal disk with a shallow conical cavity machined into its inner surface. When the ceramic contracts radially under the application of an applied AC electric field, the endcaps flex to give an amplified strain (displacement) in the direction normal to the cap surface. In addition, the moonie, and especially the cymbal, are characterized as being of small size, thin profile, and perhaps most importantly, easy and inexpensive to fabricate.

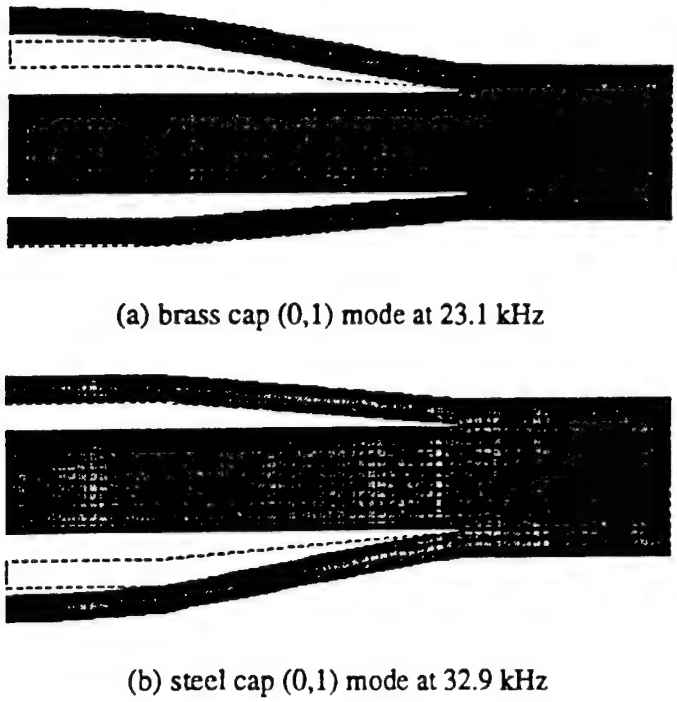

Fig. 3. Vibration mode shapes calculated by FEA for the brass/steel cap combination at (a) 23.1 kHz, and (b) 32.9 kHz. The dashed lines indicate the undeformed shape.

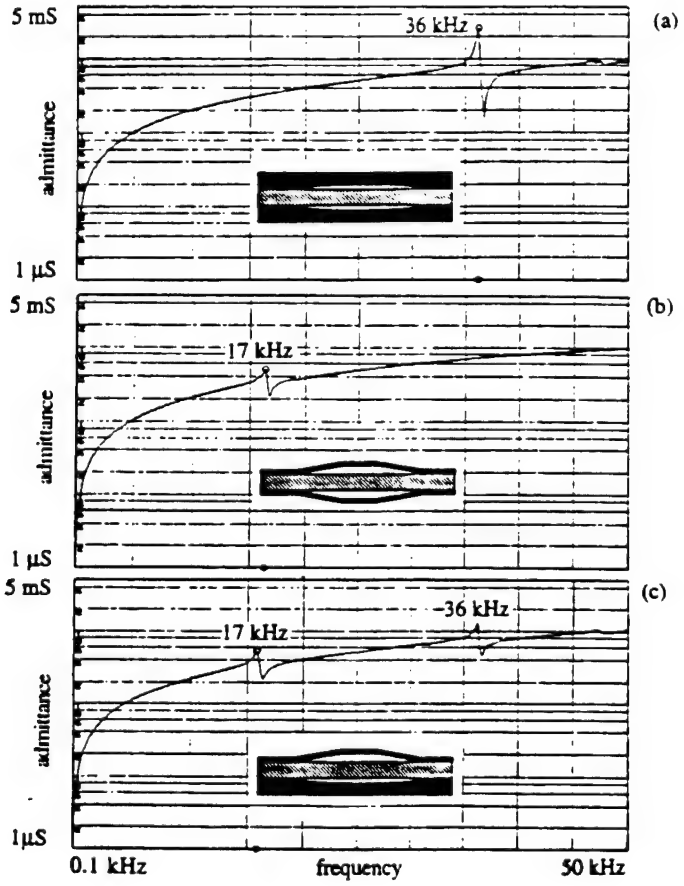

Fig. 4. Measured admittance spectra of (a) the standard brass-capped moonie transducer, (b) the standard brass-capped cymbal transducer, and (c) the moonie/cymbal cap combination transducer.

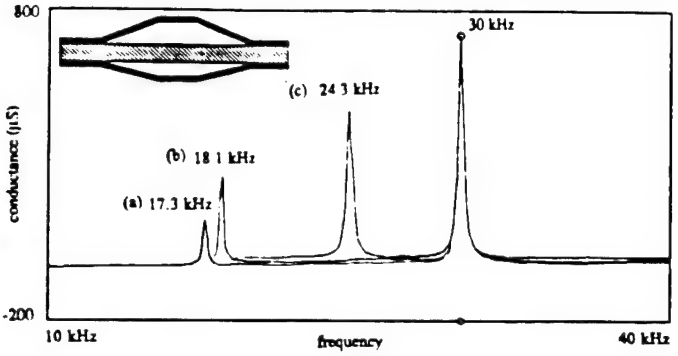

Fig. 5. Conductance vs. frequency for a cymbal transducer with two brass caps, one of which has a cavity depth of 0.47 mm and the other having a cavity depth of (a) 0.12 mm, (b) 0.18 mm, and (c) 0.32 mm. All were measured in air.

A doubly resonant cymbal-type transducer has been constructed by capping a PZT driving element asymmetrically. The focus of this paper is to demonstrate the ease by which it is possible to generate distinct resonances at any two desired frequencies between 10 and 50 kHz through proper design engineering without the need for electronic tuning or matching plates. Two configurations will be considered: two identically shaped cymbal caps of different metals, and two caps of the same material, but with different shapes.

II. Experimental Procedure

The doubly resonant cymbal transducers were made by first shaping the metal caps to the desired geometry. In the case of the cymbal caps, a die punch simultaneously cut and shaped the caps from a sheet of metal foil 0.25 mm thick. The dimensions of the cymbal caps were: diameter = 12.7 mm, thickness = 0.25 mm, the cavity diameter was tapered from 9.0 mm at the bottom of the cap to 3.0 mm at the top, and the maximum cavity depth ranged from 0.12 mm to 0.47 mm. The flange of each of the caps was bonded to a PZT-5A disk (Piezokinetics, Bellefonte, PA) poled in the thickness direction, which was 12.7 mm in diameter and 1.0 mm thick. The adhesive was a thin layer (≈ 20 μm thick, 1.5 mm wide) of Emerson and Cuming Insulating Epoxy (45LV epoxy resin, 15LV resin hardener). Great care must be taken to ensure that no epoxy leaks into the air-filled cavity and that the layer is thin enough to ensure a good metal/PZT electrode contact. The capacitance of the transducer and its admittance (or conductance) spectrum are simple and effective techniques that can be used to characterize the quality of the bonding layer, with the latter doubling as a means to observe the dual resonances. The Ansys® (Swanson Analysis Systems, Inc.) finite element software program was also used as a guide in designing the transducers. Modal analysis was used to obtain the resonance frequencies and mode shapes for a two dimensional axisymmetric model.

III. Experimental Results

The fundamental resonance frequency of a 12.7 mm diameter cymbal transducer is governed by the elastic constants of the endcap material [11], as well as the cap thickness and cavity dimensions. Fig. 1 shows the FEA calculated first resonance

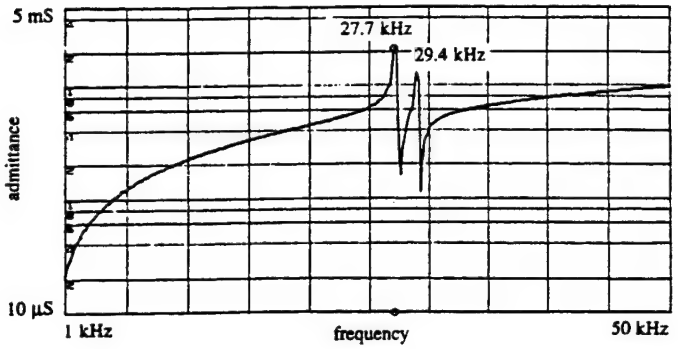

Fig. 6. Measured admittance spectrum of a brass-capped cymbal transducer showing the ability to couple the two resonances.

frequency of a cymbal transducer capped with different metals of varying cavity depth (cap thickness and cavity diameter held constant at 0.25 mm and 9.0 mm, respectively). As can be seen, by the appropriate selection of cap materials and cap geometry, the fundamental resonance frequency can be easily tailored from 15 kHz to about 45 kHz. These data imply that capping the PZT driving element asymetrically should result in a double resonance.

The first asymetrically capped cymbal transducer used two identically shaped caps of different materials, steel and brass. The measured conductance vs. frequency spectrum is shown in Fig. 2. The dual resonance behavior is quite apparent. The first resonance, at 23.1 kHz, is the (0, 1) mode associated with the brass cap and the second resonance, at 32.9 kHz, is the (0, 1) mode of the steel cap. This conclusion was arrived at from the mode shapes at these two frequencies as calculated by the Ansys® finite element program (Fig. 3). This shows that the dual resonance behavior of the steel/brass cap combination is a direct result of the individual vibrations associated with each cap. The use of two different cap types also results in a double resonance. Fig. 4 compares the measured admittance spectra of (a) the moonie-type transducer, (b) the cymbal-type transducer, and (c) the moonie/cymbal cap combination. These results experimentally verify the argument that the dual resonance behavior derives from the fundamental resonance mode of each individual cap.

As evidenced by Fig. 1, the cap geometry also strongly affects the resonance frequency. Therefore, obtaining dual resonance behavior with cymbal caps of a single material can also be accomplished by using two caps with different dimensions. The admittance spectra of cymbal transducers with brass caps each with a different cavity depth is shown in Fig. 5. The dual resonance behavior is again visible, where the first resonance, at 17.3, 18.1, or 24.3 kHz is due to the (0, 1) mode of the cap with the shallower cavity, 0.12 mm, 0.18 mm, or 0.32 mm, respectively. The second resonance, at 30 kHz, is due to the (0, 1) mode of the cap with the deeper cavity, 0.47 mm. Utilizing caps with nearly the same shape can drive the two resonances close enough that they can couple together (Fig. 6). When this occurs, it is possible to increase the operational bandwidth by lowering the mechanical Q. From this result, it appears as though the operational bandwidth of the doubly resonant cymbal is roughly twice that of the singly resonant device.

Being able to fix two individual resonances at the desired frequencies in a cymbal transducer of a given diameter by simply either capping it asymmetrically with different materials and/or with differently shaped caps provides the transducer designer the capability of working with a very simple structure and being able to manipulate the working frequency range of the device without the need for sophisticated electronics.

IV. Conclusions

A dual resonance transducer has been developed simply by capping a PZT disk driving element asymmetrically. The simple construction, small size, thin profile, inexpensive fabrication procedure, and ability to easily tailor the two resonances by changing the cap materials and/or manipulating their dimensions are the striking features of this device. It is expected that capping the ceramic driving element asymmetrically with caps of two different thicknesses or with two different cavity diameters will also generate dual resonance behavior.

References

[1] G. A. Steel, B. V. Smith, and B. K. Gazey, "Tunable sonar transducers." *Electron. Lett.*, vol. 22, pp. 758–759, July 1986.

[2] S. K. Jain and B. V. Smith, "Tunable sandwich transducer," *Electron. Lett.*, vol. 24, pp. 311–312, Mar. 1988.

[3] T. Inouye, T. Nada, A. Kameyama, K. Sugiuchi, S. Takahashi, and M. Konno, "Investigation for wide-band underwater ultrasonic transducers," *Trans. IEICE*, vol. E 70, pp. 723–734, Aug., 1987.

[4] B. V. Smith, R. L. Mansfield, D. T. I. Francis, and J. R. Dunn, "The design of a 100-kHz wideband sonar transducer," in *Proc. Third Int. Workshop Transducers Sonics Ultrason.*, M. D. McCollum, B. F. Hamonic, and O. B. Wilson, Eds., Lancaster, PA: Technomic, 1993, pp. 231–238.

[5] S. C. Thompson, M. P. Johnson, E. A. McLaughlin, and J. F. Lindberg, "Performance and recent developments with doubly resonant wideband transducers," in *Proc. Third Int. Workshop Transducers Sonics Ultrason.*, M. D. McCollum, B. F. Hamonic, and O. B. Wilson, Eds., Lancaster, PA: Technomic, 1993, pp. 239–249.

[6] S. Saitoh, M. Izumi, and Y. Mine, "A dual frequency ultrasonic probe for medical applications," *IEEE Trans. Ultrason., Ferroelect., Freq. Contr.*, vol. 42, pp. 294–300, Mar. 1995.

[7] R. E. Newnham, Q. C. Xu, and S. Yoshikawa, "Transformed stress direction acoustic transducer," U. S. Patent 4,999,819, Mar. 12, 1991.

[8] A. Dogan and R. E. Newnham, "Metal-electroactive ceramic composite actuator," U. S. Patent Pending.

[9] Q. C. Xu, S. Yoshikawa, J. R. Belsick, and R. E. Newnham, "Piezoelectric composites with high sensitivity and high capacitance for use at high pressures," *IEEE Trans. Ultrason., Ferroelect., Freq. Contr.*, vol. 38, pp. 634–639, Nov. 1991.

[10] Q. C. Xu, A. Dogan, J. Tressler, S. Yoshikawa, and R. E. Newnham, "Ceramic-metal composite actuator," *Ferroelectrics*, vol. 160, pp. 337–346, 1994.

[11] J. F. Tressler, A. Dogan, J. F. Fernandez, J. T. Fielding, Jr., K. Uchino, and R. E. Newnham, "Capped ceramic hydrophones," in *Proc. IEEE Ultrason. Symp.*, M. Levy, S. C. Schneider, and B. R. McAvoy, Eds., Piscataway, NJ: Inst. Electrical Electron. Eng., 1995, pp. 897–900.

APPENDIX 42

Finite Element Analysis of the Cymbal-Type Transducer

James F. Tressler, Wenwu Cao, Kenji Uchino, and Robert E. Newnham
Materials Research Laboratory, The Pennsylvania State University
University Park, PA 16802

Abstract -- The effect of material properties and dimensional changes on the fundamental resonance frequency of the cymbal transducer has been investigated using the ANSYS® finite element software program. Vibration mode shapes, calculated resonance frequencies and admittance spectra for both air- and water-loading are presented. Very good agreement is observed between the modeled and experimentally measured admittance spectra between 1 Hz and 200 kHz, establishing the validity of the model over this frequency range. The calculated data show that the fundamental resonance frequency can be easily manipulated simply by changing the cymbal cap material or dimensions.

I. INTRODUCTION

Flextensional transducers have seen a resurgence in interest in recent years as low frequency (i.e. typically less than 5 kHz), moderate to high acoustic output power underwater electroacoustic projectors [1]. Flextensionals consist of a piezoelectric or magnetostrictive ring, disk, or stack sandwiched between and mechanically coupled to curved metal shells or plates. Unfortunately, they are typically quite large in size and heavy.

The so-called "moonie" and "cymbal" type transducers are essentially miniaturized versions of flextensionals. These patented designs were originally developed as high sensitivity hydrophones and micropositioning actuators [2-5]. The only difference between the moonie and cymbal is in the shape of the caps. Their cross-sectional views, including

the standard dimensions, are compared in Fig. 1. The operational principle of the moonie and cymbal are the same: the caps convert and amplify the small radial displacement and vibration velocity of the piezoceramic disk into a much larger axial displacement and vibration velocity normal to the surface of the caps. Conversely, the caps can mechanically transform and amplify the incident axial direction stress, such as from a weak hydrostatic pressure wave, into a much larger radial direction stress, thereby enhancing the electrical charge developed on the electrodes of the piezoceramic disk. The advantages the cymbal transducer offers over the moonie design include an easier and less expensive fabrication procedure as well as more easily tailorable performance characteristics. The fabrication procedure has been detailed previously [4,5].

The various classes of flextensional transducers have been modeled by finite element methods quite extensively [6-9] as has the moonie design [3,10]. This paper will report on the FEA results from the cymbal and compare them with experimental data where possible. Namely, the effect of materials and design parameters on resonance frequency and admittance spectra will be described.

II. Finite Element Modeling

A. Principle

The fundamental purpose of finite element analysis is to mathematically describe, or predict, the physical behavior of an actual engineering system under various loading conditions. FEA allows the designer to manipulate and test the effects of all the possible design variables using computer analysis rather than by the more tedious alternative of actually building and testing prototype designs. Finite element analysis of the cymbal transducer was performed using the ANSYS® software package version 5.1 (Swanson Analysis Systems, Inc.) using a Sun workstation. In addition to the standard structural analyses, this modeling code also has the capability of modeling coupled-field phenomena (e.g. piezoelectricity) as well as acoustic fluid and fluid-structural interface effects. A

complete theoretical treatment of the finite element method, including derivation of the structural matrices, etc.. can be found in the ANSYS User's Manual [11] or in a large number of texts written on the subject. Basically, it is assumed that the structure being modeled consists of a finite assembly of elements which are meshed by a series of nodes, and that transmission of a load can only pass through these nodes.

ANSYS version 5.1 has the capability of performing six different types of structural analysis: static, harmonic, transient dynamic, modal, spectrum, and buckling. Harmonic analysis ascertains the steady-state response of a structure to loads that vary sinusoidally with time. In this case, the structural response is calculated at several different frequencies and a graph of the response output versus frequency is generated. Modal analysis is used to determine the natural frequencies and mode shapes of a structure. In this paper, only results from these two types of analyses will be discussed.

B. Procedure

Since the cymbal transducer exhibits axisymmetry about its central axis, it was modeled as a two dimensional axisymmetric body. A two dimensional axisymmetric model offers the advantage over the corresponding three dimensional model in that the size of the model is smaller and consequently calculation time is less.

The cymbal transducer consists of three parts: the metal caps, the active piezoelectric element, and an epoxy adhesive. For the caps and the epoxy, it was assumed that their material properties were linear and isotropic. The piezoelectric properties were taken to be linear and anisotropic. The boundary conditions were such that any translational motion of the model was prohibited and the appropriate symmetry conditions were flagged. In addition, a damping coefficient, which has to be obtained empiracally, was included.

When including the effects of water loading, the amount of water modeled was determined from the radiation impedance associated with a rigid circular piston located within an infinite baffle [12]. Assuming the piston (i.e. the cymbal) is small relative to one

wavelength, the piston added mass term (from the water) approaches a constant value of $(8/3)\rho a^3$, where ρ is the density of the medium and a is the outer radius of the cymbal cap. This term is equivalent to the mass of a cylinder of the acoustic medium with the same radius as the cymbal and a height of $8a/3\pi$, which is the minimum height of water over the surface of the cymbal that needs to be modeled and in this case is ≈ 6 mm. A radiation boundary was included at the edge of the water layer to prevent reflection of acoustic energy.

Unless otherwise noted, the results reported in this paper are for brass-capped cymbal transducers with the dimensions given in the caption of Fig. 1. The cymbal vibration modes, the in-air and in-water fundamental resonance frequencies, and a demonstration of the capability of generating the in-air and in-water admittance spectra by FEA will be shown.

III. Modeling Results

A. Vibration Modes

Fig. 2 shows the calculated cymbal cap vibration mode shapes corresponding to the (0,1), (0,2), (0,3), and PZT radial modes. The modes are designated by the ordered pair (m,n) where the integer m is the number of radial node lines and the integer n is the number of azimuthal nodal circles. Since a two dimensional axisymmetric body was modeled in this analysis, the cap vibration will always be symmetric, hence m is always zero. The (0,1) mode is known as the first, or fundamental, vibration mode of the cymbal caps. The frequency of the vibration modes depends on the cap material and geometry and will be discussed in further detail in later sections.

B. Admittance Spectra

The calculated and experimentally measured admittance spectra of a standard size brass-capped cymbal with dimensions described in Fig. 1 are compared in Fig. 3. Very

nice agreement is observed between the two, indicating that ANSYS models the cymbal behavior quite nicely in-air. When in-water, the fundamental resonance shifts to a lower frequency due to mass loading as described in section II. The calculated and experimentally obtained admittance spectra in the neighborhood of the first resonance frequency for in-air and in-water conditions are compared in Fig. 4. Again, excellent agreement is observed between the measured and calculated in-air and in-water results.

C. Resonance Frequencies

1. PZT type and thickness As evidenced by Fig. 5, the fundamental resonance frequency is affected very little by either the type of PZT driving element used or its thickness. In general, the cymbals driven by piezoelectrically hard PZT (e.g. 4 or 8) exhibit about a 1 kHz higher resonance frequency than those driven by a soft PZT (e.g. 5A or 552). The resonance frequency appears to reach a constant value when the PZT thickness exceeds about 2.5 mm and decreases by about 15% for very thin drive elements due to an overall reduction in stiffness of the structure.

2. Cap material For transducers with caps of equal dimensions but with different materials, the fundamental resonance frequency is proportional to the ultrasonic velocity of the cap material, or $\sqrt{E/\rho(1-\sigma^2)}$. The resonance frequency is plotted as such in Fig. 6a. These results show that for a transducer of fixed size, the first resonance frequency can be easily tailored simply by changing the cap material. Included on the plot is the resonance frequency when the transducer is water-loaded. The linear trend in the data is no longer observed. This is due to the variation in the densities of the cap materials. Equation 1 shows how the in-water resonance frequency ($f_{r,w}$) can be calculated from the in-air resonance frequency ($f_{r,a}$) [13]. It is based on curve deflection theory for a thin plate clamped around its rim. The term 0.7885 arises from this boundary condition. In the equation, $\emptyset$ represents the cavity diameter at the base of the cap, t is the cap thickness, ρ_w

is the water density, and ρ_c is the cap density. When plotting the percent change in resonance frequency when going from in-air to in-water as a function of the ratio of the water density to the cap density, the predicted one over square root behavior is observed (Fig. 6b). Essentially, these data show that cymbals with cap materials which have a density close to that of water (e.g. aluminum) will exhibit a much more marked shift in its fundamental resonance frequency when immersed in water than a cymbal capped with a higher density cap material, such as tungsten.

$$f_{r,w} = \frac{f_{r,a}}{\sqrt{1+\left(\frac{8\emptyset}{3\pi}\right)\left(\frac{\rho_w}{\rho_c}\right)\left(\frac{0.7885}{t}\right)}} \qquad \text{(Eq. 1)}$$

3. Cap thickness and cavity depth Fig. 7 shows the effect of both cap thickness and cavity depth on the first resonance frequency of the cymbal transducer in-air. The results clearly show that as cap thickness decreases, the first resonance frequency decreases linearly until very thin (< 100 μm) caps are reached. In contrast, as cavity depth increases, the first resonance frequency increases due to an overall increase in the stiffness of the cap. When water loaded, the graphs exhibit the same trends, albeit with the fundamental resonance frequencies shifted down as per Equation 1. The percent change in resonance frequency in going from air to water loading will increase for thinner caps, as predicted by the Equation 1, whereas the cavity depth has no effect.

4. Cavity diameter When keeping the device diameter constant, changes in the base cavity diameter have the greatest effect on the resonance frequency as compared with all other parameters (Fig. 8a). For the standard size brass-capped cymbal, the resonance frequency can be manipulated from about 10 kHz to 50 kHz when changing the cavity diameter from 12 mm to 4.5 mm and the cavity depth from 0.02 mm to 0.47 mm. Again, the water-loaded resonance frequency will be lower than the in-air value due to mass

loading. The shift down can be calculated from Equation 1, where the percent change in resonance frequency will increase as the base cavity diameter increases, which is again predicted by Equation 1. Changes in the cavity diameter at the apex of the cap typically has a smaller effect on the resonance frequency, especially for large base cavity diameters (Fig. 8b)

5. Device diameter The effect of device diameter on the fundamental resonance frequency is shown in Fig. 9. The total height of the transducer was kept constant as nearly 2 mm while the radial dimensions were scaled proportionally. These results show that a two order of magnitude increase in total diameter (from 0.25 mm to 25 mm) resulted in a resonance frequency decrease from 200 kHz to 7 kHz. The water-loaded resonance frequency is included in the graph for comparison.

IV. CONCLUSIONS

The very good agreement between the calculated and experimentally measured admittance spectra indicate that the ANSYS finite element program can model the behavior of the cymbal transducer quite well both in-air as well as when water-loaded. The first resonance frequency is controlled primarily by the cap material - from both its elastic constants as well as its dimensions (geometry). For a 12.7 mm diameter cymbal, the data show that the resonance frequency can be tailored anywhere in air between 5 kHz and 50 kHz simply by changing the cap material or the cap geometry. This capability makes the cymbal-type transducer quite versatile for a number of piezoelectric sensor and/or actuator applications.

ACKNOWLEDGMENT

Financial support was provided by the Office of Naval Research, contract number N00014-96-1-1173.

REFERENCES

[1] E. F. Rynne. "Innovative approaches for generating high power, low frequency sound." in *Transducers for Sonics and Ultrasonics: Proceedings of the Third International Workshop*, M. D. McCollum. B. F. Hamonic, and O. B. Wilson, Eds., Lancaster, PA: Technomic, 1993, pp. 38-49.

[2] Q. C. Xu, S. Yoshikawa, J. R. Belsick, and R. E. Newnham, "Piezoelectric composites with high sensitivity and high capacitance for use at high pressures," *IEEE Trans. UFFC*, vol. 38. pp. 634-639, November 1991.

[3] K. Onitsuka. A. Dogan. J. F. Tressler. Q. C. Xu. S. Yoshikawa. and R. E. Newnham. "Metal-ceramic composite transducer, the 'moonie'," *J. Intel. Mater. Sys. Struct.*, vol. 6, pp. 447-455, July 1995.

[4] J. F. Tressler, A. Dogan, J. F. Fernandez, J. T. Fielding Jr., K. Uchino, and R. E. Newnham, "Capped ceramic hydrophones," in *1995 IEEE Ultrasonics Symposium Proceedings*, M. Levy. S. C. Schneider, and B. R. McAvoy, Eds., Piscataway, NJ: IEEE, 1995, pp. 897-900.

[5] A. Dogan, K. Uchino, and R. E. Newnham, "Composite piezoelectric transducer with truncated conical endcaps 'cymbal'," *IEEE Trans. UFFC*, vol. 44, pp. 597-605, May 1997.

[6] S. C. Butler, A. L. Butler, and J. L. Butler, "Directional flextensional transducer," *J. Acoust. Soc. Am.*, vol. 92, pp. 2977-2979, November 1992.

[7] G. Bedrosian, R. Morrow, M. Palmo, and T. Sober, "SONAR3D: a 3D finite element modeling code for analyzing low frequency sonar transducer arrays," in *Transducers for Sonics and Ultrasonics: Proceedings of the Third International Workshop*, M. D. McCollum, B. F. Hamonic, and O. B. Wilson, Eds., Lancaster, PA: Technomic, 1993. pp. 386-390.

[8] H. C. Robinson, R. T. Richards, and J. B. Blottman III, "Variational modeling of class V flextensional ring-shell projectors," in *Transducers for Sonics and Ultrasonics: Proceedings of the Third International Workshop*, M. D. McCollum, B. F. Hamonic, and O. B. Wilson, Eds., Lancaster, PA: Technomic, 1993, pp. 209-221.

[9] D. F. Jones, "Comparison of class I and class III barrel-stave flextensional projectors using finite element analysis techniques." Presented at the 1997 ONR Transducer Materials and Transducers Workshop, Pennsylvania State University, May 1997.

[10] V. V. Varadan, L. C. Chin, and V. K Varadan, "Finite-element modeling of flextensional electroacoustic transducers," *Smart Mater. Struct.*, vol. 2, pp. 201-207, 1993.

[11] P. Kohnke, Ed., *ANSYS User's Manual for Revision 5.0 - Theory*, vol. IV, Houston, PA: Swanson Analysis Systems, Inc., 1992, pp. 2.1-11.19.

[12] L. E. Kinsler, A. R. Frey, A. B. Coppens, and J. V. Sanders, *Fundamentals of Acoustics*, 3rd ed., New York: John Wiley and Sons, 1982, pp. 191-193.

[13] R. S. Woollett, "Theory of the piezoelectric flexural disk transducer with applications to underwater sound," *USL Research Report No. 490, S-F001 03 04- 1*, Fort Trumbull, New London, CT: U.S. Navy Underwater Sound Laboratory, pp. 30-43, December 1960.

Figure Captions

Fig. 1 Cross-sectional views of the moonie-type (top) and cymbal-type (bottom) transducers. The cross-hatched area represents the PZT disk and the dark area the metal caps. Standard dimensions for the moonie are defined as: PZT thickness=1.0 mm, cap thickness=1.0 mm, maximum cavity diameter=9.0 mm, maximum cavity depth=0.3 mm, overall diameter=12.7 mm. The cymbal standard dimensions are defined as: PZT thickness=1.0 mm, cap thickness=0.25 mm, base cavity diameter=9.0 mm, apex cavity diameter=3.0 mm, maximum cavity depth=0.3 mm, overall diameter=12.7 mm. The standard PZT type is PZT-552 (similar properties to a PZT-5H) from Piezokinetics in Bellefonte, PA.

Fig. 2 Calculated vibration mode shapes (exaggerated scale) of the cymbal transducer. (a) is the (0,1) mode, (b) is the (0,2) mode, (c) is the (0,3) mode, and (d) is the PZT radial mode. The dashed lines show the structure at rest.

Fig. 3 (a) Calculated, and (b) experimentally measured admittance spectra for a standard size brass-capped cymbal transducer in-air.

Fig. 4 (a) Calculated, and (b) experimentally measured admittance spectra in the neighborhood of the first resonance for a standard size brass-capped cymbal transducer both in-air and in-water.

Fig. 5 Calculated first resonance frequency of brass-capped cymbal transducers with standard size brass caps utilizing PZT types of different thickness. The numeral 1 corresponds to curves associated with PZT-8 (upper) and PZT-4 (lower). The numeral 2 corresponds to curves associated with PZT-5A (upper) and PZT-552 (lower).

Fig. 6 (a) Effect of cap material on the first resonance frequency of standard size cymbals both in-air and in-water. Key: 1=brass caps, 2=tungsten, 3=steel, 4=aluminum, 5=titanium, and 6=molybdenum. (b) the percent change in first resonance frequency from in-air to in-water as a function of the ratio of water density to cap material density. The number in parenthesis is the cap density in terms of kg/m^3.

Fig. 7 Effect of cap thickness on the first resonance frequency of brass-capped cymbal transducers with different cavity depths. Curves associated with different maximum cavity depths (d_c) are represented by the numerals 1-7. Key: 1: d_c=0.02 mm, 2: d_c=0.07 mm, 3: d_c=0.12 mm, 4: d_c=0.18 mm, 5: d_c=0.25 mm, 6: d_c=0.30 mm, 7: d_c=0.47 mm.

Fig. 8 Effect of (a) base cavity diameter associated with different cavity depths on the first resonance frequency of a brass-capped cymbal transducer. Curves associated with different maximum cavity depths (d_c) are represented by the numerals 1-6, where 1: d_c=0.02 mm, 2: d_c=0.12 mm, 3: d_c=0.18 mm, 4: d_c=0.25 mm, 5: d_c=0.30 mm, 6: d_c=0.47 mm. (b) effect of apex cavity diameter associated with different base cavity diameters (Ø) on the first resonance frequency. Curves associated with different base cavity diameters (Ø) are represented by the numerals 1-6, where 1: Ø=12 mm, 2: Ø=10.5 mm, 3: Ø=9.0 mm, 4: Ø=7.5 mm, 5: Ø=6.0 mm, 6: Ø=4.5 mm.

Fig. 9 Effect of device diameter on the first resonance frequency of the brass-capped cymbal transducer. The overall thickness is maintained at ≈ 2 mm. The water-loaded resonance frequency is shown for comparison.

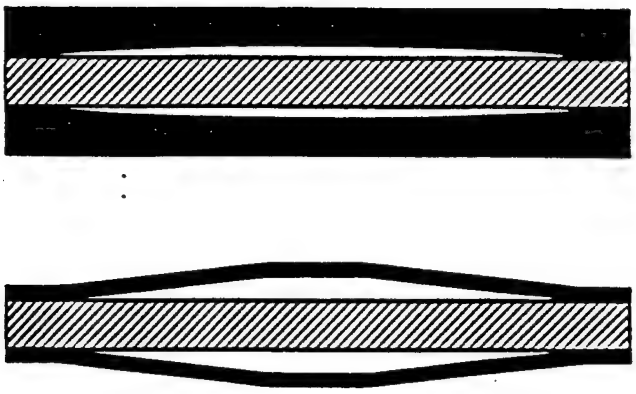

Fig. 1

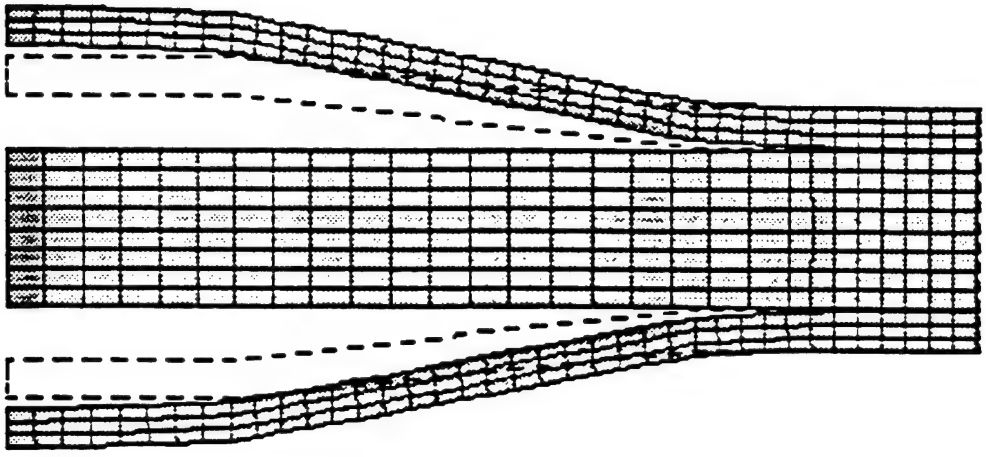

Fig 2a

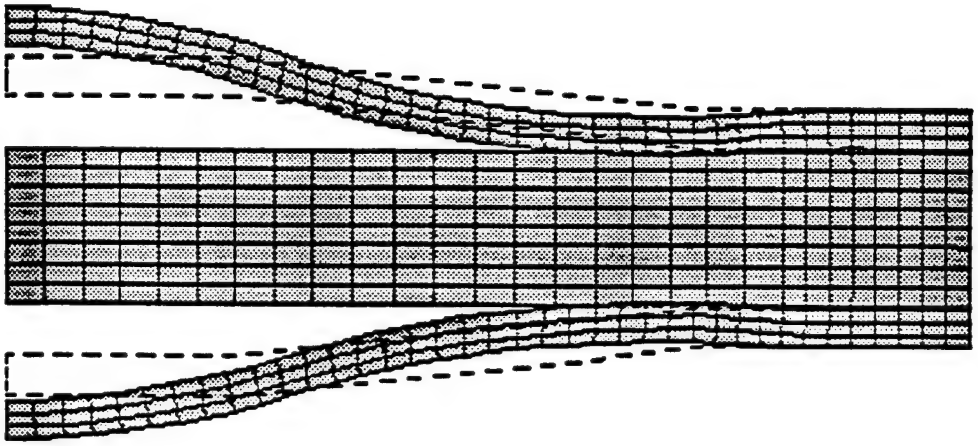

Fig. 2b

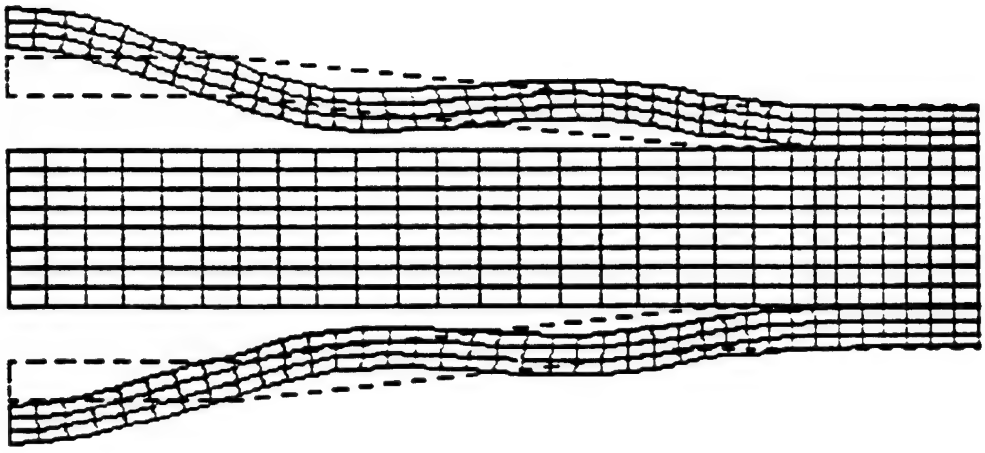

Fig 2C

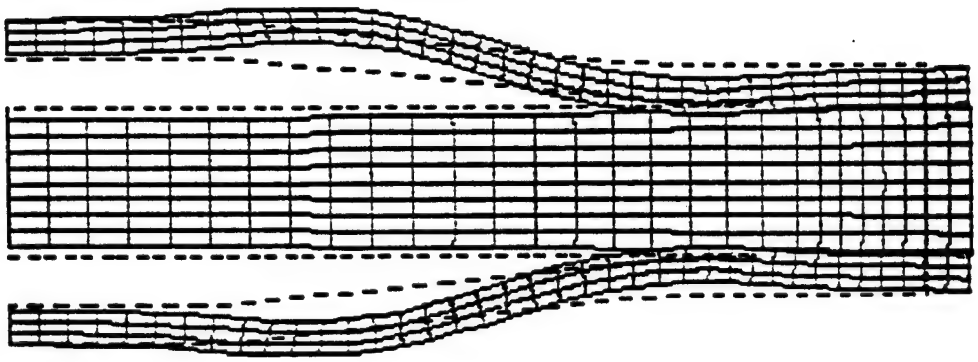

Fig 2d

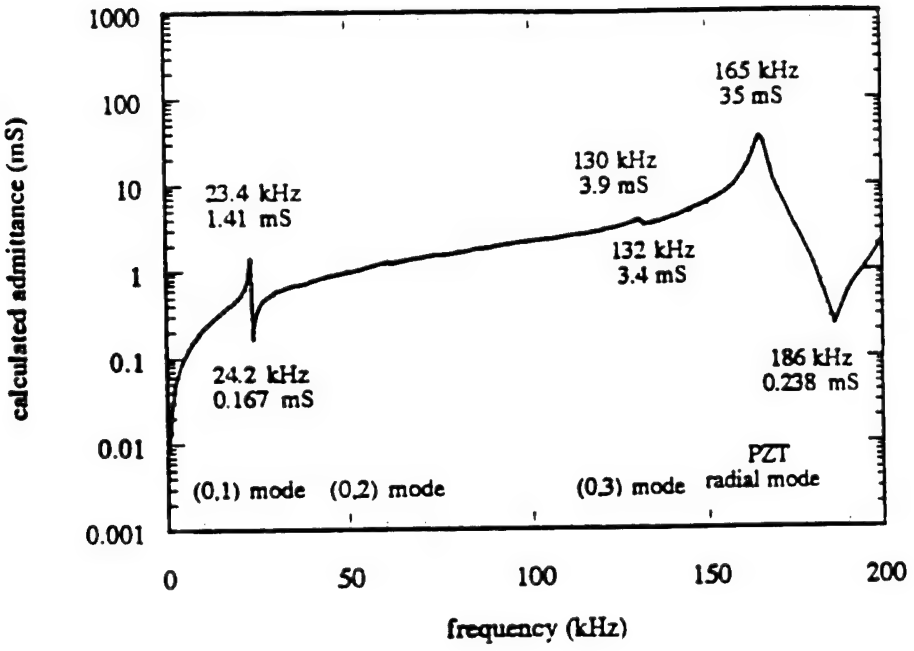
1000
100
10
1
0.1
0.01
0.001
calculated admittance (mS)
0
50
100
150
200
frequency (kHz)
165 kHz
35 mS
130 kHz
3.9 mS
23.4 kHz
1.41 mS
132 kHz
3.4 mS
186 kHz
0.238 mS
24.2 kHz
0.167 mS
PZT
radial mode
(0,1) mode
(0,2) mode
(0,3) mode

Fig 3a

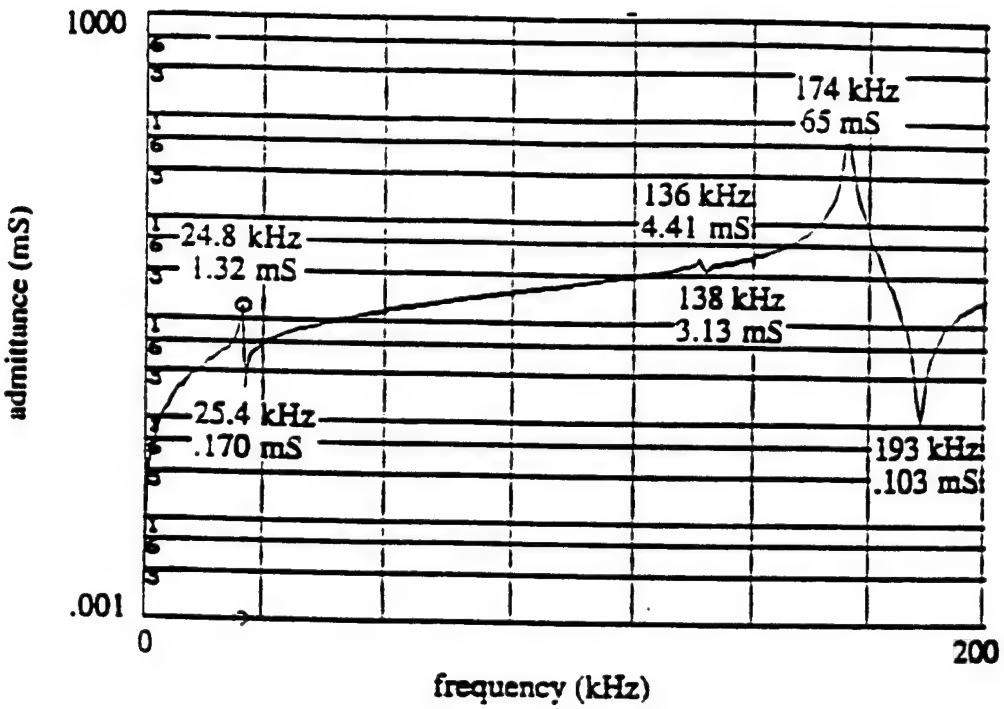
1000
.001
0
200
admittance (mS)
frequency (kHz)
174 kHz
65 mS
136 kHz
4.41 mS
24.8 kHz
1.32 mS
138 kHz
3.13 mS
25.4 kHz
.170 mS
193 kHz
.103 mS

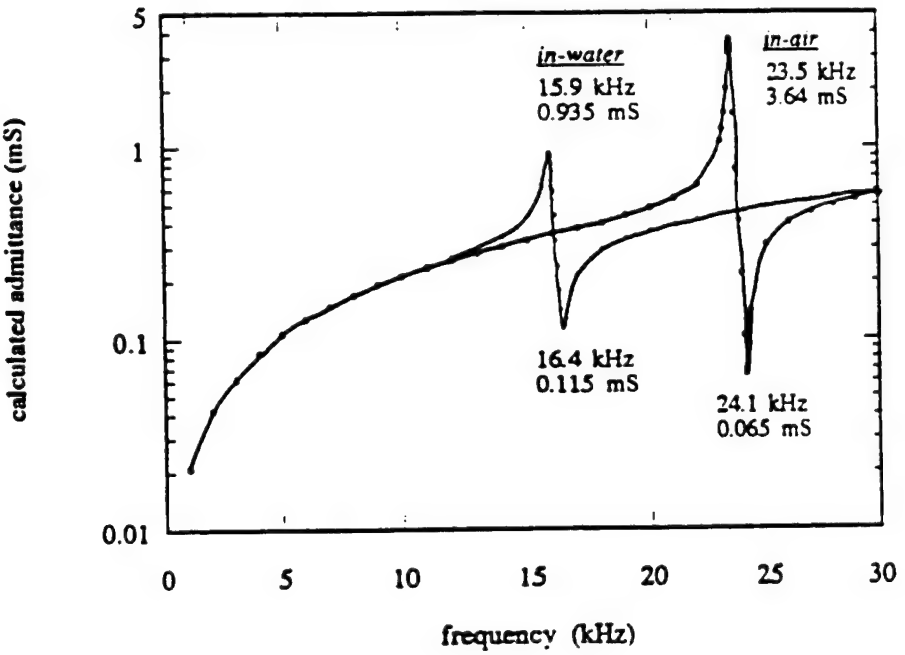
5
1
0.1
0.01
calculated admittance (mS)
in-water
15.9 kHz
0.935 mS
in-air
23.5 kHz
3.64 mS
16.4 kHz
0.115 mS
24.1 kHz
0.065 mS
0
5
10
15
20
25
30
frequency (kHz)

Fig 4a

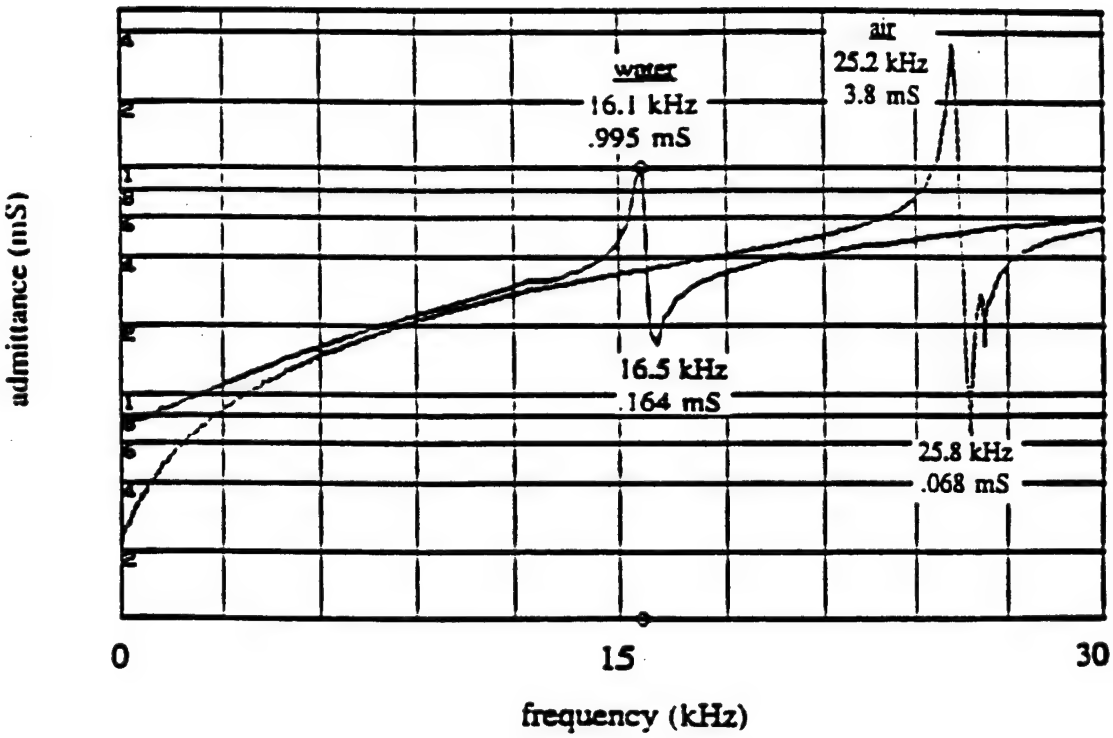
air
25.2 kHz
3.8 mS
water
16.1 kHz
.995 mS
16.5 kHz
.164 mS
25.8 kHz
.068 mS
admittance (mS)
0
15
30
frequency (kHz)

Fig 4b

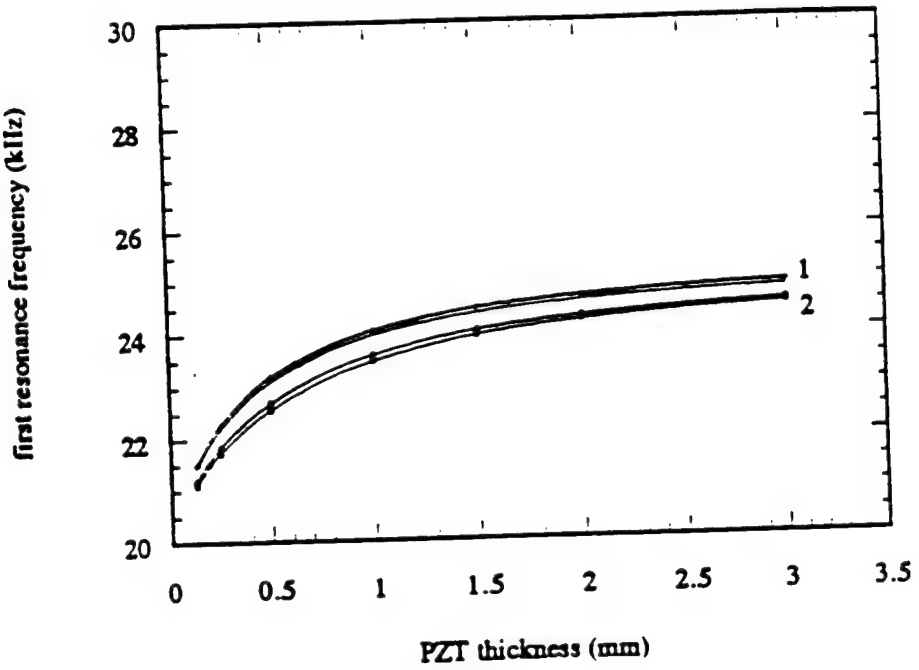
first resonance frequency (kHz)
30
28
26
24
22
20
0
0.5
1
1.5
2
2.5
3
3.5
PZT thickness (mm)
1
2

Fig 5

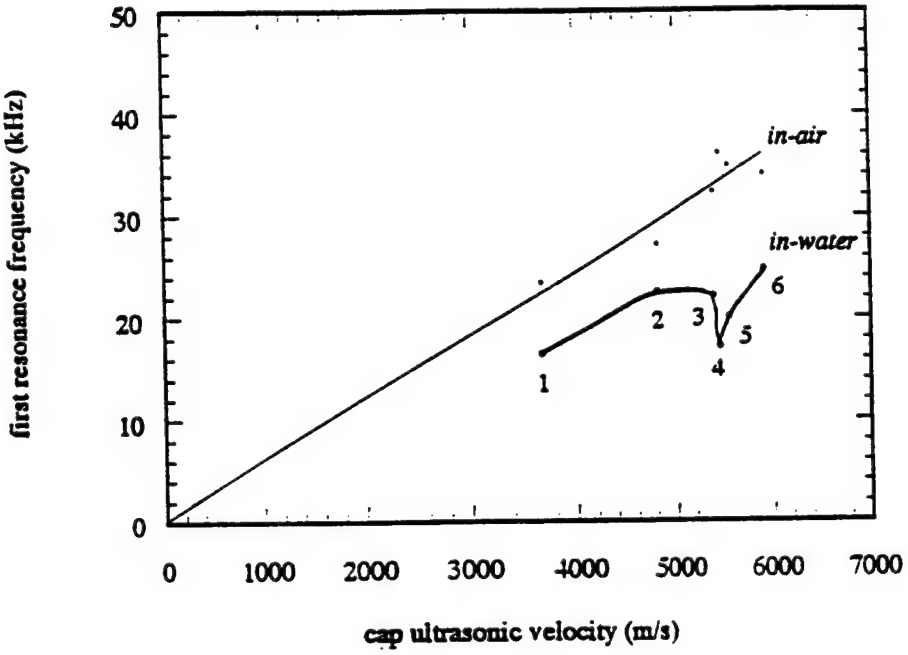
50
40
30
20
10
0
first resonance frequency (kHz)
0
1000
2000
3000
4000
5000
6000
7000
cap ultrasonic velocity (m/s)
in-air
in-water
1
2
3
4
5
6

Fig. 6a

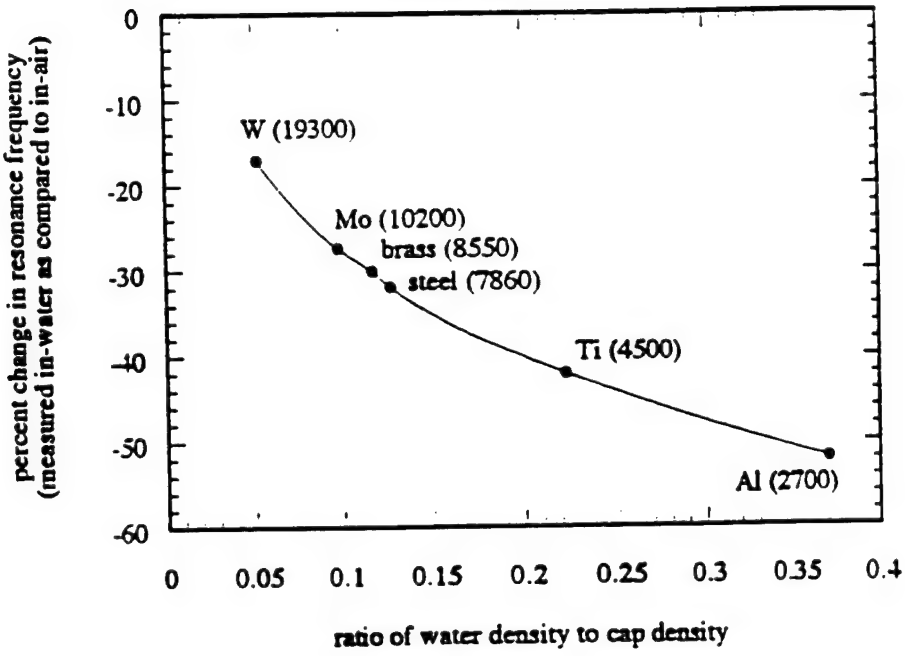
0
-10
-20
-30
-40
-50
-60
W (19300)
Mo (10200)
brass (8550)
steel (7860)
Ti (4500)
Al (2700)
0
0.05
0.1
0.15
0.2
0.25
0.3
0.35
0.4
percent change in resonance frequency
(measured in-water as compared to in-air)
ratio of water density to cap density

Fig 6b

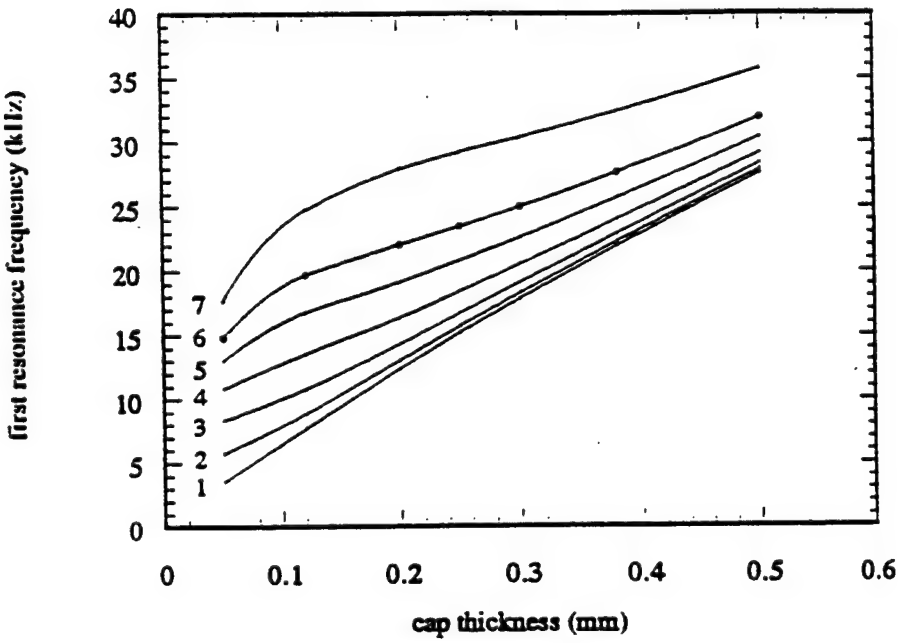
first resonance frequency (kHz)
40
35
30
25
20
15
10
5
0
7
6
5
4
3
2
1
0
0.1
0.2
0.3
0.4
0.5
0.6
cap thickness (mm)

Fig. 7

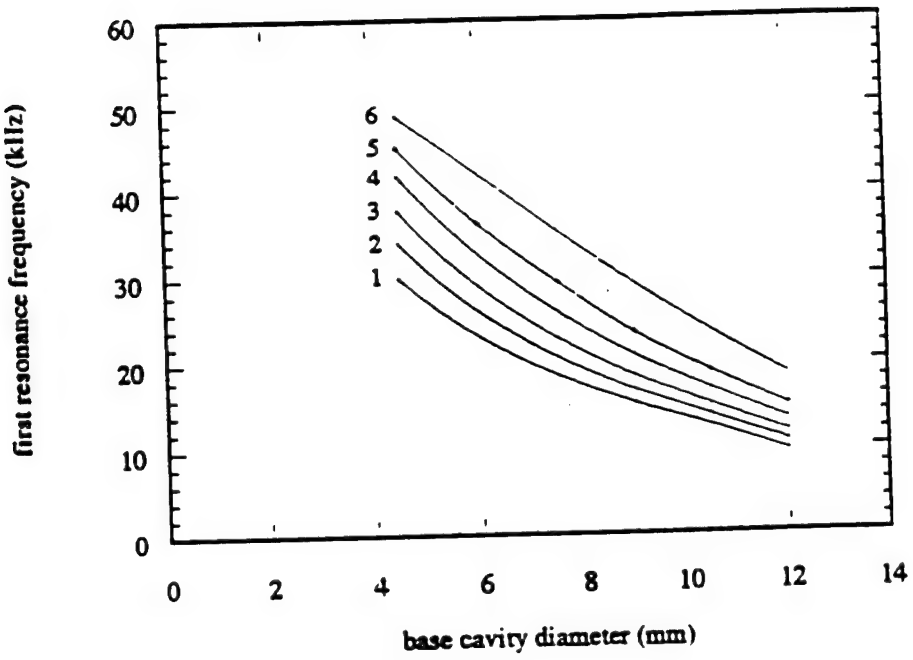
first resonance frequency (kHz)
60
50
40
30
20
10
0
0
2
4
6
8
10
12
14
base cavity diameter (mm)
6
5
4
3
2
1

Fig 8a

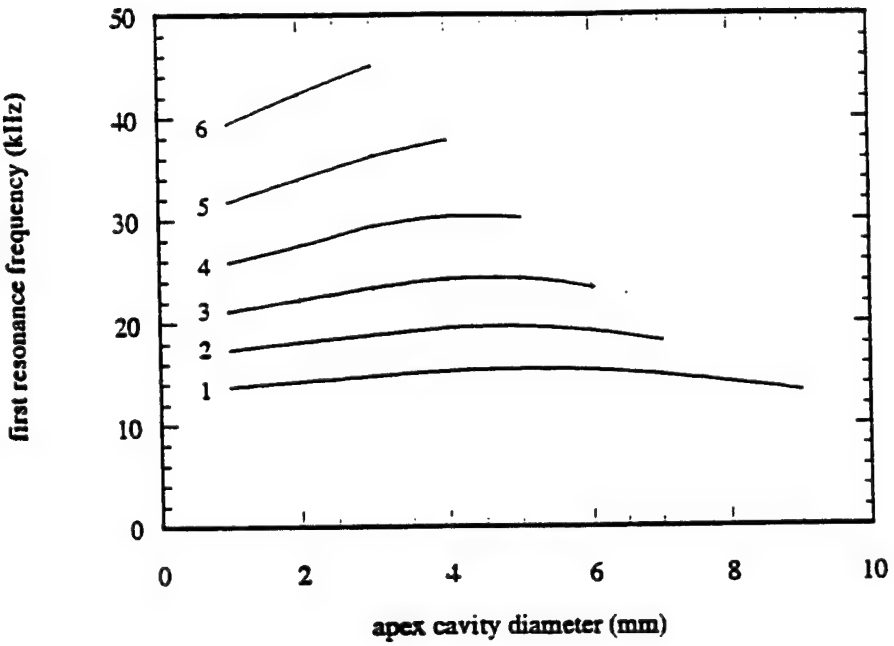
50
40
30
20
10
0
6
5
4
3
2
1
0
2
4
6
8
10
first resonance frequency (kHz)
apex cavity diameter (mm)

Fig 8b

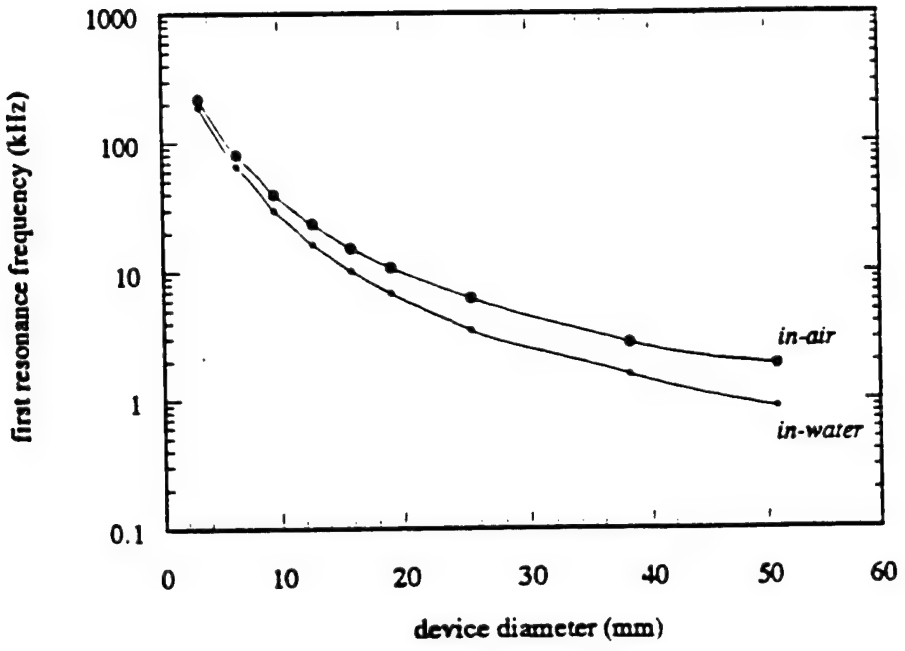
1000
100
10
1
0.1
first resonance frequency (kHz)
0
10
20
30
40
50
60
device diameter (mm)
in-air
in-water

Fig. 9

APPENDIX 43

Capped Ceramic Underwater Sound Projector

James F. Tressler, W. Jack Hughes†, Wenwu Cao, Kenji Uchino, and Robert E. Newnham
Materials Research Laboratory, †Applied Research Laboratory
The Pennsylvania State University
University Park, PA 16802 USA

Abstract -- A new type of transducer has been developed for use as a shallow water sound projector at frequencies from 5 kHz to 50 kHz. Dubbed the 'cymbal', it is similar to the more commonly known 'moonie' or class V ring/shell flextensional designs. Prototype cymbal arrays with a radiating area of 14.5 cm^2 have been developed and tested. Two mounting schemes were examined: unpotted and potted in a 5 mm thick layer of stiff polyurethane. In both cases, a transmitting response comparable to the more widely used tonpilz transducer is attainable. When tested under hydrostatic pressures, the cymbal can withstand pressures of at least 2.5 MPa (which corresponds to 250 m of water depth) without a degradation in its performance.

I. INTRODUCTION

Sound transmission is the single most effective means of directing energy transfer over large distances underwater [1]. The number of applications which utilize some form of acoustic energy is quite large, with frequencies ranging anywhere between 10^{-3} Hz to 10^{9} Hz. There is currently a great interest in the development of shallow water acoustic projectors that operate in the frequency range from 1 kHz to 100 kHz. Ideally, these transducers should be thin, lightweight, exhibit medium to high acoustic output power, be able to conform to a curved surface, and be of simple design such that they are easy and inexpensive to mass produce.

Currently, the predominant underwater projector systems that operate in the 1 kHz to 100 kHz frequency range are the tonpilz transducers and 1-3 composites. The tonpilz transducer consists of a stack of piezoceramic (typically PZT) rings connected mechanically in series and electrically in parallel. The ring stack is sandwiched between two metal masses: a heavy tailmass and a light, flared headmass which serves to transmit the generated acoustic energy into the surroundings. Tonpilz transducers are characterized by their very large acoustic output power, are typically tens of centimeters in thickness, and are designed to operate at frequencies below 100 kHz.

This work was funded by the Office of Naval Research

The 1-3 type composites consist of a number of piezoceramic rods separated by a 3-D interconnected polymer matrix. These composites have been manufactured in a number of ways [2]. The current state of the art fabrication method is by injection molding [3]. The performance of 1-3 composites is strongly affected by the elastic properties of both the ceramic and polymer phases, the volume fraction of piezoceramic rods, and most importantly, the aspect ratio of the ceramic rods [4]. Typical 1-3 composites designed for use below 100 kHz are at least 1 cm thick.

A third type of underwater projector that is seeing a resurgence in interest is the so-called flextensional transducer. Flextensionals have been in existence since the 1920s and have seen use as underwater projectors since the late 1950s [5]. Flextensionals consist of a piezoceramic drive element encapsulated by a metal shell. The shape of the shell has become quite diverse over the years and so a classification system has been established to group the common designs together [6]. Flextensional transducers typically range in size from several centimeters to several meters in length and can weigh up to hundreds of kilograms.

A miniaturized version of the class V flextensional transducer was developed in the late 1980s at the Materials Research Laboratory at The Pennsylvania State University for use as an underwater pressure sensor [7]. This transducer was named the 'moonie' due to the crescent moon shaped cavity on the inner surface of the caps. A second generation moonie-type transducer has recently been developed which consists of a thinner cap with a slightly different shape. This transducer has been dubbed the 'cymbal' due the similarity in shape of its caps to that of the musical instrument of the same name. The moonie and cymbal designs are compared in Fig. 1.

The moonie and cymbal transducers consist of a piezoceramic (usually PZT) disk poled in the thickness direction which is sandwiched between and mechanically coupled to two metal caps, each of which contains a shallow cavity on its inner surface. The presence of these cavities allows the caps to convert and amplify the small radial displacement and vibration velocity of the piezoceramic disk into a much larger axial displacement and vibration velocity normal to the surface of the caps. This enhanced displacement and vibration velocity from the caps contribute to a much larger acoustic pressure output than would occur in the uncapped ceramic. The dimensions of the standard-size moonie and cymbal transducers are presented in TABLE I.

(a) moonie structure

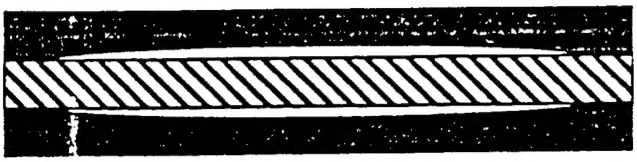

(b) cymbal structure

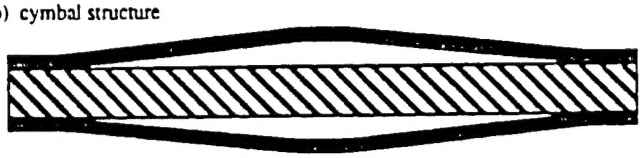

Fig. 1. Cross-sectional views of the (a) moonie-type, and (b) cymbal-type transducers. The dark areas represent the caps and the cross-hatched areas the PZT disk.

TABLE I
DIMENSIONS OF THE STANDARD MOONIE AND CYMBAL TRANSDUCERS

Moonie Parameter	Dimension
cap diameter	12.7 mm
cap thickness	1.0 mm
cavity depth	0.25 mm
cavity diameter	9.0 mm
PZT thickness	1.0 mm
PZT diameter	12.7 mm
Cymbal Parameter	
cap diameter	12.7 mm
cap thickness	0.25 mm
cavity depth	0.30 mm
cavity diameter	9.0 mm
dimple diameter	3.0 mm
PZT thickness	1.0 mm
PZT diameter	12.7 mm
weight	~ 2 grams

II. PARAMETERS TO MEASURE

Among the relevant parameters that need to be reported in order to fully characterize an underwater projector, the most important are resonance frequency, mechanical Q, electroacoustic efficiency, electromechanical coupling coefficient (k_{eff}), transmitting voltage response (TVR), source level (SL), and beam patterns. Transmitting voltage response is equal to the sound pressure produced by the projector referenced (re:) to a distance of one meter from the acoustic center of the transducer when unit voltage is applied across its electrical terminals. It is reported in terms of dB re: 1 μPa/V @ 1 m, or as 1 μPa•m/V. Source level is the intensity of the radiated sound (i.e. radiated power) relative to the intensity of a plane wave of rms pressure 1 μPa referred to a point one meter from the acoustic center of the projector. Source level is related to the transmitting voltage response through the applied input voltage as:

$$SL = TVR + 20 \cdot \log V_{in,rms} \qquad (1)$$

Thus, this parameter has the same units as TVR. In general, a source level of greater than 200 dB re: 1 μPa/V @ 1 m is desirable. The beam pattern describes the response of the transducer relative to its main acoustic axis.

III. COMPUTER MODELING

The ANSYS® finite element software program (version 5.1) was used to model the behavior of the cymbal transducer both in-air as well as when it was water-loaded. Modal analysis of a two-dimensional axisymmetric model was performed to obtain vibration mode shapes, resonance frequencies, and the stress distribution within the structure at resonance. Harmonic analysis was utilized to calculate admittance versus frequency curves, from which a theoretical effective coupling coefficient could be derived.

IV. EXPERIMENTAL PROCEDURE

Single element cymbal transducers were fabricated by first simultaneously cutting and shaping the caps in a die press. The caps were then adhered to a poled PZT disk using a very thin layer of epoxy. The bonding quality after curing was characterized by measuring the admittance spectra of the transducer.

Single element cymbal transducers were incorporated into 9-element square arrays, where the single elements were wired together electrically in parallel. Two mounting schemes were investigated: unpotted and potted in a stiff layer of polyurethane approximately 5 mm thick.

Underwater calibration tests were performed in the anechoic water tank at the Applied Research Laboratory at Penn State. The tank measures 5.5 m in depth, 5.3 m in width, and 7.9 m in length. A pure tone sinusoidal pulse signal of 2 msec duration was applied to the test transducer and its acoustic output was subsequently measured by a standard F33 hydrophone. The test transducer and the standard are positioned so that they are at a depth of 2.74 m and separated by a distance of 3.16 m.

V. Results and Discussion

TABLE II provides some typical experimentally measured values for the parameters described in section II. These are all values for standard-size single element brass-capped cymbals except where otherwise noted. The large shift in the fundamental resonance frequency is due to the mass loading effect of the water. The d_{33} coefficient is really an effective d_{33} coefficient (since it is reported for a device). The PZT type in parenthesis is the type used as the active element in the transducer.

TABLE II
Typical Air- and Water-Loaded Characteristics of the Standard-Size Brass-Capped Cymbal Transducer

	air-loading	water-loading
f_r	23.4 kHz	15.9 kHz
k_{eff}	0.20	0.25
Q_m	200	20
efficiency		90%
d_{33} (PZT-552)	12000 pC/N	
d_{33} (PZT-5A)	8000 pC/N	
d_{33} (PZT-4)	6000 pC/N	
d_{33} (PZT-8)	5000 pC/N	

Fig. 2. shows the first resonance frequency of standard-size cymbal transducers with different cap materials as calculated by FEA both in-air and in-water. The first resonance frequency in-air is proportional to the sonic velocity of the cap material, $\sqrt{E/\rho(1-\sigma^2)}$, where E is the cap Young's modulus, ρ its density, and σ its Poisson's ratio. When the resonance frequency is measured in-water, the linear trend in the data is no longer observed. This is due to the difference in the density of the caps. Cymbals which have caps with densities closer to that of water, such as titanium, will exhibit a much more marked change in its resonance frequency in going from air to water than cymbals with caps of higher density, e.g. tungsten.

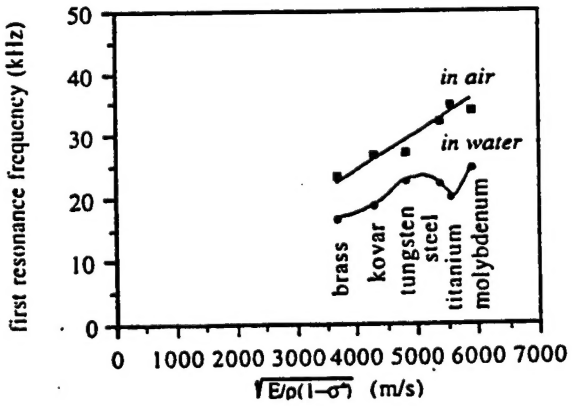

Fig. 2. First resonance frequency of standard-size cymbal transducers with different endcaps measured in-air and in-water.

The transmitting voltage response in the neighborhood of the first resonance frequency for same-size single element brass-capped cymbal transducers utilizing different PZT types is shown in Fig. 3. The transmitting response correlates with the effective d_{33} coefficient of the device, as seen from TABLE II. Single element cymbals are characterized by a relatively high Q_m (≈ 20) and consequently a narrow bandwidth.

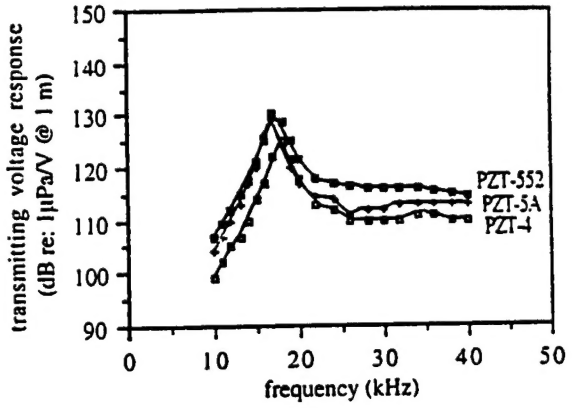

Fig. 3. Transmitting voltage response of a standard-size brass-capped cymbal utilizing different PZT types.

The transmitting voltage response of nine-element arrays of standard-size brass-capped cymbals, both potted and unpotted, are compared in Fig. 4. The fundamental resonance frequency is now strongly damped in both cases, resulting in wideband behavior. This is in part due to the array more closely approaching the idealized 'ρc' loading conditions as compared to the single element.

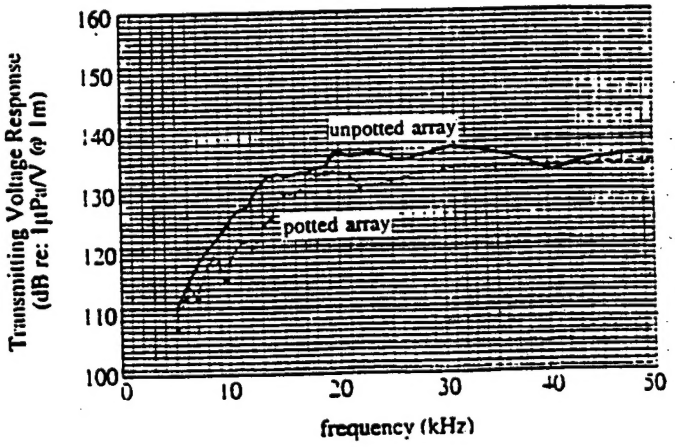

Fig. 4. Comparison of the transmitting voltage response of nine element potted and unpotted arrays of standard-size brass-capped cymbals utilizing PZT-552 driving elements.

A representative beam pattern for the nine-element arrays at 50 kHz is shown in Fig. 5. At frequencies below 50 kHz. the array exhibits near omnidirectionality. Above 50 kHz. the side lobes become more pronounced and grating lobes appear. Thus, 50 kHz is taken to be the upper use frequency for the arrays.

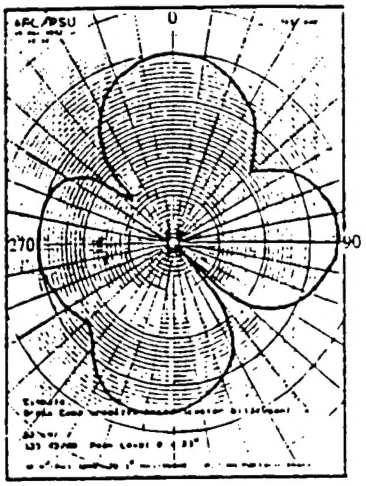

Fig. 5. Beam pattern of the array of brass-capped cymbals at 50 kHz.

Fig. 6. shows the source level as measured for the unpotted array when driven at 52 dBV both before and after failure. A source level of greater than 190 dB is generated by the array between about 18 kHz and at least 25 kHz. Although this is still less than the desired 200 dB, it is important to keep in mind that this is for an array of radiating area of only 14.5 cm^2. Increasing the radiating area by incorporating more single elements into the array will enhance the source level by a factor of 20•logA, where A is equal to the increase (i.e. multiplication factor) in radiating area.

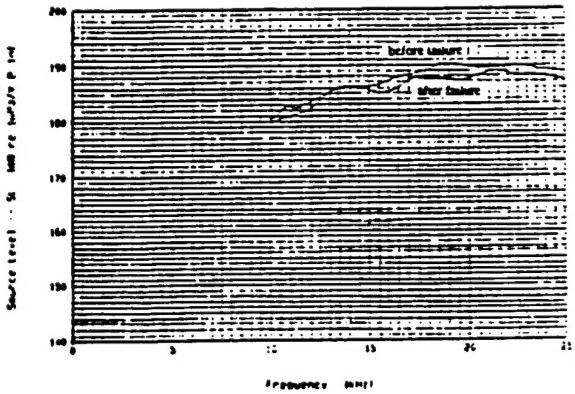

Fig. 6. Source level of the unpotted cymbal array as measured both before and after failure.

Fig. 7. shows the measured pressure dependence of the effective d_h and g_h coefficients of single-element brass-capped cymbal transducers with different cavity depths. The standard-size cymbal can withstand up to 2.5 MPa without a significant degradation in its properties.

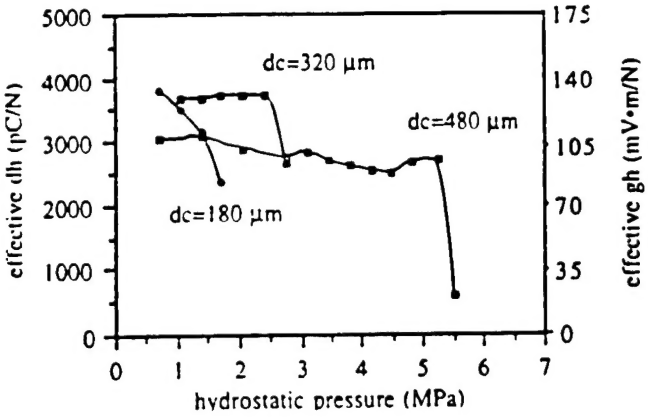

Fig. 7. Measured pressure dependence of the effective d_h and g_h coefficients for standard-size brass-capped single element cymbal transducers

VI. Conclusions

The cymbal transducer appears to be a viable candidate for medium- to high-power shallow water acoustic projector applications. Its thin profile when incorporated into arrays makes it ideal for attaching to a curved surface. In addition, its simple design renders it easy and inexpensive to mass produce.

Acknowledgments

The authors would like to thank Ender Kuntsal of ITC in Santa Barbara, CA, and Robert Dashem of the Applied Research Laboratory at Penn State for their contributions.

References

[1] R.F.W. Coates, *Underwater Acoustic Systems*, Macmillan New Electronics Series, Hong Kong, 1990.

[2] T.R. Gururaja, A. Safari, R.E. Newnham, and L.E. Cross, "Piezoelectric ceramic-polymer composites for transducer applications," in *Electronic Ceramics: Properties, Devices, and Applications*, L.M. Levinson, Ed., New York: Marcel Dekkar, Inc., 1988, pp. 92-145.

[3] L. Bowen, R. Gentilman, D. Fiore, H. Pham, W. Serwatka, C. Near, and B. Pazol,"Design, fabrication, and properties of Sonopanel" 1-3 piezocomposite transducers," *Ferroelectrics*, vol. 187, pp. 109-120, 1996.

[4] W. Cao, Q.M. Zhang, and L.E. Cross, "Theoretical study on the static performance of piezoelectric ceramic-polymer composites with 1-3 connectivity," *J. App. Phys.*, vol. 72, pp. 5814-5821, 1992.

[5] K.D. Rolt, "History of the flextensional electroacoustic transducer," *J. Acoust. Soc. Am.*, vol. 87, pp. 1340-1349, 1990.

[6] E.F. Rynne, "innovative approaches for generating high power, low frequency sound," in *Transducers for Sonics and Ultrasonics*, M.D. McCollum, B.F. Hamonic, and O.B. Wilson, Eds., Lancaster, PA: Technomic, 1993, pp. 38-49.

[7] Q.C. Xu, S. Yoshikawa, J.R. Belsick, and R.E. Newnham, "Piezoelectric composites with high sensitivity and high capacitance for use at high pressures," *IEEE Trans. UFFC*, vol. 38, pp. 634-639, 1991.